Die Rolle zytosolischer Nukleinsäurerezeptoren bei Strahlentherapie- oder Chemotherapie-induziertem intestinalen Gewebeschaden und der Graft-versus-host disease

vorgelegt von
Julius Clemens Fischer
aus München
2018

Klinik und Poliklinik für Innere Medizin III, Hämatologie und Onkologie, Klinikum rechts der Isar der Fakultät für Medizin der Technischen Universität München.

Die Rolle zytosolischer Nukleinsäurerezeptoren bei Strahlentherapie- oder Chemotherapie-induziertem intestinalen Gewebeschaden und der Graft-versus-host disease

Julius Clemens Fischer

Vollständiger Abdruck der von der Fakultät für Medizin der Technischen Universität München, zur Erlangung des akademischen Grades eines Doktors der Medizinischen Wissenschaft (Dr. med. sci.), genehmigten Dissertation.

Vorsitzender: apl. Prof. Dr. Klaus-Peter Janssen

Prüfende/-r der Dissertation:
1) Priv.-Doz. Dr. Hendrik Poeck
2) Prof. Dr. Dirk Busch
3) Prof. Dr. Percy A. Knolle

Die Dissertation wurde am 27.06.2018 bei der Technischen Universität München eingereicht und durch die Fakultät für Medizin der Technischen Universität München am 02.01.2019 angenommen.

Inhaltsverzeichnis

1. Einleitung

Zur Behandlung bestimmter schwerer onkologischer oder genetischer Erkrankungen werden allogene hämatopoetische Stammzelltransplantationen eingesetzt. In etwa der Hälfte der Fälle kommt es nach Transplantation zur Entwicklung einer akuten Graft-versus-host disease, einer oftmals tödlichen Immunerkrankung. Trotz intensiver Forschungen gibt es noch immer einen Mangel an effektiven Therapien und Lücken im Verständnis über den Entstehungsprozess der Erkrankung. Bekannt ist, dass der Beginn der Erkrankung maßgeblich durch einen Integritätsverlust der Darmbarriere geprägt ist. Neue Therapieansätze zur Prävention und Behandlung der Graft-versus-host disease zielen deshalb unter anderem darauf ab, die Epithelbarriere des Darms zu stärken, um damit das Ausmaß der Erkrankung zu reduziere. Im Zentrum der aktuellen Forschung stehen Signalwege, die zur Regeneration der intestinalen Epithelzellen beitragen und deren Aktivierung die Entwicklung einer Graft-versus-host disease abmildern könnte.

2. Medizinische und immunologische Grundlagen

2.1 Klinische Bedeutung hämatopoetischer Stammzelltransplantationen

Zu den ältesten aller in der Humanmedizin angewendeten Stammzelltherapien gehören die hämatopoetischen Stammzelltransplantationen (HSZT). Bei diesem Verfahren werden pluripotente hämatopoetische Vorläuferzellen, die zuvor aus dem Blut oder Knochenmark eines Spenders isoliert wurden, dem Empfänger per Infusion transplantiert.

HSZT bilden einen wichtigen Bestandteil der Therapie eines umfangreichen Spektrums verschiedener Erkrankungen. Bei den meisten dieser Krankheitsbilder handelt es sich um onkologische Entitäten. Zu den Pathologien gehören beispielsweise aggressive Formen der Leukämien, Varianten des Multiplen Myeloms oder solide Tumorerkrankungen wie fortgeschrittene Stadien des Hodenkrebses. Zusätzlich zu diesen klassischen onkologischen Indikationen werden HSZT z.B. auch zur Therapie seltener Erkrankungen wie der paroxysmalen nächtlichen Hämoglobinurie oder der schweren aplastischen Anämie angewendet (Brodsky, 2009; Marsh et al., 2009). Im oftmals noch klinisch experimentellen Rahmen werden HSZT außerdem zur Behandlung bestimmter genetisch bedingter Autoimmunerkrankungen wie z.B. Formen der chronisch-entzündlichen Darmerkrankungen eingesetzt (L. Zhu et al., 2017). Neue Konzepte untersuchen weitere Einsatzgebiete von HSZT wie etwa zur Therapie eines Lupus erythematodes, im Zusammenhang mit soliden Organtransplantationen oder in Kombination mit adaptivem T-Zell-Transfer (H. W. Li et al., 2012).

Zur Therapie all dieser Erkrankungen werden hochdosierte Chemotherapeutika oder Strahlentherapie (Ganzkörperbestrahlung, total body irradiation, TBI) angewendet, um die malignen, autoimmunen oder defekten Körperzellen auszulöschen. Diese hochdosierte Therapie führt zu einer Bekämpfung und

Rückgang der kranken Zellen, die durch eine gewöhnlich dosierte zytostatische Therapie nicht gewährleistet wäre. Neben dem gewünschten therapeutischen Effekt einer derartigen Hochdosistherapie beeinträchtigen solche intensiven Therapieregime auch die Hämatopoese im Knochenmark der Patienten. Diese Zerstörung des patienteneigenen Knochenmarks bewirkt einen massiven Abfall der Blutzellbildung und damit eine massive Panzytopenie, die ohne zusätzliche Maßnahmen oftmals zu Blutungen, Sauerstoffunterversorgung, Infektionen und dem Tod der Patienten führen würde. Um das Überleben der Patienten nach einer solchen Hochdosistherapie zu gewährleisten, werden HSZT mit bereits im Vorfeld gewonnenen hämatopoetischen Stammzellen (Stammzellapherese) durchgeführt. Hierbei wird primär zwischen autologen-HSZT, bei denen die Stammzellen vor Therapiebeginn von den Patienten selbst gesammelt wurden und allogenen HSZT (allo-HSZT), bei denen das Transplantat von einem fremden Spender stammt, unterschieden.

Autologe HSZT werden primär als Rescue-Therapie nach Hochdosischemotherapie eingesetzt, um die Blutbildung und damit das Überleben des Patienten zu sichern.

Im Gegensatz dazu können allo-HSZT deutlich vielseitiger eingesetzt werden. Im Allo-HSZT ermöglichen die Therapie von Erkrankungen, die bereits das eigene Knochenmark eines Patienten befallen haben oder körpereigene Immunzellen betreffen (z.B. bei Leukämien, Erkrankungen mit genetisch defekten Knochenmarkszellen oder bestimmten Autoimmunerkrankungen). Außerdem kann durch die allo-HSZT zusätzlich der Graft-versus-Tumor (GVT) Effekt therapeutisch genutzt werden. Bei diesem Effekt wird davon profitiert, dass allogene Stammzellen die Entwicklung von Immunzellen bewirken, welche auch die entarteten Zellen des Empfängers effektiv erkennen und diese damit besser als die körpereigenen Immunzellen des Empfängers bekämpfen können. Dieser

Effekt spielt v.a. nach allo-HSZT im Zuge von Leukämien als s.g. Graft-versus-Leukemia (GVL) Effekt eine entscheidende Rolle (Weiden et al., 1979).

Im Umkehrschluss tragen diese immunologischen Grundlagen des GVL Effekts zusammen mit zusätzlichen pathogenetischen Mechanismen zu einer gravierenden Komplikation nach allo-HSZT bei, der oftmals tödlich verlaufenden Graft-versus-host disease (GVHD) (Shlomchik, 2007).

2.2 Graft-versus-host disease nach allogener Stammzelltransplantation

Die bedrohlichste Komplikation nach erfolgreicher allogener hämatopoetischer Stammzelltransplantation ist die Graft-versus-host disease (GVHD), eine allo-immunologisch bedingte Multiorganerkrankung, bei der es zur Entzündung und Zerstörung zahlreicher Gewebetypen und Organe kommt (Ferrara et al., 2009). Hierbei wird zwischen der akuten GVHD (aGVHD) und der chronischen (late-onset) GVHD unterschieden, die im Gegensatz zu der aGVHD definitionsgemäß erst 100 Tage nach Transplantation auftritt (Blazar et al., 2012). Die besonders lebensbedrohliche akute GVHD tritt in 30% - 60% aller allo-HSZT auf und trägt in 15-30% maßgeblich zum Tod der Empfänger bei (Ferrara et al., 2009).

Im Vordergrund der GVHD stehen histopathologisch diagnostizierbare Pathologien des Gastrointestinaltrakts (GIT), der Haut und der Leber (Lerner et al., 1974; Stift et al., 2014; Ziemer et al., 2014). Zusätzlich kann es jedoch auch zu vielfältigen zusätzlichen Manifestationen, beispielsweise im Knochenmark, Thymus, der Lunge, den Augen, den Speicheldrüsen oder dem Urogenitalsystem der allo-HSZT-Empfänger kommen (Cooke et al., 2017; Szyska et al., 2016). Je nach Größe des Befalls und histopathologischem Grad der Pathologien lässt sich die GVHD in 4 Grade klassifizieren (Glucksberg et al., 1974). Etwa 50% aller allo-HSZT Empfänger entwickeln eine Grad II bis IV GVHD (Zeiser et al., 2016).

Zur Firstline-Therapie der GVHD erfolgt in der Regel eine Behandlung mit Glucocorticoiden (Wolff et al., 2013). Im Falle von Non-Respondern ist die Möglichkeit von Zweitlinien-Therapeutika begrenzt auf u.a. mTOR Inhibitoren, einzelne monoklonale Antikörper, wie z.B. Infliximab, Tyrosinkinaseinhibitoren (Ruxolitinib) und mesenchymale Stromazellen, zum Einsatz (Kuci et al., 2016; Lutz et al., 2016; Rager et al., 2011; Schmidt-Hieber et al., 2005; Spoerl et al., 2014; Wolff et al., 2013). Es gibt jedoch eine Vielzahl von weiteren vielversprechenden therapeutischen Ansätzen, die in den letzten Jahren in der präklinischen Forschung entwickelt wurden und bereits in ersten klinischen Studien eingesetzt werden, wie beispielsweise der Einsatz von IL-22 (Blazar et al., 2012; Zeiser et al., 2017). Trotz allem endet die Erkrankung für 5-30% aller Glucocorticoid-Therapie-refraktären GVHD Patienten tödlich (Martin et al., 2012). Die hohe Morbidität und Mortalität von allo-HSZT Empfängern betont die Notwendigkeit der weiteren Erforschung der Pathogenese der GVHD und Entwicklung neuer Therapeutika.

2.3 Pathogenese der Graft-versus-host disease

Die Pathogenese der GVHD basiert auf einem komplexen Zusammenspiel verschiedener Mechanismen. Im Zentrum der Pathogenese steht die Aktivierung der Donor-T-Zellen, die aus dem allogenen Transplantat stammen und sich entwickeln. Die Effektorfunktionen dieser allo-reaktiven Donor-T-Zellen bewirken schlussendlich den Gewebeschaden und die daraus resultierenden klinischen Symptome der GVHD. Arbeiten mit T-Zell depletierten allogenen Transplantaten konnten zeigen, dass eine Reduktion der transplantierten T-Zellen mit verminderter GVHD einhergeht (Horowitz et al., 1990). Diese Beobachtung lässt sich durch präklinische Krankheitsmodelle zur Forschung der GVHD erklären. In diversen murinen Tiermodellen kommt es nach der

Transplantation von T-Zell-deletiertem allogenen Knochenmark (und der damit verbundenen Transplantation von im Knochenmark enthaltenen hämatopoetischen Stammzellen) kaum zur Entwicklung einer GVHD. Zur Induktion einer GVHD wird deshalb in murinen GVHD Krankheitsmodellen allogenes Knochenmark gemeinsam mit zusätzlichen allogenen T-Zellen transplantiert (Reddy et al., 2008).

Die Pathogenese und damit die Schritte, die zu der T-Zell-Aktivierung, Expansion, Migration und Effektorfunktion beitragen, lassen sich vereinfacht als ein zirkuläres achtphasiges Modell beschreiben, das mit der Konditionierungstherapie der Empfänger beginnt **(Abbildung 1)** (Zeiser et al., 2016). Diese Konditionierungstherapie dient der Eradikation des Empfänger-Immunsystems und der hämatopoetischen Vorläuferzellen im Knochenmark und wird gleichzeitig zur Bekämpfung der Tumorzellen oder defekten Zellen des Empfängers genutzt (**siehe Abschnitt 2.1**). Die Konditionierungstherapie leitet gleichzeitig die erste Phase der Pathogenese der GVHD ein:

1. Im Zuge der Konditionierungstherapie durch hochdosierte Chemotherapie oder TBI werden die epithelialen Barrieren der Haut, Lunge und Gastrointestinaltrakt (GIT) des Empfängers zerstört. Einen besonders hohen Stellenwert hat hierbei die Zerstörung der Mukosa des GIT, die eine Barriere zu der luminal gelegenen mikrobiellen Besiedelung (vorwiegend Bakterien, Viren und Pilzen) des GIT schafft (Zeiser et al., 2016).

2. Im Zuge des lokalen Barriereschadens erfolgt die Translokation von Mikroorganismen und deren PAMPs (Pathogen-associated molecular pattern) in die darunter gelegenen Gewebeschichten. Zusätzlich kommt es durch die Konditionierungstherapie zur Freisetzung von DAMPs (Damage-associated molecular patterns) wie ATP oder Harnsäure aus zerstörten Körperzellen (Toubai et al., 2016; Zeiser et al., 2016).

3. DAMPs und PAMPs werden von Mustererkennungsrezeptoren (Pattern Recognition Receptors, PRRs) verschiedener lokaler Zellen erkannt und bewirken deren Aktivierung (Heidegger et al., 2014; Zeiser et al., 2016). Die Aktivierung von antigenpräsentierenden Zellen (APC) und angeborenen Effektorzellen wie z.B. neutrophilen Granulozyten bewirkt einen sich selbst weiter stimulierenden Zytokinsturm (u.a. IL-1b IL-6, TNFa) und die Verstärkung des lokalen Gewebeschadens und Zelltod z.B. durch freigesetzte reaktive Sauerstoffspezies (Zeiser et al., 2016).

4. Im Zuge der Zytokinfreisetzung und als Folge des proinflammatorischen Milieus erfolgt die Migration und Reifung von Dendritischen Zellen (DC) aus sekundären lymphatischen Organen in zentral gelegene lymphatische Organe. Auf diese Weise kommt es zu einem erhöhten Kontakt von APC und allogenen T-Zellen (Zeiser et al., 2016).

5. Die Interaktion von stark aktivierten APC und den durch den Zytokinsturm ebenfalls bereits voraktivierten allogenen T-Zellen bewirkt ein starkes T-Zell Priming und deren Aktivierung. (Zeiser et al., 2016). Die genauen Antigene, die zur T-Zell Aktivierung beitragen sind Bestandteil aktueller Forschung. Neben den spezifischen Gewebeantigenen (MHC-Komplexen) des Empfängers, spielen auch auf MHC-Komplexen präsentierte und zuvor prozessierte Antigene (incl. mikrobielle Antigene) eine entscheidende Rolle bei der T-Zell-Rezeptor Aktivierung der Spender T-Zellen (Koyama et al., 2016).

6. Im Zuge der T-Zell Aktivierung erfolgt deren Differenzierung und Expansion (Zeiser et al., 2016).

7. Im Anschluss an die Expansion erfolgt die Einwanderung der T-Zellen in die Zielorgane des stattgefundenen T-Zell-Primings und damit auch maßgeblich in den GIT (Beilhack et al., 2005; Zeiser et al., 2016).

8. Die einwandernden T-zellen bewirken in den Zielorganen einen akuten Gewebeschaden, der je nach Ausmaß der Erkrankung mit massivem Zelluntergang einhergehen kann. Der Organschaden der multiplen Zielorgane führt letztlich zu einer systemischen Entzündung mit oftmals letalen Folgen.

Schlussendlich resultiert ein *Circulus vitiosus*, da der Gewebeschaden wiederum zu Zelltod und neuem epitehlialen Barriereschaden und damit zu der erneuten Freisetzung von DAMPs und PAMPs führt (Zeiser et al., 2016).
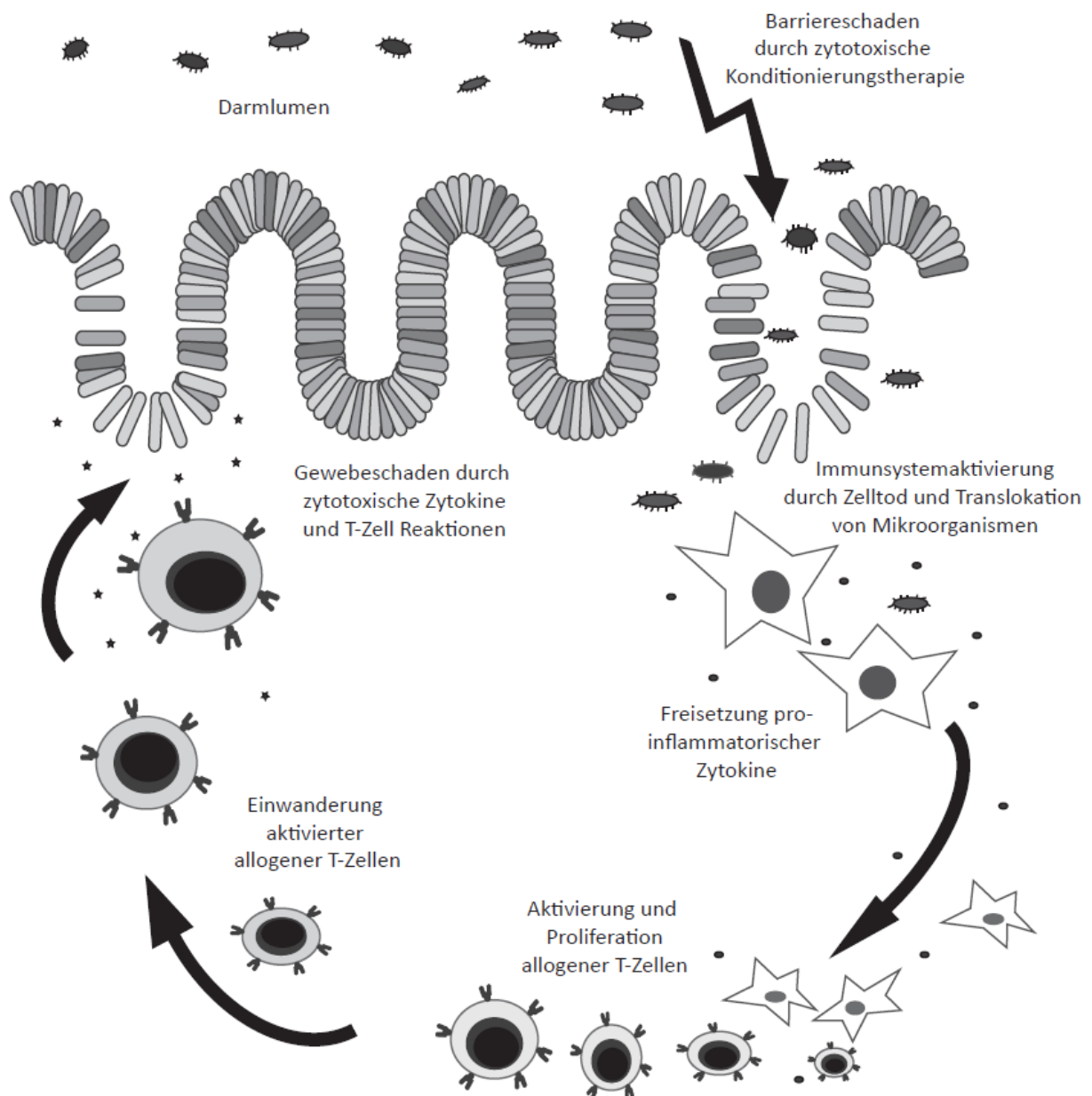

Abbildung 1: Pathogenese der GVHD initiiert durch zytotoxische Konditionierungstherapien

2.4 Die intestinale Barriere bei der Pathogenese der Graft-versus-host disease

Eine gestörte intestinale Homöostase mit beeinträchtigter Barrierefunktion gilt als Disposition für eine Vielzahl von Autoimmunerkrankungen oder Erkrankungen mit immunpathogener Komponente. Beispiele sind mikrobielle Infektionen, Morbus Crohn, Colitis Ulcerosa, Zöliakie, Diabates melitus, Metabolisches Syndrom, NAFLD (Nicht-alkoholische Fettleber) bis hin zum septischen Schock (Groschwitz et al., 2009; Sanchez de Medina et al., 2014; Yan et al., 2013). Zur epithelialen Barrierefunktion gehören in diesem Zusammenhang mindestens zwei wesentliche Funktionen: ein mechanisch intaktes Epithel wehrt das Eindringen von luminal gelegenen Organismen und Toxinen ab und verhindert im Gegenzug den Verlust von körpereigenen Stoffen, wie z.B. Flüssigkeit, Proteinen oder Elektrolyten. Außerdem gehören intestinale Epithelzellen zur Frontlinie der Immunantwort, da sie durch ihre Produktion von antimikrobiellen Peptiden (AMPs), wie z.B. Reg3γ, bei der physiologischen Keimbesiedlung des Darms eine entscheidende Rolle spielen (Peterson et al., 2014).

Bei der Pathogenese der GVHD spielen beide Komponenten eine maßgebliche Rolle. Durch die Konditionierungstherapie vor Transplantation kommt es zu zytotoxischem Schaden der Darmepithelzellen incl. deren Stammzellen und zu deren Zelltod. Die direkte Folge sind epitheliale Barrieredefekte, die eine Freilegung der physiologisch „sterilen" Lamina propria (LP) bewirken. Die in der LP gelegenen Immunzellen registrieren das Eindringen von Pathogenen oder deren PAMPs und lösen eine massive Entzündungskaskade aus (**siehe Abschnitt 2.3**). Am Ende der Entzündungskaskade steht die Einwanderung von zytotoxischen allo-reaktiven T-zellen, die das Darmepithel erneut angreifen und erneute Barrieredefekte bewirken (Heidegger et al., 2014; Zeiser et al., 2016). Zusätzlich zu dem Verlust der mechanisch intakten Gewebeschicht bewirkt die

Zerstörung des Darmepithels eine gestörte Expression von AMP. Dieser Vorgang fördert die weitere Invasion von Keimen. Zusätzlich wird die Zusammensetzung der intestinalen mikrobiellen Besiedelung und damit Wiederherstellung der intestinalen Immun- und Epithelhomöostase behindert (Weber et al., 2017). Eine gestörte intestinale Homöostase und ein in seiner Diversität kompromittiertes Mikrobiom trägt weiter zur Entwicklung und Aufrechterhaltung einer GVHD bei (Jenq et al., 2012; Shono et al., 2016).

2.5 Die zytosolischen Nukleinsäurerezeptoren RIG-I und cGAS

Zu den bedeutendsten Mustererkennungsrezeptoren für Nukleinsäureren gehören die membrangebundenen Toll-like Rezeptoren TLR3, TLR7, TLR8, TLR9, die zytosolischen RIG-I-like Rezeptoren (RLR) RIG-I und MDA5 sowie der zytosolische Rezeptor cGAS (Schlee et al., 2016).

Die Stimulation dieser Signalwege induziert jeweils sowohl die Expression von Typ-I Interferon (IFN) und IFN- stimulierten Genen (ISGs) als auch die Aktivierung von NFκB Transkriptionsfaktoren (Cai et al., 2014; Schlee et al., 2016). Die Kombination aus NFκB-Aktivierung und Typ-I IFN-Signaling spielt eine Schlüsselrolle bei der Initiierung der Immunabwehr gegen virale Infektionen durch das angeborene Immunsystem (Schlee et al., 2016). Zusätzlich tragen zytosolische Nukleinsäurerezeptoren auch zur Abwehr von intrazellulären bakteriellen Infektionen bei. Neue Erkenntnisse deuten darauf hin, dass sie auch bei der Erkennung und Kontrolle von genotoxischem Zellschaden involviert sind (Cai et al., 2014; Hu et al., 2016; Schlee et al., 2016).

In den letzten Jahren wurden die kürzlich neu entdeckten Rezeptoren RIG-I und cGAS intensiv studiert. Der RNA Rezeptor RIG-I und der DNA Rezeptor cGAS können neben viralen und bakteriellen Nukleinsäuremotiven auch durch künstliche Liganden stimuliert werden. Starke RIG-I Liganden zeichnen sich

hierbei durch eine doppelsträngige RNA Struktur mit einer Länge von ca. 18 - 300 Basenpaaren und ein am 5' Ende gelegenes Di- oder Triphosphat (2pRNA, 3pRNA) aus (Schlee et al., 2016; J. Wu et al., 2014). Liganden für den Rezeptor cGAS sind v.a. durch ihre doppelsträngige DNA Struktur und eine Länge von mehr als 25 (murine cGAS Liganden) bzw. 40 - 80 (humane cGAS Liganden) Basenpaaren charakterisiert (Schlee et al., 2016). Auch wenn es erst kürzlich gelungenen ist, RIG-I und cGAS genauer zu charakterisieren, konnte bereits mithilfe von präklinischen Modellen für v.a. Tumor- und Infektionserkrankungen mehrfach gezeigt werden, dass die gezielte Aktivierung von RIG-I und cGAS therapeutisch genutzt werden kann (Ireton et al., 2011; Ng et al., 2017; Y. Wu et al., 2017).

3. Wissenschaftliche Fragestellungen

3.1 Originalarbeit 1: Etablierung neuer Analysemethoden zur Messung von intestinalem Integritätsverlust bei akutem Gewebeschaden

Eine wichtige Funktion des Gastrointestinaltrakts ist es, eine Barriere zwischen dem sterilen Körperinneren und seinen luminalen Oberflächen zu schaffen. Bei akutem Gewebeschaden durch Traumata, Infektionen, Autoimmun-erkrankungen oder auch toxischen Nebenwirkungen von Therapien kann diese Darmintegrität Schaden nehmen. Dieser Verlust der intestinalen Integrität spielt eine entscheidende Rolle bei der Pathogenese vieler Erkrankungen, wie z.B. der GVHD nach allo-HSZT **(siehe Abschnitt 2.4).**

In der präklinischen Forschung besteht ein breites Spektrum an Methoden, um Gewebe- und Zellschäden qualitativ und quantitativ zu bestimmen. Neben morphologischen und damit v.a. histopathologischen Gewebeanalysen, kann die Aktivität und Viabilität von Zellen mithilfe verschiedener biochemischer und molekularbiologischer Techniken analysiert werden. Im Gegensatz zu diesen vielseitigen Analyseverfahren zur Charakterisierung von gewonnenen Geweben, Zellpräparaten oder einzelnen Zellen, ist das methodische Spektrum, das zur funktionellen *in vivo* Analyse ganzer Gewebe- und Organfunktionen angewendet werden kann, limitiert.

Zur Messung der intestinalen Integrität als Funktion der Darmschleimhaut ist der intestinale FITC-Dextran Permeabilitäts Assay der Goldstandard, der in vielen Krankheitsmodellen Anwendung findet (An et al., 2007; Fouts et al., 2012; Furuta et al., 2001; Hanash et al., 2012; Hartmann et al., 2013; Napolitano et al., 1996; Viaud et al., 2013). Bei diesem *in vivo* Assay wird FITC-Dextran, ein hochmolekulares, physiologisch nicht verdauliches und mit dem fluoreszierenden Farbstoff FITC (Fluorescein isothiocyanate) markiertes Polysaccharid, den Versuchstieren oral per Gavage zugeführt. Im Verlauf werden

Blutproben der Versuchstiere gewonnen und deren FITC-Dextran Gehalt bestimmt. Da FITC-Dextran bei intakter Darmepithelbarriere weder transloziert noch resorbiert wird, korreliert die im Blutkreislauf gemessene FITC-Dextran Konzentration invers mit der intestinalen Integrität.

Obwohl der intestinale FITC-Dextran-Permeabilitäs-Assay in einer Vielzahl von Krankheitsmodellen mit postuliertem intestinalem Gewebeschaden angewendet wird, sind grundlegende Charakterisierungen seiner messtechnischen Qualitäten unbekannt. Im Speziellen gibt es keine genauen Informationen zur Sensitivität, Spezifität und Versatilität des Assays. In der Zusammenschau der bisherigen Forschungsergebnisse konnte außerdem gezeigt werden, dass auch die zusätzlich bekannten funktionellen oder molekularbiologischen angewendeten Analysemethoden zur Bestimmung der intestinalen Integrität mit individuellen Limitationen behaftet sind (Bischoff et al., 2014; L. Wang et al., 2015). Aktuell sind deshalb zusätzliche qualitativ hochwertige und neue Methoden ausstehend, um zufriedenstellend valide Aussagen über die intestinale Epithelintegrität treffen zu können.

Kürzlich wurde im Rahmen von Forschungsarbeiten zur Rolle von neutrophilen Granulozyten in der GVHD gezeigt, dass es nach Chemotherapie, TBI oder GVHD induziertem akuten Gewebeschaden zu einer massiven Infiltration von neutrophilen Granulozyten in die intestinale Lamina Propria kommt (Schwab et al., 2014). In diesem Zusammenhang stellt sich nun die für die vorliegende Arbeit leitende Frage, ob die gezielte und standardisierte Quantifizierung dieser Granulozyten-Infiltration als quantifizierbarer Marker für intestinalen Integritätsverlust genutzt werden kann, welcher Mechanismus dieser Infiltration zugrunde liegt und mit welchen Qualitäten und Limitationen dieser Assay behaftet wäre. Im Speziellen stellen sich folgende Fragen:

(I)   Kann die Analyse der Infiltration von neutrophilen Granulozyten als neuer Marker für intestinalen Integritätsverlust im Rahmen eines akuten Gewebeschadens genutzt werden?

(II)   Welche messtechnischen Qualitäten (u.a. Sensitivität, Spezifität) und wissenschaftlichen Limitationen bringt die Bestimmung der intestinalen Granulozyten Infiltration bei der Messung eines intestinalen Integritätsverlusts mit sich?

(III)   Welche Vor- und Nachteile lassen sich mithilfe des neutrophilen Granulozyten-Infiltrations-Assays im Vergleich zu dem als Goldstandart bekannten intestinalen FITC-Dextran-Permeabilitäts-Assay und anderen Methoden zur Messung der intestinalen Epithelintegrität erzielen?

(IV)   Welcher Mechanismus liegt der intestinalen Infiltration der neutrophilen Granulozyten bei intestinalem Integritätsverlust zugrunde?

(V)   Lässt sich der Granulozyten-Infiltrations-Assay zur Erforschung unbekannter Signalwege in klinisch relevanten Krankheitsmodellen mit postuliertem intestinalem Integritätsverlust anwenden?

3.2. Originalarbeit 2: Charakterisierung der zytosolischen Nukleinsäure-rezeptoren RIG-I und cGAS bei akutem Gewebeschaden und der Graft-versus-host disease

Die zytosolischen Nukleinsäurerezeptoren RIG-I und cGAS spielen nicht nur bei der Erkennung von Infektionen durch das angeborene Immunsystem eine wichtige Rolle (**siehe Abschnitt 2.5**), sondern haben nach jüngsten Erkenntnissen auch entscheidende Funktionen bei der Pathogenese von intestinalen Autoimmun- und Tumorerkrankungen (X. D. Li et al., 2011; Y. Wang et al., 2007;

Q. Zhu et al., 2014). Im Speziellen wurde postuliert, dass RIG-I Aktivierung durch bakterielle RNA im Darmepithel zur intestinalen Homöostase beiträgt und die Entwicklung einer experimentellen Colitis kontrollieren kann (X. D. Li et al., 2011). Der Aktivierung von intrazellulären DNA Rezeptoren wurde eine entscheidende Rolle bei der Kontrolle intestinaler epithelialer Proliferation und experimenteller Karzinogenese sowie Regulation von akutem Gewebeschaden zugeschrieben (Ahn et al., 2015; Hu et al., 2016).

Im Gegensatz zu diesen thematisch verwandten Beobachtungen liegen aktuell keine Erkenntnisse über eine Rolle der zytosolischen Nukleinsäurerezeptoren RIG-I und cGAS bei der Reaktion auf Hochdosisbestrahlung, Chemotherapie und Entwicklung einer akuten GVHD vor. Vor diesem Hintergrund stellen sich für die vorliegende Arbeit folgende Fragen:

(I) Spielen die Rezeptoren RIG-I und cGAS eine Rolle bei der Regulation von akutem Gewebeschaden (durch alleinige TBI oder Chemotherapie) und der Entwicklung einer akuten Graft-versus-host disease?

(II) Durch welchen Mechanismus beeinflussen die Rezeptoren RIG-I und cGAS akuten Gewebeschaden und die Pathogenese der akuten Graft-versus-host disease?

a. Welche Zelltypen sind für die RIG-I oder cGAS abhängige Regulation der Pathogenese der akuten GVHD verantwortlich?

b. Welche Phasen der Pathogenese der akuten Graft-versus-host disease werden durch die Rezeptoren RIG-I und cGAS beeinflusst?

c. Spielen die Rezeptoren RIG-I und cGAS eine Rolle bei der Regulation der intestinalen Integrität und Darmpermeabilität, die im Zentrum der Pathogenese der akuten GVHD steht?

(III) Lässt sich durch die Aktivierung von RIG-I oder cGAS ein therapeutischer Effekt zur Milderung eines akuten Gewebeschadens und der akuten Graft-versus-host disease erzielen?

(IV) Durch welchen Mechanismus beeinflusst eine therapeutische Aktivierung von RIG-I oder cGAS die Pathogenese von akutem Gewebeschaden und akuter Graft-versus-host disease?

    a. Zu welchem Zeitpunkt der allo-HSCT und GVHD Entwicklung ist eine Therapie mit RIG-I oder cGAS Liganden möglich und erfolgreich?

    b. Welche Signalwege und Botenstoffe werden durch die RIG-I oder cGAS Aktivierung freigesetzt und sind für den Effekt der Therapie verantwortlich?

    c. Welche Zielzellen reagieren auf die durch RIG-I oder cGAS Aktivierung freigesetzten Botenstoffe?

    d. Welche Phase der Pathogenese einer akuten GVHD wird durch die gezielte Aktivierung von RIG-I oder cGAS beeinflusst?

    e. Spielen die gezielte Aktivierung von RIG-I und cGAS eine Rolle bei der Regulation der intestinalen Integrität und Darmpermeabilität, die im Zentrum der Pathogenese der akuten GVHD steht?

4. Methodik und Lösungsansätze

4.1 Originalarbeit 1: Charakterisierung des intestinalen Granulozyten Infiltrations-Assays zur Messung von intestinalem Integritätsverlust bei akutem Gewebeschaden

Um zu prüfen, ob die intestinale Infiltration von neutrophilen Granulozyten als wissenschaftlicher Assay zur Evaluation der intestinalen Integrität bei akutem Gewebeschaden genutzt werden kann, wurde dieser neue Assay mit dem Goldstandard, dem intestinalen FITC-Dextran-Permeabilitäts-Assay, verglichen. Bei diesem Vergleich wurden neben den Analysen der Sensitivität und Spezifität der beiden Assays auch weitere Qualitäten wie Versatilität und Breite der Detektionsbereiche berücksichtigt. Folgende Lösungsansätze wurden hierbei im Speziellen untersucht bzw. angewendet:

(I)   Da sich ein durch TBI oder Chemotherapie ausgelöster akuter Gewebeschaden zuverlässig induzieren und objektiv titrieren lässt, wurden diese beiden Modelle für die weiteren Analysen ausgewählt.

(II)   Zur Untersuchung der messtheoretischen Sensitivität und Spezifität der beiden Assays wurde die intestinale neutrophile Granulozyten-Infiltration und FITC-Dextran-Translokation in genoxotisch behandelten und unbehandelten Versuchstieren untersucht. Da die Größe der Versuchsgruppen und damit resultierende Anzahl an Messwerten aus tierversuchsmethodischen Gründen limitiert war, wurde im Anschluss die den Messwerten der Versuchsgruppen zugrundeliegenden Normalverteilungen modelliert. Mithilfe der errechneten Normalverteilungen wurde danach abgeschätzt, welche Werte sich für die Sensitivität und Spezifität der beiden Assays ergeben, um zwischen behandelten und unbehandelten Tieren zu unterscheiden.

(III) Zur Analyse der Detektionsbereiche der beiden untersuchten Assays wurden verschiedene Dosen an TBI oder Chemotherapie appliziert und die neutrophile Granulozyten-Infiltration bzw. FITC-Dextran-Translokation analysiert.

Zur Interpretation des neutrophilen Granulozyten-Infiltrations-Assays wurde außerdem die Frage beantwortet, welcher grundlegende Mechanismus der Infiltration zugrunde liegt. In diesem Zusammenhang legen neue Erkenntnisse nahe, dass die Translokation von Bakterien nach intestinalem Integritätsverlust die Einwanderung von neutrophilen Granulozyten bewirken könnte **(siehe Abschnitt 3.1)**. Diese Hypothese wurde für TBI- und Chemotherapie-induzierten intestinalen Integritätsverlust untersucht.

(IV) Um zu überprüfen, ob das bakterielle Mikrobiom bei der Infiltration von neutrophilen Granulozyten eine maßgebliche mechanistische Rolle spielt, wurde die durch akuten Gewebeschaden induzierte Infiltration von neutrophilen Granulozyten in Versuchstiere, die mit einem darmdekontaminierenden Antibiotikacocktail vorbehandelt wurden, mit nicht vorbehandelten Versuchstieren verglichen.

Zur Evaluation des wissenschaftlichen Nutzens des neutrophilen Granulozyten-Infiltrations-Assays in klinisch relevanten Krankheitsmodellen wurde der Assay im Rahmen der Analyse der Rolle von RIG-I und cGAS bei akutem intestinalen Gewebeschaden angewendet **(siehe Originalarbeit 2)**.

4.2. Originalarbeit 2: Untersuchung der Rolle der zytosolischen
Nukleinsäurerezeptoren RIG-I und cGAS bei der Graft-versus-host disease

Zur Analyse der Rolle der Signalwegen RIG-I und STING bei akutem Gewebeschaden nach TBI, Chemotherapie und der Pathogenese der akuten GVHD wurden folgende Lösungsansätze und Methoden untersucht bzw. angewendet:

(I) Zur Untersuchung der Rolle der zytosolischen Nukleinsäurerezeptoren RIG-I und cGAS bei akutem Gewebeschaden und der Entwicklung einer akuten GVHD, wurden transgene Mäuse verwendet, die Defekte in den Signalwegen von RIG-I oder cGAS tragen.

    a. Für den RNA-Rezeptor RIG-I stehen transgene knock-out (KO) Mäuse zu Verfügung, in denen RIG-I nicht exprimiert wird (Y. Wang et al., 2007). Da RIG-I KO (RIG-I$^{-/-}$) Tiere autoimmune Krankheitszeichen entwickeln, wurden für einen Großteil der mechanistischen *in vivo* und *in vitro* Analysen MAVS KO (MAVS$^{-/-}$) Tiere verwendet, für die keine spontanen pathologischen Phänotypen bekannt sind (Meylan et al., 2005; Y. Wang et al., 2007). MAVS$^{-/-}$ Tieren fehlt in allen Körperzellen das mitochondrionale Adapterprotein MAVS, an welches RIG-I nach seiner Aktivierung bindet. Nach Bildung des RIG-I/MAVS Komplexes fungiert MAVS als Signalplattform und unumgängliche Grundlage für die Induktion von Typ-I IFN, IIGs und NFκB-Aktivierung.

    b. Zur Analyse des cGAS Signalwegs wurden uns zur Verfügung stehende STING KO Tiere verwendet (Sauer et al., 2011). Analog zu MAVS im Zusammenspiel mit RIG-I fungiert STING als ein essentielles Adapterprotein für cGAS und dessen Funktion nach Aktivierung (Schlee et al., 2016). Zur Analyse eines möglichen therapeutischen Nutzens der gezielten cGAS/STING Aktivierung wurde komplexierte interferon-stimulierende DNA (ISD) angewendet, für die eine Aktivierung des STING Signalwegs bekannt ist (Ishikawa et al., 2009).

(II) Zur Identifikation der Zellen, in denen der RIG-I/MAVS oder cGAS/STING Signalweg bei den untersuchten Krankheitsmodellen eine Rolle spielt,

wurden murine Knochenmarkschimären hergestellt: Hierbei wurde transgenen und regulären (Wild-typ) Empfängertieren nach einer Konditionierungstherapie mit TBI syngenes Knochenmark transplantiert, das entweder aus transgenen oder Wild-Typ Empfängertieren gewonnen wurde. Zwei Monate nach dieser syngenen HSZT konnten diese generierten Chimären, deren hämatopoetische Zellen jetzt aus dem Spenderknochenmark stammten, für weitere Analysen verwendet werden.

(III) Zur Untersuchung eines möglichen therapeutischen Effekts der RIG-I Aktivierung im Rahmen von akutem Gewebeschaden nach TBI, Chemotherapie und der akuten GVHD wurde 3pRNA verwendet **(siehe Abschnitt 2.5).** 3pRNA kann mit einem lipophilen Carrier komplexiert *in vivo* angewendet werden und führt zu einer starken RIG-I Aktivierung (Poeck et al., 2008).

(IV) Zur Untersuchung eines möglichen therapeutischen Effekts der gezielten cGAS/STING Aktivierung wurde komplexierte interferon-stimulierende DNA (ISD) angewendet, für die eine Aktivierung des STING Signalwegs bekannt ist (Ishikawa et al., 2009).

(V) Zur Analyse des Zeitpunktes, an dem die RIG-I oder cGAS Aktivierung bzw. deren Botenstoffe einen therapeutischen Effekt induzieren, wurden die Liganden zu unterschiedlichen Zeitpunkten (u.a. am Tag vor allo-HSZT, am Tag der allo-HSZT und am Folgetag der allo-HSZT) appliziert und die Effekte auf die Pathogenese der GVHD studiert.

(VI) Zur Analyse der Botenstoffe und Signalwege, die durch eine therapeutische RIG-I oder cGAS Aktivierung beeinflusst werden, wurden Typ-I Interferon neutralisierende Antikörper eingesetzt. Zur genaueren Analyse der Zellen, auf die Typ-I Interferon wirkt, wurden

konditionale KO Mäuse verwendet, in denen der Typ-I Interferon Rezeptor nur auf bestimmten Körperzellen nicht exprimiert wird.

(VII) Zur Analyse der Rolle der Signalwege RIG-I/MAVS und cGAS/STING bei der Regulation der intestinalen Darmintegrität und Permeabilität im Rahmen von akutem Gewebeschaden, wurden die Versuchstiere nach TBI, Chemotherapie oder während akuter GVHD mit dem intestinalen FITC-Dextran-Translokation-Assay sowie dem intestinalen Granulozyten-Infiltrations-Assay **(siehe Originalarbeit 1**) analysiert. Analoge Analysen erfolgten nach Applikation der Liganden 3pRNA und ISD zur Untersuchung der intestinalen Integrität nach Aktivierung von RIG-I oder cGAS.

(VIII) Zur Untersuchung der Rolle der RIG-I/MAVS und cGAS/STING Signalwege auf die intestinale Epithelregeneration wurden Stammzellkulturen (sogenannte intestinale Organoid Kulturen) mit intestinalen Epithelzellen aus transgenen Mäusen mit defekten Signalwegen generiert und analysiert. Zur Analyse der Effekte der RIG-I oder cGAS Aktivierung auf die intestinale Organoidformation wurde das Organoidwachstum von Kulturen studiert, die mit RIG-I oder cGAS Liganden stimuliert worden waren. Außerdem wurde die Entwicklung von Organoiden analysiert, die aus Mäusen gewonnen worden waren, die zuvor mit RIG-I- oder cGAS-Liganden behandelten worden waren.

5. Zusammenfassung der Ergebnisse der Originalarbeiten

5.1. Fischer et al „Assessment of mucosal integrity by quantifying neutrophil granulocyte influx in murine models of acute intestinal injury"

In dieser Arbeit zeigen wir, dass sich das Ausmaß eines durch TBI oder Chemotherapie ausgelösten intestinalen epithelialen Integritätsverlusts durch die quantitative Bestimmung der Invasion von neutrophilen Granulozyten in die intestinale Lamina Propria scharf abbilden lässt.

Gängige Verfahren zur Bestimmung des Verlusts der intestinalen epithelialen Integrität, wie der intestinale FITC-Dextran-Permeabilitäts-Assay, sind in der Lage, stark ausgeprägten intestinalen Gewebeschaden, wie z.B. während der akuten GVHD nach allogener hämatopoetischer Stammzelltransplantation, nachzuweisen. Hat der Schaden, der untersucht werden soll, jedoch ein geringeres Ausmaß, wie z.B. nach der alleinigen Applikation einer hohen Dosis TBI oder Chemotherapie, stößt der FITC-Dextran-Permeabilitäts-Assay an seine Nachweisgrenze und verliert bei der Differenzierung von behandelten und unbehandelten Tieren an Sensitivität und Spezifität.

Die Messung der neutrophilen Granulozyten-Invasion ermöglicht es hingegen, intestinalen akuten Gewebeschaden nach Applikation von hohen TBI und Chemotherapie Dosen nachzuweisen und zwischen behandelten und unbehandelten Mäusen mit sehr hoher Genauigkeit zu differenzieren. Zusätzlich ist die quantitative Erfassung der neutrophilen Granulozyten Invasion auch in der Lage, intestinalen Gewebeschaden nach Behandlung mit einer reduzierten TBI oder Chemotherapie Dosis sensitiv zu erfassen.

Mechanistisch können wir belegen, dass die Reduktion der Darmbakterienlast der Versuchstiere die Invasion von neutrophilen Granulozyten nach TBI oder Chemotherapie induziertem intestinalen Gewebeschaden reduziert und damit für die Invasion der neutrophilen Granulozyten verantwortlich ist.

In Summe lassen sich diese Beobachtungen zu folgendem Modell zusammenführen: TBI und Chemotherapie bewirken einen dosisabhängigen Darmschaden, der einen Verlust der Integrität des Darmepithels bewirkt. Dieser Integritätsverlust wiederum hat eine Translokation von Darmbakterien in die unter dem Epithel gelegene Lamina Propria zur Folge. Im Zuge dieser Translokation erfolgt eine Einwanderung von neutrophilen Granulozyten in die Lamina Propria. Die Bestimmung des Ausmaßes dieser neutrophilen Granulozyten-Invasion stellt damit eine neue Vorgehensweise zur Messung der intestinalen Epithelintegrität dar.

Diese neutrophile Granulozyten-Infiltrations-Analyse kann ergänzend zu bereits verwendeten Methoden, wie z.B. dem intestinalen FITC-Dextran-Permeabilitäts-Assay, der Bestimmung von Tight-Junction-Protein Expressionen, fäkalen Albumin-Konzentrationen oder Calprotectin-Konzentrationen im Blut verwendet werden, um ein vollständiges Bild der intestinalen Darmintegrität in Modellen von akutem intestinalem Gewebeschaden zu erhalten.

Julius Clemens Fischer, der Erstautor der Veröffentlichung „Assessment of mucosal integrity by quantifying neutrophil granulocyte influx in murine models of acute intestinal injury" entwickelte die Grundidee für die Studie, konzipierte die durchgeführten Versuche, führte die Experimente durch, analysierte die Ergebnisse und verfasste das Manuskript.

5.2. Fischer et al. „RIG-I/MAVS and STING signaling promote gut integrity during irradiation- and immune-mediated tissue injury"

In dieser Arbeit zeigen wir, dass sowohl die endogene als auch die zielgerichtete therapeutische Aktivierung von RIG-I/MAVS und cGAS/STING akuten

Darmschaden nach Bestrahlung, Chemotherapie und im Zuge der akuten GVHD reduziert.

In MAVS-defizienten Mäusen führt akuter Gewebeschaden nach TBI, Chemotherapie und im Verlauf der akuten GVHD nach allogener hämatopoetischer Stammzelltransplantation zu erhöhtem intestinalem Gewebeschaden und einem Funktionsverlust der intestinalen epithelialen Barriere. Dieses Defizit zeigt sich durch eine reduzierte epitheliale Integrität, die mit einer erhöhten Infiltration von neutrophilen Granulozyten, erhöhter FITC-Dextran-Translokation sowie einer verminderten Expression von AMP durch das Darmepithel verbunden ist. Schlussendlich bewirkt dieser epitheliale Funktionsverlust ein reduziertes Überleben im Verlauf der akuten GVHD nach allogener HSZT. Mechanistisch lässt sich diese Beobachtung auf den defekten MAVS-Signalweg im nicht-hämatopoetischen System zurückführen, der zu einer reduzierten intestinalen Epithelregeneration des intestinalen Stammzellkompartments führt.

Umgekehrt führt die zielgerichtete therapeutische Aktivierung des RIG-I/MAVS Signalwegs durch 3pRNA vor der Applikation von TBI, Chemotherapie oder einer allogenen HSZT zu gegensätzlichen Effekten. Die Target-Therapie von RIG-I bewirkt eine erhöhte intestinale epitheliale Barrierefunktion (reduzierte Permeabilität, verminderte Infiltration von neutrophilen Granulozyten und erhöhte Produktion von AMPs) und ein erhöhtes Überleben im Verlauf der akuten GVHD nach allogener HSZT. Mechanistisch sind diese Beobachtungen auf eine durch 3pRNA induzierte Typ-I IFN Antwort zurückzuführen, die bei genauen Timing der Wirkung eine erhöhte Epithelregeneration des intestinalen epithelialen Stammzellkompartments bewirkt. Die therapeutische Aktivierung von RIG-I führt dabei zu einer verminderten T-Zell Aktivierung, ohne den durch allogene T-Zellen vermittelten GVL-Effekt zu kompromittieren.

Analog zu RIG-I und MAVS-defizienten Mäusen führt ein defekter STING Signalweg ebenfalls zu vermindertem Überleben nach allo-HSZT und verstärkter Entwicklung einer akuten GVHD. Analog zu der therapeutischen Applikation von 3pRNA führt auch der zielgerichtete Einsatz von ISD zu therapeutischen Effekten, die ebenfalls eine erhöhte Epithelfunktion, Regeneration des intestinalen Stammzellkompartments und Überleben nach allo-HSZT, bewirken.

Julius Clemens Fischer, der Erstautor der Veröffentlichung „RIG-I/MAVS and STING signaling promote gut integrity during irradiation- and immune-mediated tissue injury" entwickelte Ideen für die Studie, konzipierte die durchgeführten Versuche, führte einen Großteil der Experimente durch oder analysierte deren Ergebnisse und verfasste das Manuskript.

6. Bezug zur bestehenden Literatur und Schlussfolgerungen

In der derzeitigen präklinischen Forschung ist es von entscheidender Bedeutung, ein verbessertes Verständnis über die intestinale Epithelfunktion, Epithelregeneration und Immunhomöostase des GIT zu erlangen (Peterson et al., 2014). Um den aktuellen Fragestellungen zur Veränderung der Epithelfunktion in klinisch relevanten Krankheitsmodellen gerecht zu werden, sind zusätzliche und an die neuen Fragestellungen angepasste Methoden essentiell (Bischoff et al., 2014). Unsere Etablierung und Charakterisierung des intestinalen neutrophilen Granulozyten-Infiltrations-Assays stellt eine entscheidende Ergänzung zu den derzeitig verbreiteten Methoden zur Analyse der intestinalen Epithelfunktion und intestinalen Integrität dar. Die intestinale Granulozyten-Infiltration korreliert dosisabhängig mit dem applizierten Schaden durch Bestrahlung oder Chemotherapie und bringt eine höhere Sensitivität als der derzeitige Goldstandard, der intestinale FITC-Dextran-Permeabilität-Assay, mit sich. Im Rahmen unserer Studie zur Rolle der zytosolischen Nukleinsäure-Rezeptoren und Signalwege RIG-I/MAVS und cGAS/STING bei akutem Gewebeschaden und der akuten GVHD nach allo-HSZT haben wir diese Qualitäten erstmals direkt nutzen können. Wir haben gezeigt, dass ein defekter RIG-I/MAVS Signalweg bei akutem intestinalen Gewebeschaden zu einer verstärkten intestinalen Infiltration von neutrophilen Granulozyten führt. Diese Beobachtung korrelierte mit weiteren Charakteristika einer verminderten intestinalen Integrität, wie etwa der erhöhten FITC-Dextran Permeabilität in MAVS$^{-/-}$ Mäusen während einer akuten GVHD. Wir konnten hierbei mechanistisch aufdecken, dass die RIG-I/MAVS oder cGAS/STING Signalwege die intestinale Epithelregeneration beeinflussen können. Bezüglich der Steuerung der intestinalen Epithelfunktion und Regeneration konnte kürzlich gezeigt werden, dass der IL-22 Signalweg einen Schlüsselregulator darstellt. Mäuse mit

defektem IL-22 Signalweg weisen im Rahmen akuter intestinaler Gewebeschädigung einen erhöhten intestinalen Integritätsverlust auf (Hanash et al., 2012). Folgearbeiten konnten zeigen, dass IL-22 die intestinale Epithelregeneration über das intestinale Stammzellkompartiment steuert (Lindemans et al., 2015). Stimulationen des intestinalen Stammzellkompartiments im Allgemeinen und des IL-22 Signalwegs im Speziellen stellen damit hochaktuelle und vielversprechende neue molekulare Ziele für die therapeutische Modulation akuter intestinaler Gewebeschädigungen dar (Lamarthee et al., 2016). Unsere Arbeiten offenbaren, dass die RIG-I/MAVS und cGAS/STING- Signalwege die intestinale Epithelregeneration ebenfalls beeinflussen können und dabei ähnliche Charakteristika wie die durch IL-22 vermittelte Effekte aufweisen. Ähnlich wie Tiere mit defektem IL-22 Signalweg zeigen RIG-I$^{-/-}$, MAVS$^{-/-}$ oder Tiere mit defektem STING Signalweg vermindertes Überleben im Rahmen der akuten GVHD. Umgekehrt lässt sich durch die Applikation von RIG-I oder cGAS Liganden ein durch Typ-I IFN vermittelter therapeutischer Effekt erzielen, der analog zu den Effekten des IL-22 Signalwegs eine erhöhte intestinale Epithelregeneration und intestinale Integrität bewirkt.

Auch wenn weitere Arbeiten ebenfalls eine entscheidende Rolle des Typ-I IFN Signalwegs im Rahmen von akuter intestinaler Schädigung und Epithelregeneration vermuten lassen (Robb et al., 2011; Sun et al., 2015; Tschurtschenthaler et al., 2014), konnten frühe klinische Studien des Typ-I IFN Einsatzes im Rahmen der allo-HSZT keine positiven Resultate erbringen, sondern zeigten vielmehr relevante Risiken auf (Hehlmann et al., 1999; Kolb et al., 1990; Morton et al., 1998; Porter et al., 1994). Alle diese klinischen Studien haben jedoch gemeinsam, dass Typ-I IFN über lange Zeiträume und oftmals bereits über mehrere Wochen oder Monate vor Transplantation verabreicht wurde. Im

Gegensatz dazu konnten wir in unserer präklinischen Studie zeigen, dass die 3pRNA oder ISD Gabe nur direkt vor Transplantation der Entwicklung einer akuten GVHD vorbeugen kann. Diese „gezielte" oder „targeted"-Therapie bewirkt eine auf wenige Stunden begrenzte Typ-I IFN Induktion. Wir konnten zeigen, dass nur ein enges Zeitfenster von wenigen Stunden vor Transplantation bis zum Tag der Transplantation existiert, in dem die Typ-I IFN Induktion therapeutische Effekte erzielen kann. Spätere „targeted"-Therapie führt zu gegensätzlichen Effekten und bewirkt reduzierte Epithelfunktion und reduziertes Überleben nach allo-HSZT. Aus diesen Daten lassen sich klare Konzepte für neue klinische Studien ableiten, die den gezielten Einsatz von humanen RIG-I- oder cGAS-Liganden sowie von rekombinanten Typ-I IFN direkt vor allo-HSZT untersuchen.

Um das Risiko der Entwicklung einer GVHD nach allo-HSZT oder die Entwicklung von intestinalen Nebenwirkungen nach Strahlentherapie und Chemotherapie besser abschätzen zu können, sind außerdem klinische Studien ausstehend, die Polymorphismen der RIG-I/MAVS, cGAS/STING und Typ-I IFN Signalwege im Menschen untersuchen und diese mit dem Auftreten intestinaler Krankheitsbilder, wie dem der akuten GVHD nach allo-HSZT, korrelieren.

6. Abkürzungsverzeichnis

2pRNA	Diphosphat-RNA
3pRNA	Triphosphat-RNA
aGVHD	Akute GVHD
allo-HSZT	allogenen-HSZT
AMP	Antimikrobielles Peptid
APC	Antigenpräsentierende Zelle
cGAS	Cyclic GMP-AMP synthase
DAMP	Damage-associated molecular pattern
DC	Dendritische Zelle
EAE	Experimentelle autoimmune Enzephalomyelitis
FITC	Fluorescein isothiocyanate
GIT	Gastrointestinaltrakt
GVHD	Graft-versus-host disease
GVL	Graft-versus-Leukemia
GVT	Graft-versus-Tumor
HSZT	Hämatopoetische Stammzelltransplantation
IFN	Interferon
ISD	Interferon stimulierende DNA
ISGs	IFN- stimulierte Gene
KO	Knock-out
LP	Lamina propria
MAVS	Mitochondrial antiviral-signaling protein
MDA5	Melanoma Differentiation-Associated protein 5
mTOR	Mammalian target of rapamycin
NAFLD	Nicht-alkoholische Fettleber
NFκB	Nuclear factor 'kappa-light-chain-enhancer' of activated B-cells
PAMP	Pathogen-associated molecular pattern
PRR	Mustererkennungsrezeptor (Pattern Recognition Receptor)
Reg3γ	Regenerating islet-derived protein 3 gamma
RIG-I	Retinoic acid inducible gene I
RLR	RIG-I like Rezeptor
TBI	Ganzkörperbestrahlung (total body irradiation)
TLR	Toll-like Rezeptor

7. Literaturverzeichnis

Ahn, J., Konno, H., & Barber, G. N. (2015). Diverse roles of STING-dependent signaling on the development of cancer. *Oncogene, 34*(41), 5302-5308. doi:10.1038/onc.2014.457

An, G., Wei, B., Xia, B., McDaniel, J. M., Ju, T., Cummings, R. D., Braun, J., & Xia, L. (2007). Increased susceptibility to colitis and colorectal tumors in mice lacking core 3-derived O-glycans. *J Exp Med, 204*(6), 1417-1429. doi:10.1084/jem.20061929

Beilhack, A., Schulz, S., Baker, J., Beilhack, G. F., Wieland, C. B., Herman, E. I., Baker, E. M., Cao, Y. A., Contag, C. H., & Negrin, R. S. (2005). In vivo analyses of early events in acute graft-versus-host disease reveal sequential infiltration of T-cell subsets. *Blood, 106*(3), 1113-1122. doi:10.1182/blood-2005-02-0509

Bischoff, S. C., Barbara, G., Buurman, W., Ockhuizen, T., Schulzke, J. D., Serino, M., Tilg, H., Watson, A., & Wells, J. M. (2014). Intestinal permeability--a new target for disease prevention and therapy. *BMC Gastroenterol, 14*, 189. doi:10.1186/s12876-014-0189-7

Blazar, B. R., Murphy, W. J., & Abedi, M. (2012). Advances in graft-versus-host disease biology and therapy. *Nat Rev Immunol, 12*(6), 443-458. doi:10.1038/nri3212

Brodsky, R. A. (2009). How I treat paroxysmal nocturnal hemoglobinuria. *Blood, 113*(26), 6522-6527. doi:10.1182/blood-2009-03-195966

Cai, X., Chiu, Y. H., & Chen, Z. J. (2014). The cGAS-cGAMP-STING pathway of cytosolic DNA sensing and signaling. *Mol Cell, 54*(2), 289-296. doi:10.1016/j.molcel.2014.03.040

Cooke, K. R., Luznik, L., Sarantopoulos, S., Hakim, F. T., Jagasia, M., Fowler, D. H., van den Brink, M. R. M., Hansen, J. A., Parkman, R., Miklos, D. B., Martin, P. J., Paczesny, S., Vogelsang, G., Pavletic, S., Ritz, J., Schultz, K. R., & Blazar, B. R. (2017). The Biology of Chronic Graft-versus-Host Disease: A Task Force Report from the National Institutes of Health Consensus Development Project on Criteria for Clinical Trials in Chronic Graft-versus-Host Disease. *Biol Blood Marrow Transplant, 23*(2), 211-234. doi:10.1016/j.bbmt.2016.09.023

Ferrara, J. L. M., Levine, J. E., Reddy, P., & Holler, E. (2009). Graft-versus-host disease. *The Lancet, 373*(9674), 1550-1561. doi:10.1016/s0140-6736(09)60237-3

Fouts, D. E., Torralba, M., Nelson, K. E., Brenner, D. A., & Schnabl, B. (2012). Bacterial translocation and changes in the intestinal microbiome in mouse models of liver disease. *J Hepatol, 56*(6), 1283-1292. doi:10.1016/j.jhep.2012.01.019

Furuta, G. T., Turner, J. R., Taylor, C. T., Hershberg, R. M., Comerford, K., Narravula, S., Podolsky, D. K., & Colgan, S. P. (2001). Hypoxia-inducible factor 1-dependent induction of intestinal trefoil factor protects barrier function during hypoxia. *J Exp Med, 193*(9), 1027-1034.

Glucksberg, H., Storb, R., Fefer, A., Buckner, C. D., Neiman, P. E., Clift, R. A., Lerner, K. G., & Thomas, E. D. (1974). Clinical manifestations of graft-versus-host disease in human recipients of marrow from HL-A-matched sibling donors. *Transplantation, 18*(4), 295-304.

Groschwitz, K. R., & Hogan, S. P. (2009). Intestinal barrier function: molecular regulation and disease pathogenesis. *J Allergy Clin Immunol, 124*(1), 3-20; quiz 21-22. doi:10.1016/j.jaci.2009.05.038

Hanash, A. M., Dudakov, J. A., Hua, G., O'Connor, M. H., Young, L. F., Singer, N. V., West, M. L., Jenq, R. R., Holland, A. M., Kappel, L. W., Ghosh, A., Tsai, J. J., Rao, U. K., Yim, N. L., Smith, O. M., Velardi, E., Hawryluk, E. B., Murphy, G. F., Liu, C., Fouser, L. A., Kolesnick, R., Blazar, B. R., & van den Brink, M. R. (2012). Interleukin-22 protects intestinal stem cells from immune-mediated tissue damage and regulates sensitivity to graft versus host disease. *Immunity, 37*(2), 339-350. doi:10.1016/j.immuni.2012.05.028

Hartmann, P., Chen, P., Wang, H. J., Wang, L., McCole, D. F., Brandl, K., Starkel, P., Belzer, C., Hellerbrand, C., Tsukamoto, H., Ho, S. B., & Schnabl, B. (2013). Deficiency of intestinal mucin-2 ameliorates experimental alcoholic liver disease in mice. *Hepatology, 58*(1), 108-119. doi:10.1002/hep.26321

Hehlmann, R., Hochhaus, A., Kolb, H. J., Hasford, J., Gratwohl, A., Heimpel, H., Siegert, W., Finke, J., Ehninger, G., Holler, E., Berger, U., Pfirrmann, M., Muth, A., Zander, A., Fauser, A. A., Heyll, A., Nerl, C., Hossfeld, D. K., Loffler, H., Pralle, H., Queisser, W., & Tobler, A. (1999). Interferon-alpha before allogeneic bone marrow transplantation in chronic myelogenous leukemia does not affect outcome adversely, provided it is discontinued at least 90 days before the procedure. *Blood, 94*(11), 3668-3677.

Heidegger, S., van den Brink, M. R., Haas, T., & Poeck, H. (2014). The role of pattern-recognition receptors in graft-versus-host disease and graft-versus-leukemia after allogeneic stem cell transplantation. *Front Immunol, 5*, 337. doi:10.3389/fimmu.2014.00337

Horowitz, M. M., Gale, R. P., Sondel, P. M., Goldman, J. M., Kersey, J., Kolb, H. J., Rimm, A. A., Ringden, O., Rozman, C., Speck, B., & et al. (1990). Graft-versus-leukemia reactions after bone marrow transplantation. *Blood, 75*(3), 555-562.

Hu, B., Jin, C., Li, H. B., Tong, J., Ouyang, X., Cetinbas, N. M., Zhu, S., Strowig, T., Lam, F. C., Zhao, C., Henao-Mejia, J., Yilmaz, O., Fitzgerald, K. A., Eisenbarth, S. C., Elinav, E., & Flavell, R. A. (2016). The DNA-sensing AIM2 inflammasome controls radiation-induced cell death and tissue injury. *Science, 354*(6313), 765-768. doi:10.1126/science.aaf7532

Ireton, R. C., & Gale, M., Jr. (2011). RIG-I like receptors in antiviral immunity and therapeutic applications. *Viruses, 3*(6), 906-919. doi:10.3390/v3060906

Ishikawa, H., Ma, Z., & Barber, G. N. (2009). STING regulates intracellular DNA-mediated, type I interferon-dependent innate immunity. *Nature, 461*(7265), 788-792. doi:10.1038/nature08476

Jenq, R. R., Ubeda, C., Taur, Y., Menezes, C. C., Khanin, R., Dudakov, J. A., Liu, C., West, M. L., Singer, N. V., Equinda, M. J., Gobourne, A., Lipuma, L., Young, L. F., Smith, O. M., Ghosh, A., Hanash, A. M., Goldberg, J. D., Aoyama, K., Blazar, B. R., Pamer, E. G., & van den Brink, M. R. (2012). Regulation of intestinal inflammation by microbiota following allogeneic bone marrow transplantation. *J Exp Med, 209*(5), 903-911. doi:10.1084/jem.20112408

Kolb, H. J., Mittermuller, J., Clemm, C., Holler, E., Ledderose, G., Brehm, G., Heim, M., & Wilmanns, W. (1990). Donor leukocyte transfusions for treatment of recurrent chronic myelogenous leukemia in marrow transplant patients. *Blood, 76*(12), 2462-2465.

Koyama, M., & Hill, G. R. (2016). Alloantigen presentation and graft-versus-host disease: fuel for the fire. *Blood, 127*(24), 2963-2970. doi:10.1182/blood-2016-02-697250

Kuci, Z., Bonig, H., Kreyenberg, H., Bunos, M., Jauch, A., Janssen, J. W., Skific, M., Michel, K., Eising, B., Lucchini, G., Bakhtiar, S., Greil, J., Lang, P., Basu, O., von Luettichau, I., Schulz, A., Sykora, K. W., Jarisch, A., Soerensen, J., Salzmann-Manrique, E., Seifried, E., Klingebiel, T., Bader, P., & Kuci, S. (2016). Mesenchymal stromal cells from pooled mononuclear cells of multiple bone marrow donors as rescue therapy in pediatric severe steroid-refractory graft-versus-host disease: a multicenter survey. *Haematologica, 101*(8), 985-994. doi:10.3324/haematol.2015.140368

Lamarthee, B., Malard, F., Saas, P., Mohty, M., & Gaugler, B. (2016). Interleukin-22 in Graft-Versus-Host Disease after Allogeneic Stem Cell Transplantation. *Front Immunol, 7*, 148. doi:10.3389/fimmu.2016.00148

Lerner, K. G., Kao, G. F., Storb, R., Buckner, C. D., Clift, R. A., & Thomas, E. D. (1974). Histopathology of graft-vs.-host reaction (GvHR) in human recipients of marrow from HL-A-matched sibling donors. *Transplant Proc, 6*(4), 367-371.

Li, H. W., & Sykes, M. (2012). Emerging concepts in haematopoietic cell transplantation. *Nat Rev Immunol, 12*(6), 403-416. doi:10.1038/nri3226

Li, X. D., Chiu, Y. H., Ismail, A. S., Behrendt, C. L., Wight-Carter, M., Hooper, L. V., & Chen, Z. J. (2011). Mitochondrial antiviral signaling protein (MAVS) monitors commensal bacteria and induces an immune response that prevents experimental colitis. *Proc Natl Acad Sci U S A, 108*(42), 17390-17395. doi:10.1073/pnas.1107114108

Lindemans, C. A., Calafiore, M., Mertelsmann, A. M., O'Connor, M. H., Dudakov, J. A., Jenq, R. R., Velardi, E., Young, L. F., Smith, O. M., Lawrence, G., Ivanov, J. A., Fu, Y. Y., Takashima, S., Hua,

G., Martin, M. L., O'Rourke, K. P., Lo, Y. H., Mokry, M., Romera-Hernandez, M., Cupedo, T., Dow, L., Nieuwenhuis, E. E., Shroyer, N. F., Liu, C., Kolesnick, R., van den Brink, M. R. M., & Hanash, A. M. (2015). Interleukin-22 promotes intestinal-stem-cell-mediated epithelial regeneration. *Nature, 528*(7583), 560-564. doi:10.1038/nature16460

Lutz, M., & Mielke, S. (2016). New perspectives on the use of mTOR inhibitors in allogeneic haematopoietic stem cell transplantation and graft-versus-host disease. *Br J Clin Pharmacol, 82*(5), 1171-1179. doi:10.1111/bcp.13022

Marsh, J. C., Ball, S. E., Cavenagh, J., Darbyshire, P., Dokal, I., Gordon-Smith, E. C., Keidan, J., Laurie, A., Martin, A., Mercieca, J., Killick, S. B., Stewart, R., Yin, J. A., & British Committee for Standards in, H. (2009). Guidelines for the diagnosis and management of aplastic anaemia. *Br J Haematol, 147*(1), 43-70. doi:10.1111/j.1365-2141.2009.07842.x

Martin, P. J., Rizzo, J. D., Wingard, J. R., Ballen, K., Curtin, P. T., Cutler, C., Litzow, M. R., Nieto, Y., Savani, B. N., Schriber, J. R., Shaughnessy, P. J., Wall, D. A., & Carpenter, P. A. (2012). First- and second-line systemic treatment of acute graft-versus-host disease: recommendations of the American Society of Blood and Marrow Transplantation. *Biol Blood Marrow Transplant, 18*(8), 1150-1163. doi:10.1016/j.bbmt.2012.04.005

Meylan, E., Curran, J., Hofmann, K., Moradpour, D., Binder, M., Bartenschlager, R., & Tschopp, J. (2005). Cardif is an adaptor protein in the RIG-I antiviral pathway and is targeted by hepatitis C virus. *Nature, 437*(7062), 1167-1172. doi:10.1038/nature04193

Morton, A. J., Gooley, T., Hansen, J. A., Appelbaum, F. R., Bruemmer, B., Bjerke, J. W., Clift, R., Martin, P. J., Petersdorf, E. W., Sanders, J. E., Storb, R., Sullivan, K. M., Woolfrey, A., & Anasetti, C. (1998). Association between pretransplant interferon-alpha and outcome after unrelated donor marrow transplantation for chronic myelogenous leukemia in chronic phase. *Blood, 92*(2), 394-401.

Napolitano, L. M., Koruda, M. J., Meyer, A. A., & Baker, C. C. (1996). The impact of femur fracture with associated soft tissue injury on immune function and intestinal permeability. *Shock, 5*(3), 202-207.

Ng, K. W., Marshall, E. A., Bell, J. C., & Lam, W. L. (2017). cGAS-STING and Cancer: Dichotomous Roles in Tumor Immunity and Development. *Trends Immunol*. doi:10.1016/j.it.2017.07.013

Peterson, L. W., & Artis, D. (2014). Intestinal epithelial cells: regulators of barrier function and immune homeostasis. *Nat Rev Immunol, 14*(3), 141-153. doi:10.1038/nri3608

Poeck, H., Besch, R., Maihoefer, C., Renn, M., Tormo, D., Morskaya, S. S., Kirschnek, S., Gaffal, E., Landsberg, J., Hellmuth, J., Schmidt, A., Anz, D., Bscheider, M., Schwerd, T., Berking, C., Bourquin, C., Kalinke, U., Kremmer, E., Kato, H., Akira, S., Meyers, R., Hacker, G., Neuenhahn, M., Busch, D., Ruland, J., Rothenfusser, S., Prinz, M., Hornung, V., Endres, S., Tuting, T., & Hartmann, G. (2008). 5'-Triphosphate-siRNA: turning gene silencing and Rig-I activation against melanoma. *Nat Med, 14*(11), 1256-1263. doi:10.1038/nm.1887

Porter, D. L., Roth, M. S., McGarigle, C., Ferrara, J. L., & Antin, J. H. (1994). Induction of graft-versus-host disease as immunotherapy for relapsed chronic myeloid leukemia. *N Engl J Med, 330*(2), 100-106. doi:10.1056/NEJM199401133300204

Rager, A., Frey, N., Goldstein, S. C., Reshef, R., Hexner, E. O., Loren, A., Luger, S. M., Perl, A., Tsai, D., Davis, J., Vozniak, M., Smith, J., Stadtmauer, E. A., & Porter, D. L. (2011). Inflammatory cytokine inhibition with combination daclizumab and infliximab for steroid-refractory acute GVHD. *Bone Marrow Transplant, 46*(3), 430-435. doi:10.1038/bmt.2010.117

Reddy, P., Negrin, R., & Hill, G. R. (2008). Mouse models of bone marrow transplantation. *Biol Blood Marrow Transplant, 14*(1 Suppl 1), 129-135. doi:10.1016/j.bbmt.2007.10.021

Robb, R. J., Kreijveld, E., Kuns, R. D., Wilson, Y. A., Olver, S. D., Don, A. L., Raffelt, N. C., De Weerd, N. A., Lineburg, K. E., Varelias, A., Markey, K. A., Koyama, M., Clouston, A. D., Hertzog, P. J., Macdonald, K. P., & Hill, G. R. (2011). Type I-IFNs control GVHD and GVL responses after transplantation. *Blood, 118*(12), 3399-3409. doi:10.1182/blood-2010-12-325746

Sanchez de Medina, F., Romero-Calvo, I., Mascaraque, C., & Martinez-Augustin, O. (2014). Intestinal inflammation and mucosal barrier function. *Inflamm Bowel Dis, 20*(12), 2394-2404. doi:10.1097/MIB.0000000000000204

Sauer, J. D., Sotelo-Troha, K., von Moltke, J., Monroe, K. M., Rae, C. S., Brubaker, S. W., Hyodo, M., Hayakawa, Y., Woodward, J. J., Portnoy, D. A., & Vance, R. E. (2011). The N-ethyl-N-nitrosourea-induced Goldenticket mouse mutant reveals an essential function of Sting in the in vivo interferon response to Listeria monocytogenes and cyclic dinucleotides. *Infect Immun, 79*(2), 688-694. doi:10.1128/IAI.00999-10

Schlee, M., & Hartmann, G. (2016). Discriminating self from non-self in nucleic acid sensing. *Nat Rev Immunol, 16*(9), 566-580. doi:10.1038/nri.2016.78

Schmidt-Hieber, M., Fietz, T., Knauf, W., Uharek, L., Hopfenmuller, W., Thiel, E., & Blau, I. W. (2005). Efficacy of the interleukin-2 receptor antagonist basiliximab in steroid-refractory acute graft-versus-host disease. *Br J Haematol, 130*(4), 568-574. doi:10.1111/j.1365-2141.2005.05631.x

Schwab, L., Goroncy, L., Palaniyandi, S., Gautam, S., Triantafyllopoulou, A., Mocsai, A., Reichardt, W., Karlsson, F. J., Radhakrishnan, S. V., Hanke, K., Schmitt-Graeff, A., Freudenberg, M., von Loewenich, F. D., Wolf, P., Leonhardt, F., Baxan, N., Pfeifer, D., Schmah, O., Schonle, A., Martin, S. F., Mertelsmann, R., Duyster, J., Finke, J., Prinz, M., Henneke, P., Hacker, H., Hildebrandt, G. C., Hacker, G., & Zeiser, R. (2014). Neutrophil granulocytes recruited upon translocation of intestinal bacteria enhance graft-versus-host disease via tissue damage. *Nat Med, 20*(6), 648-654. doi:10.1038/nm.3517

Shlomchik, W. D. (2007). Graft-versus-host disease. *Nat Rev Immunol, 7*(5), 340-352. doi:10.1038/nri2000

Shono, Y., Docampo, M. D., Peled, J. U., Perobelli, S. M., Velardi, E., Tsai, J. J., Slingerland, A. E., Smith, O. M., Young, L. F., Gupta, J., Lieberman, S. R., Jay, H. V., Ahr, K. F., Porosnicu Rodriguez, K. A., Xu, K., Calarfiore, M., Poeck, H., Caballero, S., Devlin, S. M., Rapaport, F., Dudakov, J. A., Hanash, A. M., Gyurkocza, B., Murphy, G. F., Gomes, C., Liu, C., Moss, E. L., Falconer, S. B., Bhatt, A. S., Taur, Y., Pamer, E. G., van den Brink, M. R. M., & Jenq, R. R. (2016). Increased GVHD-related mortality with broad-spectrum antibiotic use after allogeneic hematopoietic stem cell transplantation in human patients and mice. *Sci Transl Med, 8*(339), 339ra371. doi:10.1126/scitranslmed.aaf2311

Spoerl, S., Mathew, N. R., Bscheider, M., Schmitt-Graeff, A., Chen, S., Mueller, T., Verbeek, M., Fischer, J., Otten, V., Schmickl, M., Maas-Bauer, K., Finke, J., Peschel, C., Duyster, J., Poeck, H., Zeiser, R., & von Bubnoff, N. (2014). Activity of therapeutic JAK 1/2 blockade in graft-versus-host disease. *Blood, 123*(24), 3832-3842. doi:10.1182/blood-2013-12-543736

Stift, J., Baba, H. A., Huber, E., Federmann, B., Fischer, H. P., Schmitt-Graeff, A., Baurmann, H., Bethge, W., Schirmacher, P., Wrba, F., Greinix, H., Fend, F., Schwerdtfeger, R., Shulman, H. M., Wolff, D., Longerich, T., & Liver Pathology Group of the German-Austrian-Swiss Working Group on Gv, H. D. (2014). Consensus on the histopathological evaluation of liver biopsies from patients following allogeneic hematopoietic cell transplantation. *Virchows Arch, 464*(2), 175-190. doi:10.1007/s00428-013-1528-8

Sun, L., Miyoshi, H., Origanti, S., Nice, T. J., Barger, A. C., Manieri, N. A., Fogel, L. A., French, A. R., Piwnica-Worms, D., Piwnica-Worms, H., Virgin, H. W., Lenschow, D. J., & Stappenbeck, T. S. (2015). Type I interferons link viral infection to enhanced epithelial turnover and repair. *Cell Host Microbe, 17*(1), 85-97. doi:10.1016/j.chom.2014.11.004

Szyska, M., & Na, I. K. (2016). Bone Marrow GvHD after Allogeneic Hematopoietic Stem Cell Transplantation. *Front Immunol, 7*, 118. doi:10.3389/fimmu.2016.00118

Toubai, T., Mathewson, N. D., Magenau, J., & Reddy, P. (2016). Danger Signals and Graft-versus-host Disease: Current Understanding and Future Perspectives. *Front Immunol, 7*, 539. doi:10.3389/fimmu.2016.00539

Tschurtschenthaler, M., Wang, J., Fricke, C., Fritz, T. M., Niederreiter, L., Adolph, T. E., Sarcevic, E., Kunzel, S., Offner, F. A., Kalinke, U., Baines, J. F., Tilg, H., & Kaser, A. (2014). Type I interferon

signalling in the intestinal epithelium affects Paneth cells, microbial ecology and epithelial regeneration. *Gut, 63*(12), 1921-1931. doi:10.1136/gutjnl-2013-305863

Viaud, S., Saccheri, F., Mignot, G., Yamazaki, T., Daillere, R., Hannani, D., Enot, D. P., Pfirschke, C., Engblom, C., Pittet, M. J., Schlitzer, A., Ginhoux, F., Apetoh, L., Chachaty, E., Woerther, P. L., Eberl, G., Berard, M., Ecobichon, C., Clermont, D., Bizet, C., Gaboriau-Routhiau, V., Cerf-Bensussan, N., Opolon, P., Yessaad, N., Vivier, E., Ryffel, B., Elson, C. O., Dore, J., Kroemer, G., Lepage, P., Boneca, I. G., Ghiringhelli, F., & Zitvogel, L. (2013). The intestinal microbiota modulates the anticancer immune effects of cyclophosphamide. *Science, 342*(6161), 971-976. doi:10.1126/science.1240537

Wang, L., Llorente, C., Hartmann, P., Yang, A. M., Chen, P., & Schnabl, B. (2015). Methods to determine intestinal permeability and bacterial translocation during liver disease. *J Immunol Methods, 421*, 44-53. doi:10.1016/j.jim.2014.12.015

Wang, Y., Zhang, H. X., Sun, Y. P., Liu, Z. X., Liu, X. S., Wang, L., Lu, S. Y., Kong, H., Liu, Q. L., Li, X. H., Lu, Z. Y., Chen, S. J., Chen, Z., Bao, S. S., Dai, W., & Wang, Z. G. (2007). Rig-I-/- mice develop colitis associated with downregulation of G alpha i2. *Cell Res, 17*(10), 858-868. doi:10.1038/cr.2007.81

Weber, D., Frauenschlager, K., Ghimire, S., Peter, K., Panzer, I., Hiergeist, A., Weber, M., Kutny, D., Wolff, D., Grube, M., Huber, E., Oefner, P., Gessner, A., Hehlgans, T., Herr, W., & Holler, E. (2017). The association between acute graft-versus-host disease and antimicrobial peptide expression in the gastrointestinal tract after allogeneic stem cell transplantation. *PLoS One, 12*(9), e0185265. doi:10.1371/journal.pone.0185265

Weiden, P. L., Flournoy, N., Thomas, E. D., Prentice, R., Fefer, A., Buckner, C. D., & Storb, R. (1979). Antileukemic effect of graft-versus-host disease in human recipients of allogeneic-marrow grafts. *N Engl J Med, 300*(19), 1068-1073. doi:10.1056/NEJM197905103001902

Wolff, D., Ayuk, F., Elmaagacli, A., Bertz, H., Lawitschka, A., Schleuning, M., Meyer, R. G., Gerbitz, A., Hilgendorf, I., Hildebrandt, G. C., Edinger, M., Klein, S., Halter, J., Mousset, S., Holler, E., & Greinix, H. T. (2013). Current practice in diagnosis and treatment of acute graft-versus-host disease: results from a survey among German-Austrian-Swiss hematopoietic stem cell transplant centers. *Biol Blood Marrow Transplant, 19*(5), 767-776. doi:10.1016/j.bbmt.2013.01.018

Wu, J., & Chen, Z. J. (2014). Innate immune sensing and signaling of cytosolic nucleic acids. *Annu Rev Immunol, 32*, 461-488. doi:10.1146/annurev-immunol-032713-120156

Wu, Y., Wu, X., Wu, L., Wang, X., & Liu, Z. (2017). The anticancer functions of RIG-I-like receptors, RIG-I and MDA5, and their applications in cancer therapy. *Transl Res*. doi:10.1016/j.trsl.2017.08.004

Yan, L., Yang, C., & Tang, J. (2013). Disruption of the intestinal mucosal barrier in Candida albicans infections. *Microbiol Res, 168*(7), 389-395. doi:10.1016/j.micres.2013.02.008

Zeiser, R., & Blazar, B. R. (2017). Acute Graft-versus-Host Disease - Biologic Process, Prevention, and Therapy. *N Engl J Med, 377*(22), 2167-2179. doi:10.1056/NEJMra1609337

Zeiser, R., Socie, G., & Blazar, B. R. (2016). Pathogenesis of acute graft-versus-host disease: from intestinal microbiota alterations to donor T cell activation. *Br J Haematol, 175*(2), 191-207. doi:10.1111/bjh.14295

Zhu, L., Shi, T., Zhong, C., Wang, Y., Chang, M., & Liu, X. (2017). IL-10 and IL-10 Receptor Mutations in Very Early Onset Inflammatory Bowel Disease. *Gastroenterology Res, 10*(2), 65-69. doi:10.14740/gr740w

Zhu, Q., Man, S. M., Gurung, P., Liu, Z., Vogel, P., Lamkanfi, M., & Kanneganti, T. D. (2014). Cutting edge: STING mediates protection against colorectal tumorigenesis by governing the magnitude of intestinal inflammation. *J Immunol, 193*(10), 4779-4782. doi:10.4049/jimmunol.1402051

Ziemer, M., Haeusermann, P., Janin, A., Massi, D., Ziepert, M., Wolff, D., Greinix, H., & Hillen, U. (2014). Histopathological diagnosis of graft-versus-host disease of the skin: an interobserver comparison. *J Eur Acad Dermatol Venereol, 28*(7), 915-924. doi:10.1111/jdv.12215

8. Anhänge

I. Lebenslauf

Wissenschaftliche Tätigkeiten

Seit 07/2017	Assistenzarzt der Klinik und Poliklinik für Radioonkologie und Strahlentherapie des Klinikums rechts der Isar der TU München (TUM)
01/2017 – 06/2017	Wissenschaftlicher Mitarbeiter der AG Poeck & Haas, Hämatologie und Onkologie des Klinikums rechts der Isar
2013 – 2016	Bearbeitung des Promotionsprojekts: *„Die Rolle zytosolischer Nukleinsäurerezeptoren bei Strahlentherapie- oder Chemotherapie-induziertem intestinalen Gewebeschaden und der Graft-versus-host disease"*
2012	Doktorand der AG Poeck & Haas

Hochschulpolitische Tätigkeiten

2011 – 2013	Studierendenvertreter im Fakultätsrat der Medizinischen Fakultät der TUM
2010 – 2013	Studierendenvertreter in der Curriculums- und Studienkommission der Medizinischen Fakultät der TUM

Praktisches Jahr

11/2015 – 10/2016	3. Tertial: Pädiatrie (Dr. von Haunersches Kinderspital, LMU München)
	2. Tertial: Chirurgie (Klinikum rechts der Isar)
	1. Tertial: Innere Medizin (Klinikum rechts der Isar)

Ausbildung

10/2008 – 11/2016	Humanmedizinstudium mit der Gesamtnote „sehr gut" (1,5) abgeschlossen an der TUM
09/1995 – 06/2008	Abitur (Abschlussnote 1,1) abgeschlossen an dem Gymnasium am Ostring in Bochum

Stipendien

2013 – 2016	Stipendiat der Studienstiftung des deutschen Volkes
2011 – 2015	Stipendiat der Konrad-Adenauer-Stiftung
2012 – 2013	Promotionsstipendium *„Translationale Medizin"* der Medizinischen Fakultät der TUM

II. Publikationsverzeichnis

I) Originalarbeiten in peer-reviewed Journalen als Erstautor:

1) **Julius C. Fischer**, Alexander Wintges, Tobias Haas and Hendrik Poeck.
Assessment of mucosal integrity by quantifying neutrophil granulocyte influx in murine models of acute intestinal injury
Cellular Immunology. 2017 Jun;316:70-76.

2) **Julius C. Fischer**, Michael Bscheider, Gabriel Eisenkolb, Chia-Ching Lin, Alexander Wintges, Vera Otten, Caroline Lindemans, Simon Heidegger, Martina Rudelius, Sébastien Monette, Kori A. Porosnicu Rodriguez, Marco Calafiore, Sophie Liebermann, Chen Liu, Stefan Lienenklaus, Siegfried Weiss, Ulrich Kalinke, Jürgen Ruland, Christian Peschel, Yusuke Shono, Melissa Docampo, Enrico Velardi, Robert Jenq, Alan M. Hanash, Jarrod A. Dudakov, Tobias Haas, Marcel R.M. van den Brink and Hendrik Poeck.
RIG-I/MAVS and STING signaling promote gut integrity during irradiation- and immune-mediated tissue injury
Science Translational Medicine. 2017 Apr 19;9(386).

3) **Julius C. Fischer**, Vera Otten, Maike Kober, Christoph Drees, Mark Rosenbaum, Martina Schmickl, Simon Heidegger, Rudi Beyaert, Geert van Loo, Xian C. Li, Christian Peschel, Marc Schmidt-Supprian, Tobias Haas, Silvia Spoerl and Hendrik Poeck.
A20 restrains thymic regulatory T cell development
The Journal of Immunology. 2017 Oct 1;199(7):2356-2365.

4) **Julius C. Fischer**, Vera Otten, Katja Steiger, Martina Schmickl, Julia Slotta-Huspenina, Rudi Beyaert, Geert van Loo, Christian Peschel, Marc Schmidt-Supprian, Hendrik Poeck, Tobias Haas and Silvia Spoerl.
A20 deletion in T cells modulates acute graft-versus-host disease in mice
European Journal of Immunology. 2017 Nov;47(11):1982-1988.

II) Originalarbeiten in peer-reviewed Journalen als Co-Author:

1) Jankovic D, Ganesan J, Bscheider M, Stickel N, Weber FC, Guarda G, Follo M, Pfeifer D, Tardivel A, Ludigs K, Bouazzaoui A, Kerl K, **Fischer JC**, Haas T, Schmitt-Gräff A, Manoharan A, Müller L, Finke J, Martin SF, Gorka O, Peschel C, Ruland J, Idzko M, Duyster J, Holler E, French LE, Poeck H, Contassot E, Zeiser R.
The Nlrp3 inflammasome regulates acute graft-versus-host disease
Journal of Experimental Medicine. 2013 Sep 23;210(10):1899-910

2) Spoerl S, Mathew NR, Bscheider M, Schmitt-Graeff A, Chen S, Mueller T, Verbeek M, **Fischer J**, Otten V, Schmickl M, Maas-Bauer K, Finke J, Peschel C, Duyster J, Poeck H, Zeiser R, von Bubnoff N.
Activity of therapeutic JAK 1/2 blockade in graft-versus-host disease
Blood. 2014 Jun 12;123(24):3832-42

3) Vahl JC, Drees C, Heger K, Heink S, **Fischer JC**, Nedjic J, Ohkura N, Morikawa H, Poeck H, Schallenberg S, Rieß D, Hein MY, Buch T, Polic B, Schönle A, Zeiser R, Schmitt-Gräff A, Kretschmer K, Klein L, Korn T, Sakaguchi S, Schmidt-Supprian M.
Continuous T cell receptor signals maintain a functional regulatory T cell pool
Immunity. 2014 Nov 20;41(5):722-36.

4) Christoph Drees, J Christoph Vahl, Sabrina Bortoluzzi, Klaus D. Heger, **Julius C. Fischer**, Thomas Wunderlich, Christian Peschel and Marc Schmidt-Supprian.
Roquin paralogs differentially regulate functional NKT cell subsets
The Journal of Immunology. 2017 Apr 1;198(7):2747-2759.

5) Tobias Haas, Simon Heidegger, Alexander Wintges, Michael Bscheider, Sarah Bek, **Julius C. Fischer**, Gabriel Eisenkolb, Martina Schmickl, Silvia Spörl, Christian Peschel, Hendrik Poeck, Jürgen Ruland.
Card9 controls Dectin-1-induced T-cell cytotoxicity and prevention of tumor growth
European Journal of Immunology. *2017 May;47(5):872-879*

6) Fabian Mohr, **Julius C. Fischer**, Mark Nikolaus, Christian Stemberger, Stefan Dreher, Admar Verschoor, Tobias Haas, Hendrik Poeck, Dirk H. Busch.
Minimally manipulated murine regulatory T cells purified by reversible Fab Multimers are potent suppressors for adoptive T-cell therapy
European Journal of Immunology. 2017 Dec;47(12):2153-2162.

III) Editoriale

Julius C. Fischer & Hendrik Poeck
Targeting RIG-I or STING promotes epithelial regeneration
Oncotarget. 2017 Dec 6;8(70):114418-114419.

III. Originalarbeiten

CrossMark
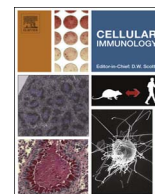
Short communication

Assessment of mucosal integrity by quantifying neutrophil granulocyte influx in murine models of acute intestinal injury

Julius Clemens Fischer[*], Alexander Wintges, Tobias Haas[1], Hendrik Poeck[1]

III. Medizinische Klinik, Klinikum rechts der Isar, Technische Universität, München, Germany

ABSTRACT

Intact epithelial body surfaces represent physical barriers which protect the organism from invading pathogens and loss of nutrients. Barrier malfunction is closely linked to disorders such as inflammatory bowel disease and graft-versus-host disease. In fact, several pharmacological or radiobiological therapeutic strategies have side effects that affect epithelial surfaces. In this context, assays that accurately assess epithelial barrier integrity in patients and animal models are crucial to create a better understanding of the mechanisms leading to disease or limiting therapeutic approaches due to barrier disruption. Here, we tested the ability of the widely used FITC-dextran intestinal permeability analysis to evaluate loss of intestinal barrier integrity in different murine models of gut mucosal damage and established influx of neutrophil granulocytes into the intestinal lamina propria (LP) as an alternative approach. We demonstrate that the sensitivity and specificity of FITC-dextran intestinal permeability analysis is relatively low: Although it did represent severe forms of mucosal damage due to intensive conditioning therapy (high doses of either total body irradiation (TBI) or chemotherapy) or after conditioning and allogeneic stem cell transplantation, it did not recognize less severe forms of damage as after lower doses of TBI or chemotherapy alone. In addition, discrimination of untreated from irradiated mice by differences in FITC-dextran translocation was not exact. In contrast, influx of neutrophil granulocytes into the intestinal LP, which reflects immune activation due to translocation of microbes and microbial products during intestinal barrier breech, quantitatively correlated with the severity of intestinal barrier damage. It accurately represented both severe and less severe forms of intestinal damage as after high or lower dose TBI or chemotherapy and correctly discriminated treated from untreated animals. Taken together, we demonstrate the limitations of FITC-dextran intestinal permeability analysis and identify intestinal neutrophil influx as a powerful additional tool to measure breakdown of intestinal barrier function.

1. Introduction

Mucosal barriers like the intestinal epithelial cell layer protect sterile compartments from physical, chemical and microbial challenge [1]. Inherited or acquired barrier malfunction is closely linked to disorders like inflammatory bowel disease (IBD) [1,2]. In addition to genetically driven diseases and barrier dysfunction resulting from chronically disrupted mucosal homeostasis, acute exogenous triggers can also cause damage to the intestinal barrier and favor the pathogenesis of illnesses like IBD or Graft-versus-host disease (GVHD), which can follow allogeneic stem cell transplantation (allo-HSCT) [2,3]. GVHD occurs in as many as 65% of transplant recipients and is caused by alloreactive T cells that attack host tissue, predominantly of the gut, liver and skin [4]. A crucial step in the development of acute GVHD is pre-transplant conditioning therapy by chemotherapy (CTX) or total body irradiation (TBI). Both can result in acute breakdown of intestinal barrier function followed by translocation of microbes and Pathogen-associated molecular patterns (PAMPs) into underlying sterile compartments. Activated intestinal immune cells prime donor T cells which attack host tissue and augment intestinal damage [4,5]. Although such collateral damage to mucosal integrity limits several pharmacological or radiobiological therapeutic strategies, recent evidence shows that certain aspects of collateral intestinal barrier disruption can be beneficial as there seems to be a complex interplay between side effects and direct anti-tumor effects of chemotherapeutic tumor therapy: In certain settings, efficient tumor control requires intestinal microbiota and reduced intestinal integrity during chemotherapy [6]. To create a better understanding of the mechanisms leading to enhanced or reduced intestinal integrity, it is crucial to be able to quantify changes in barrier function sufficiently. To date, efforts to evaluate the intestinal

barrier function in patients mainly rely on biomarkers (e.g. fecal calprotectin, fecal albumin), biopsies (e.g. tight junction protein expression) and diagnostic permeability tests (lactulose/mannitol urinary excretion etc.), all of which are flawed by certain limitations [2,7]. Several assays are used to measure intestinal permeability in mice [7]. FITC–dextran-intestinal permeability analysis, for example, uses dextran molecules as inert, non-digestible test probes of variable size linked to the fluorescent marker fluorescein isothiocyanate (FITC). In mice with a severely damaged intestinal mucosa, FITC-dextran molecules that were applied orally can leave the gut lumen and enter the systemic blood circulation, where FITC-fluorescence can be measured. This assay is used to assess intestinal permeability during gastrointestinal GVHD after allo-HSCT [8] as well as in models of colitis, hypoxia, liver disease, trauma and CTX [6,7]. Nevertheless, clear descriptions of the characteristics and limitations of FITC-dextran intestinal permeability analysis are lacking. In this report, we discuss our experience with the FITC-dextran permeability assay to measure intestinal integrity after TBI, CTX and allo-HSCT. We demonstrate that this assay suffers from limited sensitivity and specificity to detect loss of intestinal barrier integrity as after reduced doses of TBI. Alternatively, we propose quantitative evaluation of neutrophil influx into the intestinal lamina propria (LP) as a powerful additional tool to more accurately evaluate intestinal integrity. We confirm that neutrophil chemotaxis depends on intestinal microbiota [9] and show that neutrophil influx quantitatively correlates with the severity of acute intestinal tissue damage, offering higher sensitivity and specificity when using FITC-dextran intestinal permeability analysis.

2. Methods

2.1. Mice

C57BL/6 and Balb/c mice were purchased from Janvier Labs (France). Mice were used between 6 and 8 weeks of age (onset of experiments) and were maintained in specific pathogen free conditions. Animal studies were approved by the local regulatory agencies (Regierung von Oberbayern, Munich).

2.2. Models of intestinal mucosal damage

2.2.1. Intestinal damage by total body irradiation + allo-HSCT

Allo-HSCT was performed as previously described [10]. Briefly, Balb/c recipient mice received 2×4.5 Gy TBI and were then given 5×10^6 T cell-depleted donor (C57BL/6) bone marrow (TCD-BM) cells $\pm$ 0.5×10^6 donor T cells to induce acute GVHD (CD4/CD8 enrichment, Miltenyi). T cell depletion of BM cells was performed using CD90.2 MACS sorting beads (Miltenyi). Total TBI and T cell doses were chosen to ensure a strong T cell mediated damage within one week after transplantation [11]. TBI was split into two doses (2×4.5 Gy) to reconcile reduced collateral toxicity with optimal eradication of recipient/engraftment of donor hematopoietic compartments [12].

2.2.2. Intestinal damage by total body irradiation alone

6–8 weeks old Balb/c or C57BL/6 mice were irradiated with different TBI doses (0–11 Gy) to achieve different levels of damage to the intestinal mucosa, as indicated in the text and figure legends. The maximal TBI doses (9 Gy Balb/c, 11 Gy C57BL/6) were chosen according to commonly applied myeloablative TBI doses (as used for conditioning therapy before allo-HSCT of respective recipients) depending on the radio sensitivity of the mouse strain used [11].

2.2.3. Intestinal damage by chemotherapy alone

C57BL/6 mice were treated with Doxorubicin injected intraperitoneally (7.5 or 20.0 mg/KG body weight) as indicated in the text and figure legends.

2.3. Intestinal FITC-dextran intestinal permeability analysis

FITC-dextran intestinal permeability analysis was performed similar to what was previously described [8]. Mice were kept without food and water for 8 h. Then, FITC-dextran (#FD4-1G, Sigma) was administered by oral gavage at a concentration of 50 mg/ml in water (750 mg/kg). 4.5 h later, plasma was collected from peripheral blood (8800 rcf, 10 min), then mixed 1:1 with PBS and analyzed on a plate reader at 485 nm excitation wavelength and 535 nm emission wavelength.

2.4. Assessment of intestinal neutrophil granulocyte influx

Mice were sacrificed, lamina propria leukocytes (LPL) were isolated and neutrophils within LPL were analyzed by flow cytometry. Isolation of lamina propria leukocytes was performed as previously described [10]. Colon and/or ileum (defined as distal 1/3 of small intestine) were flushed with cold PBS and cut into 2 cm pieces. Longitudinally opened intestines were washed and then incubated with HBSS solution containing 2 mM EDTA, 10 mM HEPES, 5% FCS (Hyclone), 1% Penicillin-Streptomycin, 1% ʟ-Glutamine and 1 mM DTT (all Sigma-Aldrich). After incubation on a shaker (225 rpm) at 37 °C for 15 min, tissues were washed and filtered through a 100 μm strainer (BD 352360). Next, intestines were incubated for 45 min in PBS$^{+Ca/+Mg}$ supplemented with FCS (10%), Collagenase II (200 U/ml; Worthington), and DNase I (0.05 mg/ml; Roche) on a shaker at 37 °C. Cells in suspension were filtered through a 100 μm strainer and purified on a 40/80% Percoll gradient (Biochrom).

2.5. Flow cytometry

Cell suspensions were stained in PBS with 3% FCS. After live/dead staining (Cat-No: 65-0866-18, eF506, ebioscience) and Fc-Block (Cat-No 101330, BioLegend) according to manufacturer's instructions, indicated clones of fluorochrome-coupled anti-mouse antibodies (BioLegend) were used for surface staining: CD11b (M1/70, APC), CD11c (N418, FITC), Gr-1 (RB6-8C5, PerCP-Cy5.5), Ly6G (1A8, PE-Cy7), CD19 (1D3/CD19, PE), CD3 (17A2, PE), Ly6C (HK1.4, APC-Cy7), NK1.1 (PK136, PE). Neutrophils were generally identified as CD11b^{hi} Gr-1^{hi} live cells (simplified analysis). In the experiments depicted in Supplementary Fig. 2, an extended analysis using CD11b^{hi} Ly6G$^+$ CD3$^-$ CD11c^{hi-} CD19$^-$ Ly6C^{int} NK1.1$^-$ live cells [13] was performed to validate simplified analysis for the general purpose of this manuscript. Stainings performed are indicated in the figure legends. Data was acquired on a FACS Canto II (BD Biosciences) and analyzed using FlowJo software (TreeStar).

2.6. Reduction of intestinal bacterial load

Reduction of intestinal bacterial load was performed with C57BL/6 mice as previously described [14]. 6 weeks old C57BL/6 mice were given a combination of four antibiotics in the drinking water for at least 4 weeks: vancomycin (0.5 g/L), ampicillin (1.0 g/L), neomycin (1.0 g/L) and metronidazole (1.0 g/L). Reduction of intestinal bacterial load was confirmed after incubation of supernatants of diluted fecal pellets on Schaedler Agar (aerobic incubation) and Columbia Agar (anaerobic incubation).

2.7. Statistics

GraphPad Prism version 6 was used for statistical analysis. Statistical tests applied to evaluate differences between means of experimental groups are indicated in the respective figure legends. Experiments were analyzed using two-tailed unpaired *t* test or ordinary one-way Anova, corresponding to the distribution shape of our observations. We used ordinary one-way Anova for multiple comparisons and performed Dunnett's test for Multiple-test corrections. P

values less than 0.05 were considered to be statistically significant.

For further statistical analysis it was assumed that observations $X_1,…,X_n$ from untreated and treated mice were i.i.d. (independent and identically distributed). To be more specific, each random sample was considered to be normally distributed with unknown mean μ and variance $σ^2$. The estimation of these parameters was performed by applying standard maximum-likelihood techniques, i.e., the probability to exactly obtain the given sample was maximized. This two-dimensional maximization problem yields the standard estimators $\hat{μ} = \frac{1}{n}\sum_{i=1}^{n} X_i$ and $\hat{σ}^2 = \frac{1}{n}\sum_{i=1}^{n}(X_i - \hat{μ})^2$. In a second step, these estimates were used to obtain acceptance regions in statistical tests to allow for distinguishing healthy untreated from treated mice. With the null hypothesis H_0, the observation originates from an untreated mouse, the common test errors are defined as follows: A type-I-error (α-error) occurs when erroneously identifying an untreated mouse as treated and a type-II-error (β-error) falsely identifies a treated mouse as untreated. Setting the type-I-error to a specific level α directly yields a cut-off value for accepting or rejecting the null hypothesis. Here, this is simply the $(1-α)$-quantile of the respective Gaussian distribution under the null hypothesis. Once the cut-off value was determined, both the type-II-error and the power of the test $1-β$ could be obtained. Note that the power of a statistical test is the key property to compare the significance of different tests with same level α. In the sequel, we also refer to the terms *expected* sensitivity $(1-β)$ and specificity $(1-α)$ to emphasize that in future test settings it might not be known if mice are treated or not. Note that commonly the terms sensitivity and specificity are applied in the context of relative frequencies, thus being able to verify the null hypothesis with independent diagnostics.

3. Results

3.1. Translocation of FITC-dextran detects barrier loss with low sensitivity and specificity

First, we assessed the ability of a commonly used tool to evaluate the integrity of mucosal barrier function, the FITC-dextran permeability analysis. To do so, we measured FITC-dextran fluorescence in the blood following oral application in a mouse model of allo-HSCT after conditioning with TBI. Allo-HSCT was performed with Balb/c recipients after split dose TBI (2×4.5 Gy), which is optimal to eradicate recipient and allow engraftment of donor hematopoietic compartments with reduced collateral damage. As expected [8,15], we observed a robust increase of FITC-dextran serum levels in recipient mice 7 days after allo-HSCT with donor T cell-depleted BM + T cells (TBI 2×4.5 Gy + TCD-BM + T cells). In contrast, there was no significant difference in translocated FITC-dextran levels on day +7 between healthy untreated mice (no allo-HSCT) and mice that had received TBI and donor BM but no donor T cells (TBI 2×4.5 Gy + TCD-BM control mice) (Fig. 1A). These data suggest that FITC-dextran intestinal permeability analysis detects severe forms of mucosal damage (split dose TBI + allo-HSCT with T cells) but is less sensitive for less severe forms of mucosal damage (split dose TBI only). To address whether FITC-dextran intestinal permeability analysis can detect radiation-induced intestinal barrier damage at all, we next assessed FITC-dextran translocation after single dose 9 Gy TBI, which is expected to be more disruptive than split dose TBI [12]. Furthermore, we analyzed FITC-dextran levels in the serum on day + 3, which is when we expect maximum levels after TBI. Although irradiated mice showed significantly increased FITC-dextran serum levels (Fig. 1B) 3 days after 9 Gy TBI, those levels were much lower than 7 days after TBI 2×4.5 Gy + TCD-BM + T cells. These results were in line with the current understanding that TBI leads to intestinal barrier dysfunction and translocation of bacteria and PAMPs, followed by an inflammatory response which augments intestinal tissue damage through activated allogenic T cells [4,5]. To statistically evaluate the estimated sensitivity and specificity of FITC-dextran

intestinal permeability analysis that can be expected in further experiments, we fitted the probability density functions (Fig. 1C) of FITC-dextran serum levels after 9 Gy TBI vs no treatment from Fig. 1B, using maximum-likelihood estimates (see Section 2.7) and assuming that values in both groups were normally distributed. We illustrated our results in an ROC curve, a common way to illustrate the power of a test for different levels α (for details see Section 2.7), and studied the statistical inference of using various cut-off values (Supplementary Fig. 1A). Setting the level α to a usual threshold of 5% led to a cut-off value of 2505 ng/ml, resulting in a type-II-error of 23% (false negatives) and related power of 77%. While 5% of the untreated mice would be misidentified as irradiated mice (false positives), 77% of all irradiated mice would be correctly identified (Fig. 1C). Such rather low expected values of sensitivity (77%) and specificity (95%) (Table 1) indicated that FITC-dextran translocation may not represent intestinal barrier dysfunction with sufficient accuracy in this setting.

3.2. Neutrophil granulocyte migration into the intestinal lamina propria reflects barrier breech and translocation of microbiota

A recent publication demonstrated that TBI leads to neutrophil granulocyte chemotaxis into the intestinal LP. Since neutrophil influx was dramatically reduced in germfree mice [9], it was hypothesized that reduced intestinal integrity after TBI leads to translocation of bacteria and PAMPs which results in an inflammatory and chemotactic response with recruitment of neutrophils into the LP. We could confirm that relative amounts of neutrophils (as percentage of total lamina propria leukocytes) in the small and large intestine are strongly increased after TBI and observed the peak of this dynamic process on day three after TBI (Fig. 2A). We observed that about 97% of infiltrating CD11b^{hi} Gr-1^{hi} cells are in fact Ly6C^{int} Ly6G$^+$ neutrophil granulocytes but not Ly6C^{hi} Ly6G^{lo} macrophages or other immune cells (Supplementary Fig. 2A, B, C) [13]. Furthermore, we corroborated the assertion that translocation of bacteria and PAMPs contribute to this process since mice that had received antibiotics in the drinking water to reduce the intestinal microbial burden showed significantly decreased neutrophil levels after TBI compared to mice that had not received antibiotics (Fig. 2B).

3.3. Lamina propria neutrophil analysis is sensitive and specific

Next, we examined the power of lamina propria neutrophil analysis as a read-out to discriminate between untreated and irradiated mice (Fig. 2C). Here as well, the percentages of neutrophils of all LPL of untreated and irradiated mice were assumed to be Gaussian. The probability density functions of lamina propria neutrophil levels of healthy untreated and irradiated mice were fitted as described before (Fig. 2D). Accepting a very low type-I-error of 0.001% (false positives) yields a cut-off value of 0.45% CD11b^{hi} Gr-1^{hi} and a very high power of 99.995% (Fig. 2D, Supplementary Fig. 1B). Thus, nearly all mice were correctly identified as either untreated or treated, indicating the considerable expected sensitivity (99.5%) and specificity (99.9%) (Table 1).

3.4. Lamina propria neutrophil analysis provides an enhanced detection range

We further evaluated the detection range of LP neutrophil vs FITC-dextran intestinal permeability analysis by testing lower dose levels of TBI. In fact, mice that received 5.5 Gy TBI already showed significantly enhanced neutrophil levels compared to untreated mice. Neutrophil levels of mice that received 9 Gy TBI were further significantly increased (Fig. 2E). In contrast, FITC-dextran intestinal permeability analysis did not detect intestinal barrier damage after 5.5 Gy TBI, as FITC-dextran levels in the serum after irradiation with 5.5 Gy were not increased compared to untreated control mice (Fig. 2E). As tight
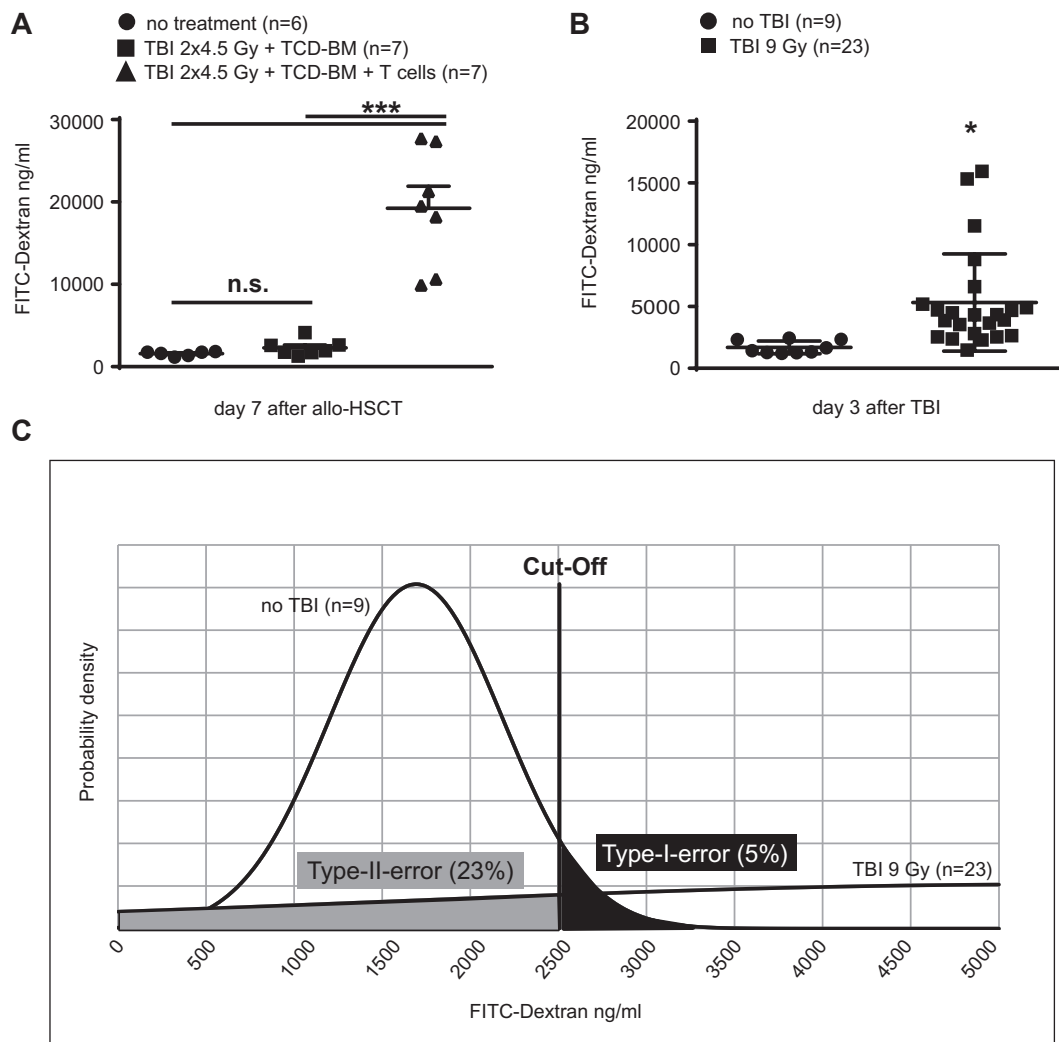
Fig. 1. FITC-dextran intestinal permeability analysis detects barrier loss with low sensitivity and specificity (A) Balb/c mice were either left untreated (n = 6) or received split dose 2×4.5 Gy TBI followed by allo-HSCT with T cell-depleted bone marrow (TCD-BM) only (n = 7) or with 2×4.5 Gy TBI + TCD-BM + T cells (n = 7) on day 0 and were then challenged with oral gavage of FITC-dextran on day + 7. Depicted are FITC-dextran concentrations in the serum. Data from one representative experiment. (B) Balb/c mice were either left untreated (n = 9) or received single dose 9 Gy TBI (n = 23) on day 0 and were then challenged with oral gavage of FITC-dextran on day + 3. Depicted are FITC-dextran concentrations in the serum. Pooled data of 3 independent experiments. (C) Fitted Gaussian distribution of mice depicted in (B) and statistical analysis of Type-I-error (5%) and resulting Type-II-error. Experiments were analyzed using parametric two-tailed unpaired *t* test and ordinary one-way Anova for multiple comparisons. Significance was set at P values < 0.05, p < 0.01 and p < 0.001 and was then indicated with asterisks (*, ** and ***). Data are presented as mean ± S.E.M.

Table 1
Detection of mucosal damage by high dose TBI.

Test characteristics:	Sensitivity	Specificity
FITC dextran intestinal permeability analysis	77%	95%
Neutrophil infiltration analysis	99.5%	99.9%

junctions are central constituents of epithelial barrier function in the gut, we next analyzed the effect of different dose levels of TBI on the gene expression levels of several relevant tight junctional proteins [2,16,17]. We observed several significant changes in gene expression levels of Claudin 2, Claudin 4 Claudin 11, Occludin, JAM-A and ZO-1 between untreated mice and mice that received 5.5 Gy or 9 Gy TB, respectively (Supplementary Fig. 3). Irradiation is known to affect mRNA expression levels of tight junctional proteins differentially with respect to time after exposure and intestinal segment affected [16]. Whether these changes in mRNA expression of tight-junctional proteins translate into differential protein expression and whether they reflect damage or regeneration of barrier function remains to be determined. We believe that dose-sensitive, differential mRNA expression of tight-

junctional proteins reflects individual damage levels to the intestinal barrier integrity which can be assessed by LP neutrophil quantification.

3.5. Lamina propria neutrophil analysis is versatile

To establish that LP neutrophil quantification can be used to measure different levels of damage to intestinal barrier integrity in general, we used an alternative damage model with CTX. First, we analyzed FITC-dextran translocation into the blood after doxorubicin treatment i.p. to show that intestinal integrity was affected. High dose doxorubicin (20 mg/kg body weight) led to significantly increased FITC-dextran levels in the serum, whereas reduced dose doxorubicin (7.5 mg/kg) did not (Fig. 3A). In contrast, animals that received doxorubicin showed significantly enhanced influx of neutrophils into the small intestinal LP in both treatment groups. As with TBI, pretreatment with oral antibiotics also reduced neutrophil levels after doxorubicin treatment (Fig. 3B). Quantitative representation of different levels of intestinal damage was thus similar after CTX and after TBI (Figs. 3A and 2E), indicating the versatility of this test.
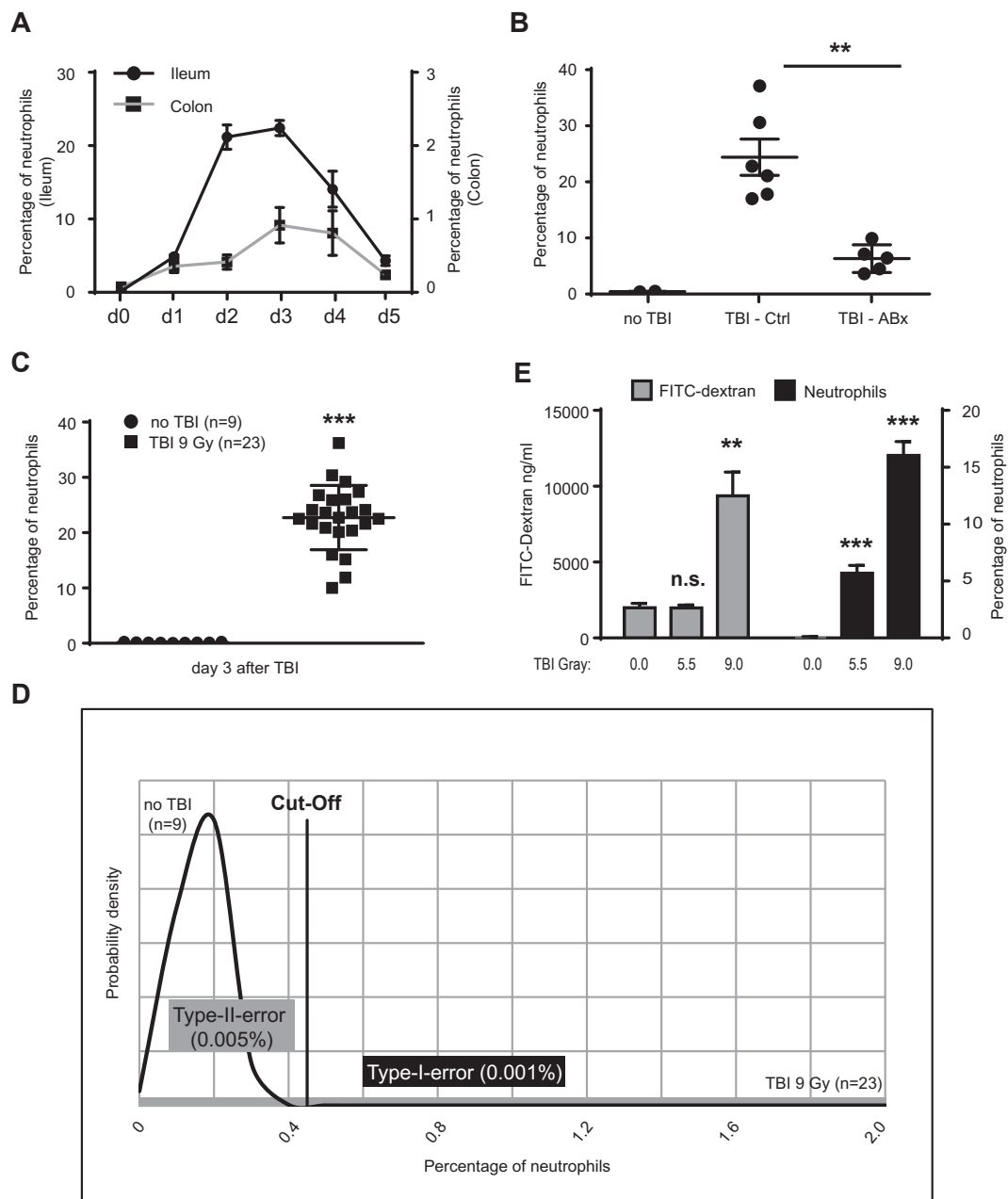
Fig. 2. Quantification of neutrophil granulocytes in the intestinal lamina propria detects barrier breech with high sensitivity and specificity. (A) Lamina propria leukocytes (LPL) isolated from small (Ileum) and large intestines of Balb/c mice were analyzed by flow cytometry at different time points after 9 Gy TBI. Percentages of neutrophils (CD11b^{hi} Gr-1^{hi}) of all live cells are depicted. D0 (n = 2), d1 (n = 3), d2 (n = 3), d3 (n = 4), d4 (n = 4) and d5 (n = 4). Pooled data of 2 independent experiments. (B) C57BL/6 mice were treated with antibiotics for 4 weeks (n = 5) or left untreated (n = 6) and then received 11 Gy TBI. On day 3 after TBI LPL isolated from small intestines (Ileum) were analyzed by flow cytometry. Percentages of neutrophils (CD11b^{hi} Gr-1^{hi}) of all live cells are depicted. Pooled data of 2 independent experiments. (C) LPL isolated from small intestines (Ileum) of Balb/c mice were analyzed by flow cytometry on day 3 after 9 Gy TBI (n = 23) and were compared with untreated mice (n = 9). Percentages of neutrophils (CD11b^{hi} Gr-1^{hi}) of all live cells are depicted. Pooled data of 3 independent experiments. (D) Fitted Gaussian distribution of mice depicted in (C) and statistical analysis of Type-I-error (0.001%) and resulting Type-II-error (0.005%). (E) Untreated Balb/c mice (n = 8), mice that received 5.5 Gy (n = 8) or 9 Gy (n = 8) TBI were challenged with oral gavage of FITC-dextran on day 3. FITC-dextran concentrations in the serum and percentages of neutrophils (CD11b^{hi} Gr-1^{hi}) of all live LPL isolated from small intestine (Ileum) are depicted. Pooled data of 4 independent experiments. Experiments were analyzed using parametric two-tailed unpaired t test and ordinary one-way Anova for multiple comparisons. Significance was set at P values < 0.05, p < 0.01 and p < 0.001 and was then indicated with asterisks (*, ** and ***). Data are presented as mean ± S.E.M.

4. Discussion

In this report, we characterize and compare two techniques to detect loss of intestinal barrier integrity after pharmacological, radiation-induced or immune mediated epithelial injury through CTX, TBI or TBI + allo-HSCT, respectively. FITC-dextran intestinal permeability analysis, commonly used by researchers to evaluate mucosal barrier function, can detect barrier disruption after high doses of CTX or TBI and after TBI + allo-HSCT. However, FITC-dextran levels in the serum cannot reflect more subtle forms of epithelial damage such as after lower doses of CTX or TBI alone, indicating low sensitivity. Statistical analysis of our observations revealed that even with high doses of TBI, as applied before murine allo-HSCT, this assay does not accurately discriminate between untreated vs irradiated mice. Setting the level α to 5% resulted in a type-II-error (false negatives) of 23%. While 5% of all untreated mice would be misidentified as irradiated mice (false positives), only 77% of all irradiated mice would be correctly identified. Naturally, a test with such low expected sensitivity (77%) and
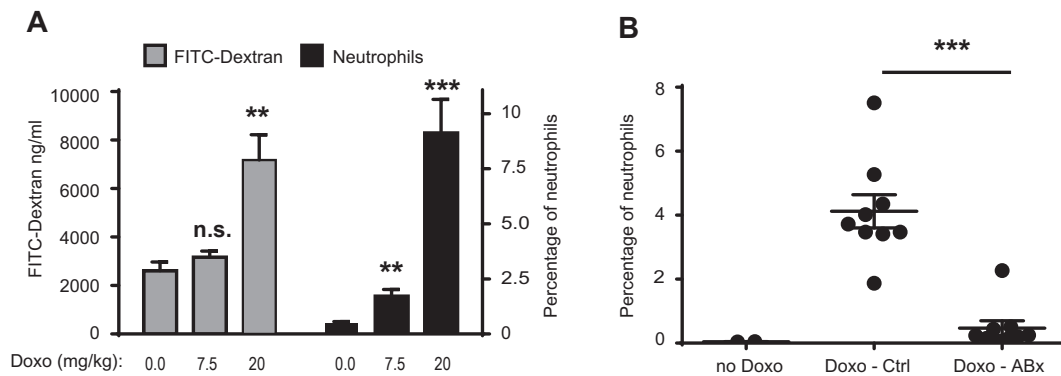
Fig. 3. Quantification of neutrophil granulocytes in the intestinal lamina propria reflects barrier breech after different doses of chemotherapy. (A) Untreated Balb/c mice and Balb/c mice that received Doxorubicin 7,5 mg/kg or Doxorubicin 20 mg/kg i.p. on day 0 were challenged with oral gavage of FITC-dextran on day 3. FITC-dextran concentrations in the serum and percentages of neutrophils (CD11b^{hi} Gr-1^{hi}) of all live LPL isolated from small intestines (Ileum) are depicted. Pooled data of 4 independent experiments with 4–12 mice per group. (B) C57BL/6 mice were treated with antibiotics (n = 9) for 4 weeks or were left untreated (n = 9) and then received Doxorubicin (20 mg/kg) i.p. On day 3 after treatment LPL isolated from small intestines (Ileum) were analyzed by flow cytometry. Percentages of neutrophils (CD11bhi Gr-1^{hi}) of all live cells are depicted. Pooled data of 2 independent experiments. Experiments were analyzed using parametric two-tailed unpaired *t* test and ordinary one-way Anova for multiple comparisons. Significance was set at P values < 0.05, p < 0.01 and p < 0.001 and was then indicated with asterisks (*, ** and ***). Data are presented as mean ± S.E.M.

specificity (95%) values will be insufficient to detect minor differences in severity of intestinal barrier damage such as it might become relevant when analyzing effects of different modalities and dose levels between clinically relevant experimental procedures and groups. Searching for more reliable parameters, we here established neutrophil influx into the intestinal LP as a sensitive marker, which indeed quantitatively reflected different levels of damage to the mucosal barrier. It detected lower levels of damage and allowed to discriminate different damage intensities as after TBI or CTX, displaying extremely limited expected error rates. Nearly all untreated vs irradiated mice would be identified correctly using this approach. Consequently, expected values for sensitivity (99.5%) and specificity (99.9%) were high. We thus postulate that quantifying neutrophil influx into the intestinal LP is a conclusive and versatile test to detect and represent different levels of damage to the mucosal barrier as might be encountered between (I) transgenic mice with defects that result in enhanced or reduced capacity to maintain intestinal integrity (II) different treatment modalities or toxic insults (III) scenarios that influence the intestinal barrier indirectly via systemic mediators as during shock or sepsis. Interestingly, a well-established biomarker for intestinal inflammation in human IBD is fecal calprotectin, an anti-microbial peptide shed into the intestinal lumen by neutrophil granulocytes that infiltrate the intestinal mucosa. This underscores that quantification of neutrophil influx into the gut LP in mice may be a valid test for intestinal integrity with direct correlations to the human system. A limitation to this approach however is that mucosal neutrophil influx reflects translocation of bacteria or PAMPs across the mucosal barrier and is thus biased by both intestinal microbiota and the functional status of the immune system. Direct measurement of translocated microbes (e.g. by culturing or ribosomal RNA sequencing) or microbial products (e.g. LPS) in the portal or systemic circulation would be an alternative but can be technically challenging, suffer from rather insensitive detection ranges and limited culture options and are prone to contamination.

5. Conclusion

As previously reported, all established tests to evaluate intestinal barrier function have relevant advantages and limitations [2,7]. There is no universal marker that reliably reflects mucosal permeability, a prerequisite for a better understanding of the pathophysiology of systemic inflammatory disorders like IBD or GVHD as well as certain aspects of immune and cancer therapy. A combination of methods might therefore be most useful to assess intestinal barrier integrity [7]. Here we show that the analysis of neutrophil influx into the gut lamina

propria is a sensitive, specific and versatile method to accurately detect and quantify injury to the integrity of the intestinal barrier, appropriate to complement other, less powerful tools such as FITC-dextran intestinal permeability analysis.

Author contributions

J.C.F designed, performed and analyzed experiments. A.W. helped to perform experiments. T.H. and H.P. guided the study. J.C.F., T.H. and H.P. wrote the manuscript. This work is part of the thesis of J.C.F at the Technical University of Munich (TUM).

Appendix A. Supplementary data

Supplementary data associated with this article can be found, in the online version, at http://dx.doi.org/10.1016/j.cellimm.2017.04.003.

References

[1] L.W. Peterson, D. Artis, Intestinal epithelial cells: regulators of barrier function and immune homeostasis, Nat. Rev. Immunol. 14 (2014) 141–153.

[2] S.C. Bischoff, G. Barbara, W. Buurman, T. Ockhuizen, J.D. Schulzke, M. Serino, H. Tilg, A. Watson, J.M. Wells, Intestinal permeability–a new target for disease prevention and therapy, BMC Gastroenterol 14 (2014) 189.

[3] S.C. Nalle, J.R. Turner, Intestinal barrier loss as a critical pathogenic link between inflammatory bowel disease and graft-versus-host disease, Mucosal Immunol. 8 (2015) 720–730.

[4] B.R. Blazar, W.J. Murphy, M. Abedi, Advances in graft-versus-host disease biology and therapy, Nat. Rev. Immunol. 12 (2012) 443–458.

[5] S. Heidegger, M.R. van den Brink, T. Haas, H. Poeck, The role of pattern-recognition receptors in graft-versus-host disease and graft-versus-leukemia after allogeneic stem cell transplantation, Front. Immunol. 5 (2014) 337.

[6] S. Viaud, F. Saccheri, G. Mignot, T. Yamazaki, R. Daillere, D. Hannani, D.P. Enot,

C. Pfirschke, C. Engblom, M.J. Pittet, A. Schlitzer, F. Ginhoux, L. Apetoh, E. Chachaty, P.L. Woerther, G. Eberl, M. Berard, C. Ecobichon, D. Clermont, C. Bizet, V. Gaboriau-Routhiau, N. Cerf-Bensussan, P. Opolon, N. Yessaad, E. Vivier, B. Ryffel, C.O. Elson, J. Dore, G. Kroemer, P. Lepage, I.G. Boneca, F. Ghiringhelli, L. Zitvogel, The intestinal microbiota modulates the anticancer immune effects of cyclophosphamide, Science 342 (2013) 971–976.

[7] L. Wang, C. Llorente, P. Hartmann, A.M. Yang, P. Chen, B. Schnabl, Methods to determine intestinal permeability and bacterial translocation during liver disease, J. Immunol. Methods 421 (2015) 44–53.

[8] A.M. Hanash, J.A. Dudakov, G. Hua, M.H. O'Connor, L.F. Young, N.V. Singer, M.L. West, R.R. Jenq, A.M. Holland, L.W. Kappel, A. Ghosh, J.J. Tsai, U.K. Rao, N.L. Yim, O.M. Smith, E. Velardi, E.B. Hawryluk, G.F. Murphy, C. Liu, L.A. Fouser, R. Kolesnick, B.R. Blazar, M.R. van den Brink, Interleukin-22 protects intestinal stem cells from immune-mediated tissue damage and regulates sensitivity to graft versus host disease, Immunity 37 (2012) 339–350.

[9] L. Schwab, L. Goroncy, S. Palaniyandi, S. Gautam, A. Triantafyllopoulou, A. Mocsai, W. Reichardt, F.J. Karlsson, S.V. Radhakrishnan, K. Hanke, A. Schmitt-Graeff, M. Freudenberg, F.D. von Loewenich, P. Wolf, F. Leonhardt, N. Baxan, D. Pfeifer, O. Schmah, A. Schonle, S.F. Martin, R. Mertelsmann, J. Duyster, J. Finke, M. Prinz, P. Henneke, H. Hacker, G.C. Hildebrandt, G. Hacker, R. Zeiser, Neutrophil granulocytes recruited upon translocation of intestinal bacteria enhance graft-versus-host disease via tissue damage, Nat. Med. 20 (2014) 648–654.

[10] D. Jankovic, J. Ganesan, M. Bscheider, N. Stickel, F.C. Weber, G. Guarda, M. Follo, D. Pfeifer, A. Tardivel, K. Ludigs, A. Bouazzaoui, K. Kerl, J.C. Fischer, T. Haas, A. Schmitt-Graff, A. Manoharan, L. Muller, J. Finke, S.F. Martin, O. Gorka,

C. Peschel, J. Ruland, M. Idzko, J. Duyster, E. Holler, L.E. French, H. Poeck, E. Contassot, R. Zeiser, The Nlrp3 inflammasome regulates acute graft-versus-host disease, J. Exp. Med. 210 (2013) 1899–1910.

[11] P. Reddy, R. Negrin, G.R. Hill, Mouse models of bone marrow transplantation, Biol. Blood Marrow Transplant. 14 (2008) 129–135.

[12] Y.Z. Cui, H. Hisha, G.X. Yang, T.X. Fan, T. Jin, Q. Li, Z. Lian, S. Ikehara, Optimal protocol for total body irradiation for allogeneic bone marrow transplantation in mice, Bone Marrow Transplant. 30 (2002) 843–849.

[13] S. Rose, A. Misharin, H. Perlman, A novel Ly6C/Ly6G-based strategy to analyze the mouse splenic myeloid compartment, Cytometry A 81 (2012) 343–350.

[14] S. Rakoff-Nahoum, J. Paglino, F. Eslami-Varzaneh, S. Edberg, R. Medzhitov, Recognition of commensal microflora by toll-like receptors is required for intestinal homeostasis, Cell 118 (2004) 229–241.

[15] A. Beilhack, S. Schulz, J. Baker, G.F. Beilhack, C.B. Wieland, E.I. Herman, E.M. Baker, Y.A. Cao, C.H. Contag, R.S. Negrin, In vivo analyses of early events in acute graft-versus-host disease reveal sequential infiltration of T-cell subsets, Blood 106 (2005) 1113–1122.

[16] S. Garg, J. Zheng, J. Wang, S. Authier, M. Pouliot, M. Hauer-Jensen, Segmental differences in radiation-induced alterations of tight junction-related proteins in non-human primate jejunum, ileum and colon, Radiat. Res. 185 (2016) 50–59.

[17] I. Hwang, B.S. An, H. Yang, H.S. Kang, E.M. Jung, E.B. Jeung, Tissue-specific expression of occludin, zona occludens-1, and junction adhesion molecule A in the duodenum, ileum, colon, kidney, liver, lung, brain, and skeletal muscle of C57BL mice, J. Physiol. Pharmacol. 64 (2013) 11–18.

Supplementary Materials for

Assessment of mucosal integrity by quantifying neutrophil granulocyte influx in murine models of acute intestinal injury

Julius Clemens Fischer, Alexander Wintges, Tobias Haas & Hendrik Poeck

This PDF file includes:
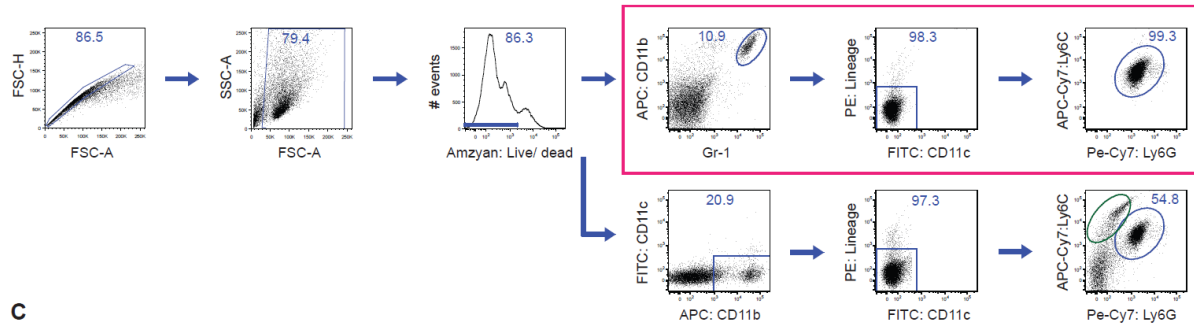
1. Supplementary methods

2. Supplementary Figure 1: Receiver operating characteristic (ROC) curves of FITC-dextran and neutrophil granulocytes to detect barrier loss induced by TBI

3. Supplementary Figure 2: FACS gating strategy to detect intestinal LP neutrophil granulocytes

4. Supplementary Figure 3: Total body irradiation affects gene expression of intestinal tight junction proteins in a dose dependent manner

1. Supplementary methods

1.1 Quantitative PCR

RNA was isolated from whole tissue homogenates lysed in TRIzol (ambion). Tissue homogenates were prepared as follows: A sample from the small intestine (1cm, terminal ileum) was flushed and longitudinally opened and was frozen in 500ul TRIzol reagent using liquid nitrogen. After thawing, samples were supplemented with stainless steel beads 5mm (Qiagen) and homogenized using a Tissuelyser II (Qiagen) 1 min with 30Hz (1800 oscillations/minute). Total RNA was isolated and transcribed using standard methods and kits according to manufacturer´s protocols (RNeasy Mini Kit, Qiagen; SuperScript III Reverse Transcriptase, invitrogen). The specific primer pairs were as follows: mActin fwd CACACCCGCCACCAGTTCG, rev CACCATCACACCCTGGTGC; mZO-1 fwd ACTCCCACTTCCCCAAAAAC, rev CCACAGCTGAAGGACTCACA; mJAM-A fwd CTGATCTTTGACCCCGTGAC, rev ACCAGACGCCAAAAATCAAG; mOccludin fwd GGTGCATAATGATTGGGTTTG, rev GTCCGTGAGGCCTTTTGA; mClaudin-2 fwd ACAGAGAACCATCCTCCCTTC, rev CTCTTCTTCACCCCCATGC; mClaudin-4 fwd GTCCTGGGAATCTCCTTGGC, rev TCTGTGCCGTGACGATGTTG; mClaudin-11 fwd GGACATCCTCATCCTTCCAG, rev TGCAGGGGAGAACTGTCAA. The qPCR Core kit for SYBR Green I (Eurogentec) and a LightCycler 480 II (Roche) Real-Time PCR System were used as indicated by the manufacturer. The relative transcript level of each gene was calculated according to the 2^{-Ct}, for unnormalized genes, and the $2^{-\Delta\Delta Ct}$ method, for genes normalized to β-Actin**.**
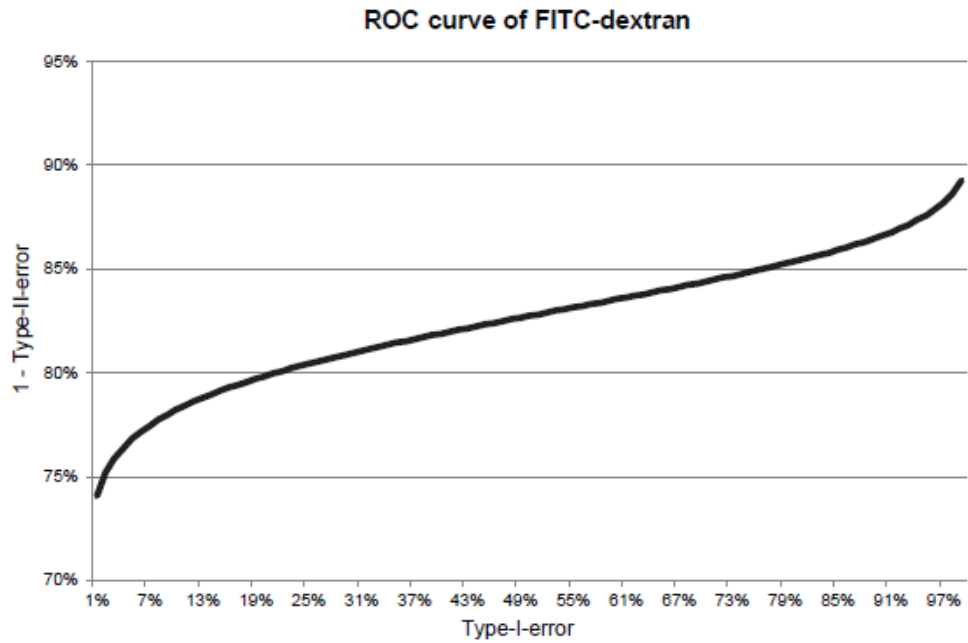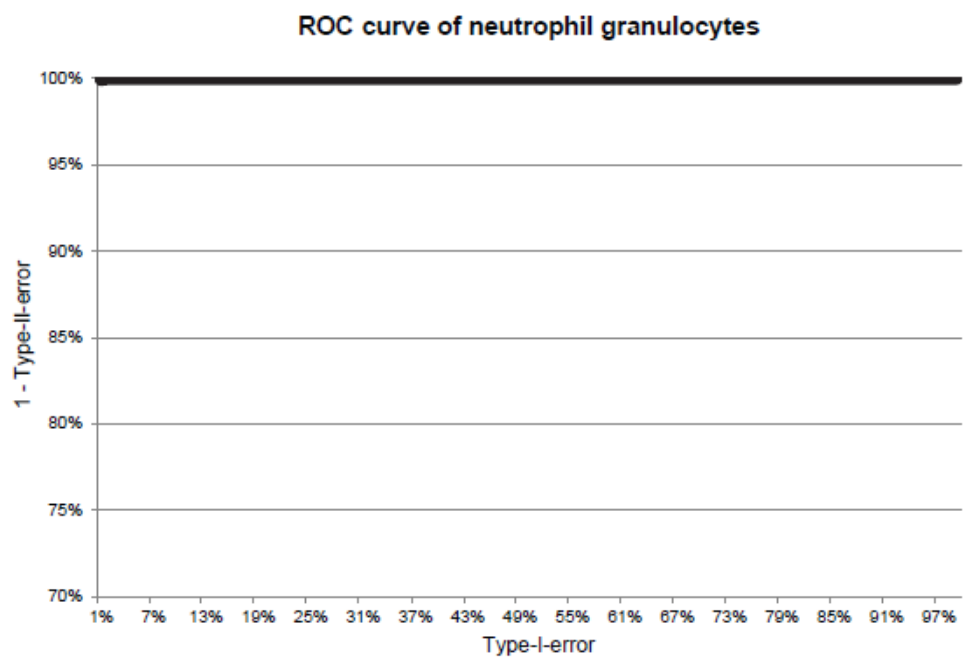
Supplementary Figure 1: Receiver operating characteristic (ROC) curves of FITC-dextran and neutrophil granulocytes to detect barrier loss induced by TBI

A) ROC curve is calculated using the data presented in Figure 1B **B)** ROC curve is calculated using the data presented in Figure 2C.
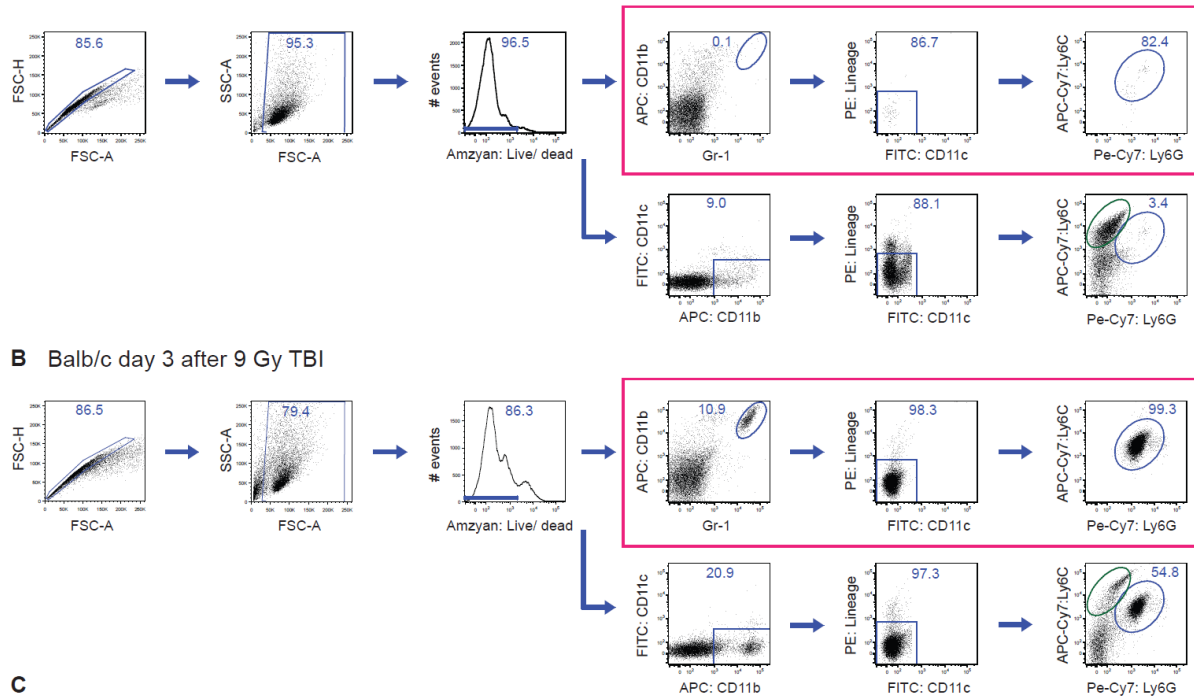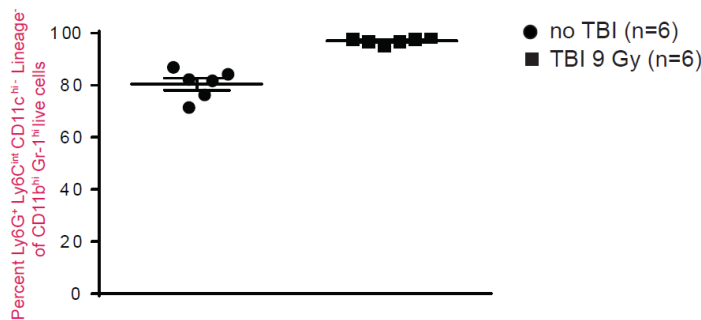
Supplementary Figure 2: FACS gating strategy to detect intestinal LP neutrophil granulocytes

FACS gating strategy to detect small intestinal lamina propria neutrophil granulocytes isolated from Balb/c mice that were left untreated (**A**) or received 9 Gy TBI and were analyzed on day +3 (**B**). Upper panel: Doublets (FSC-H vs. FSC-A) and debris (SSC-A vs. FSC-A) were excluded and live neutrophil granulocytes were detected using live/dead staining (amin), anti-mouse CD11b and Gr-1 Abs. Neutrophil granulocytes were identified as CD11b^{hi} Gr-1^{hi} live cells (simplified gating strategy of neutrophil granulocytes). Next, CD11c^{hi} and lineage$^+$ (gated out using a CD3, CD19, NK1.1 PE dump channel) cells were excluded from his population and remaining cells were gated on Ly6C^{int} Ly6G$^+$ cells to identify neutrophils more specifically (extended gating strategy of neutrophil granulocytes). Lower panel: live cells were gated only on CD11b$^+$ cells and CD11c^{hi} and lineage$^+$ cells were excluded. Remaining cells were then sub-gated on Ly6C^{hi} Ly6G$^-$ monocytes (green circle) and

Ly6G$^+$ Ly6C^{int} neutrophils (blue circle). This panel and gating strategy shows that excluding the CD11b^{hi} Gr-1^{hi} gating (upper panel) reveals a prominent Ly6C^{hi} Ly6G$^-$ population of monocytes. One representative mouse per group (no TBI n=6, 9 Gy TBI n=6) is shown. **C)** Percentage of Ly6G$^+$ Ly6C^{int} CD11c^{hi-} lineage$^-$ live cells of CD11b^{hi} Gr-1^{hi} single live cells. Animal numbers (n) per group are depicted. Data are presented as mean ± S.E.M.
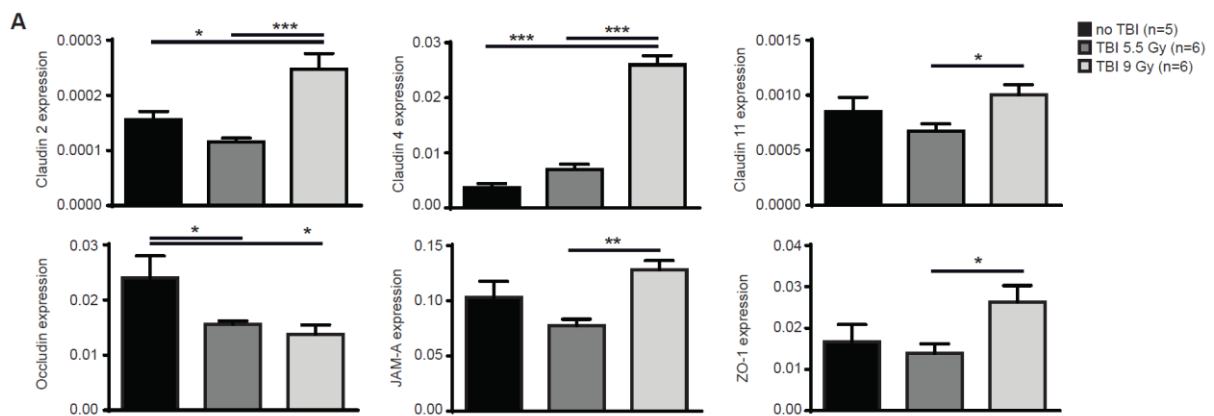
Supplementary Figure 3: Dosage of total body irradiation differentially affects gene expression of intestinal tight junction proteins

A) Gene expression of indicated genes of small intestinal tissue determined by quantitative PCR (qPCR). Balb/c mice received total body irradiation (TBI) with different doses (0Gy, 5.5Gy, 9Gy) and were analyzed 72h after treatment. Animals per group (n) are depicted. Experiments were analyzed using ordinary one-way Anova for multiple comparisons. Significance was set at P values < 0.05, p < 0.01 and p < 0.001 and was then indicated with asterisks (*, ** and ***). Data are presented as mean ± S.E.M.

GRAFT-VERSUS-HOST DISEASE

RIG-I/MAVS and STING signaling promote gut integrity during irradiation- and immune-mediated tissue injury

Julius C. Fischer,[1]* Michael Bscheider,[1]*† Gabriel Eisenkolb,[1,2]* Chia-Ching Lin,[1]
Alexander Wintges,[1] Vera Otten,[1] Caroline A. Lindemans,[3,4] Simon Heidegger,[1] Martina Rudelius,[5]
Sébastien Monette,[6] Kori A. Porosnicu Rodriguez,[2] Marco Calafiore,[4] Sophie Liebermann,[2]
Chen Liu,[7] Stefan Lienenklaus,[8] Siegfried Weiss,[9] Ulrich Kalinke,[8] Jürgen Ruland,[10,11,12]
Christian Peschel,[1] Yusuke Shono,[2] Melissa Docampo,[2] Enrico Velardi,[2] Robert R. Jenq,[4]
Alan M. Hanash,[4] Jarrod A. Dudakov,[2‡] Tobias Haas,[1§]
Marcel R. M. van den Brink,[2,4§||] Hendrik Poeck[1,2§||]

The molecular pathways that regulate the tissue repair function of type I interferon (IFN-I) during acute tissue damage are poorly understood. We describe a protective role for IFN-I and the RIG-I/MAVS signaling pathway during acute tissue damage in mice. Mice lacking mitochondrial antiviral-signaling protein (MAVS) were more sensitive to total body irradiation– and chemotherapy-induced intestinal barrier damage. These mice developed worse graft-versus-host disease (GVHD) in a preclinical model of allogeneic hematopoietic stem cell transplantation (allo-HSCT) than did wild-type mice. This phenotype was not associated with changes in the intestinal microbiota but was associated with reduced gut epithelial integrity. Conversely, targeted activation of the RIG-I pathway during tissue injury promoted gut barrier integrity and reduced GVHD. Recombinant IFN-I or IFN-I expression induced by RIG-I promoted growth of intestinal organoids in vitro and production of the antimicrobial peptide regenerating islet–derived protein 3 γ (RegIIIγ). Our findings were not confined to RIG-I/MAVS signaling because targeted engagement of the STING (stimulator of interferon genes) pathway also protected gut barrier function and reduced GVHD. Consistent with this, STING-deficient mice suffered worse GVHD after allo-HSCT than did wild-type mice. Overall, our data suggest that activation of either RIG-I/MAVS or STING pathways during acute intestinal tissue injury in mice resulted in IFN-I signaling that maintained gut epithelial barrier integrity and reduced GVHD severity. Targeting these pathways may help to prevent acute intestinal injury and GVHD during allogeneic transplantation.

INTRODUCTION

RIG-I belongs to the pattern recognition family of cytoplasmic RIG-I–like receptors. Its primary function is to detect double-stranded 5′-triphosphate RNA (3pRNA) during viral or bacterial infection (1–3). In contrast, the cytosolic DNA receptor cyclic guanosine monophosphate–adenosine monophosphate (cGAMP) synthase (cGAS) and its adapter protein STING (stimulator of interferon genes; TMEM173) recognize DNA in various contexts, for example, microbial DNA or nuclear DNA released into the cytosol by necrotic cells (4). Upon binding of ligand, RIG-I recruits the adaptor mitochondrial antiviral-signaling protein (MAVS) to induce proinflammatory cytokines, type I interferons (IFN-Is), and inflammasome activation (1, 5–8), orchestrating a diverse innate and adaptive immune response. cGAS binds to double-stranded DNA (dsDNA) and catalyzes the formation of cyclic dinucleotides. The latter can form cGAMP that activates STING to trigger innate immune gene transcription and IFN-I production (4). Whereas the role of IFN-I in initiating host defense against pathogens is well established, recent work highlights the regenerative function of this cytokine family, particularly at epithelial surfaces. IFN-I produced by plasmacytoid dendritic cells (pDCs) promotes skin repair upon mechanical barrier disruption (9) and increases intestinal epithelial turnover and repair of chemically damaged tissue. The effects of IFN-I on gut epithelial turnover have been attributed to both macrophage-dependent mechanisms (10) and Toll-like receptor stimulation of pDCs (11). However, the role of cytosolic nucleic acid sensors in this context is poorly understood. Similarly, the involvement of IFN-I in the repair of acute tissue damage by genotoxic insults has not been addressed. Unlike chemical injury of intestinal mucosa, irradiation- or chemotherapy-induced intestinal barrier dysfunction is a problem clinically.

Mucosal barriers like the intestinal epithelial cell (IEC) layer protect sterile microenvironments from physical, chemical, and microbial challenge. Epithelial integrity depends on constant and inducible IEC renewal by pluripotent intestinal stem cells (ISCs), which reside in the stem cell niche at the base of each intestinal crypt (12). Genotoxic

Fischer et al., Sci. Transl. Med. 9, eaag2513 (2017)   19 April 2017

1 of 13

stress by total body irradiation (TBI) or chemotherapy affects ISC and results in damage to the intestinal epithelium, ultimately causing translocation of microbes to sterile compartments and subsequent immune activation (*13*). During allogeneic hematopoietic stem cell transplantation (allo-HSCT), alteration of intestinal barrier function by chemotherapy or TBI administered before transplant has detrimental consequences: "Misplaced" bacterial components together with endogenous danger signals released during epithelial cell death are sensed by pattern recognition receptors on antigen-presenting cells, which then produce proinflammatory cytokines and prime donor–derived T cells (*13*). These alloreactive T cells attack and destroy host tissues, primarily the gastrointestinal tract, liver, and skin, causing morbidity and mortality in a process called acute graft-versus-host disease (GVHD). GVHD is the leading complication after allo-HSCT and occurs in as many as 50% of transplant recipients.

Thus, investigating molecular mechanisms that promote intestinal epithelial integrity and repair during tissue injury is fundamental to the development of new approaches to prevent treatment-associated inflammation and GVHD. The RIG-I/MAVS and STING signaling pathways are important regulators of IFN-I production, and IFN-I can initiate epithelial repair. Thus, we hypothesized that activation of these pathways during pretransplant bone marrow (BM) ablative therapy in mice and during allo-HSCT may protect epithelial integrity and could be exploited to promote intestinal barrier function and prevent GVHD.

RESULTS

Endogenous RIG-I/MAVS signaling reduces intestinal tissue damage induced by conditioning therapy and attenuates GVHD in mice

We first assessed genotoxic tissue damage and regeneration in wild-type (WT) mice and mice genetically deficient in MAVS (*Mavs*$^{-/-}$). Mice were exposed to lethal TBI, which caused damage to dividing cells and induced loss of intestinal epithelial barrier function (*14, 15*). Compared to *Mavs*$^{+/+}$ littermates, *Mavs*$^{-/-}$ mice exhibited worse mucosal damage in the small intestine with increased crypt apoptosis, villus atrophy, crypt abscesses, and granulocytic infiltrates (Fig. 1, A and B). Neutrophil influx into the gut mucosa, a surrogate marker for intestinal integrity (*16*), was higher in *Mavs*$^{-/-}$ compared to *Mavs*$^{+/+}$ littermates after TBI (Fig. 1C) or chemotherapy with doxorubicin (fig. S1A) (*17*). Consequently, in an acute GVHD model, where conditioning-associated intestinal damage is crucial for subsequent allogeneic T cell–mediated pathology, we observed that *Mavs*$^{-/-}$ recipients of allogeneic donor BM and T cells had increased mortality compared to *Mavs*$^{+/+}$ littermates (Fig. 1D). In addition, *Mavs*$^{-/-}$ allo-HSCT recipients exhibited greater weight
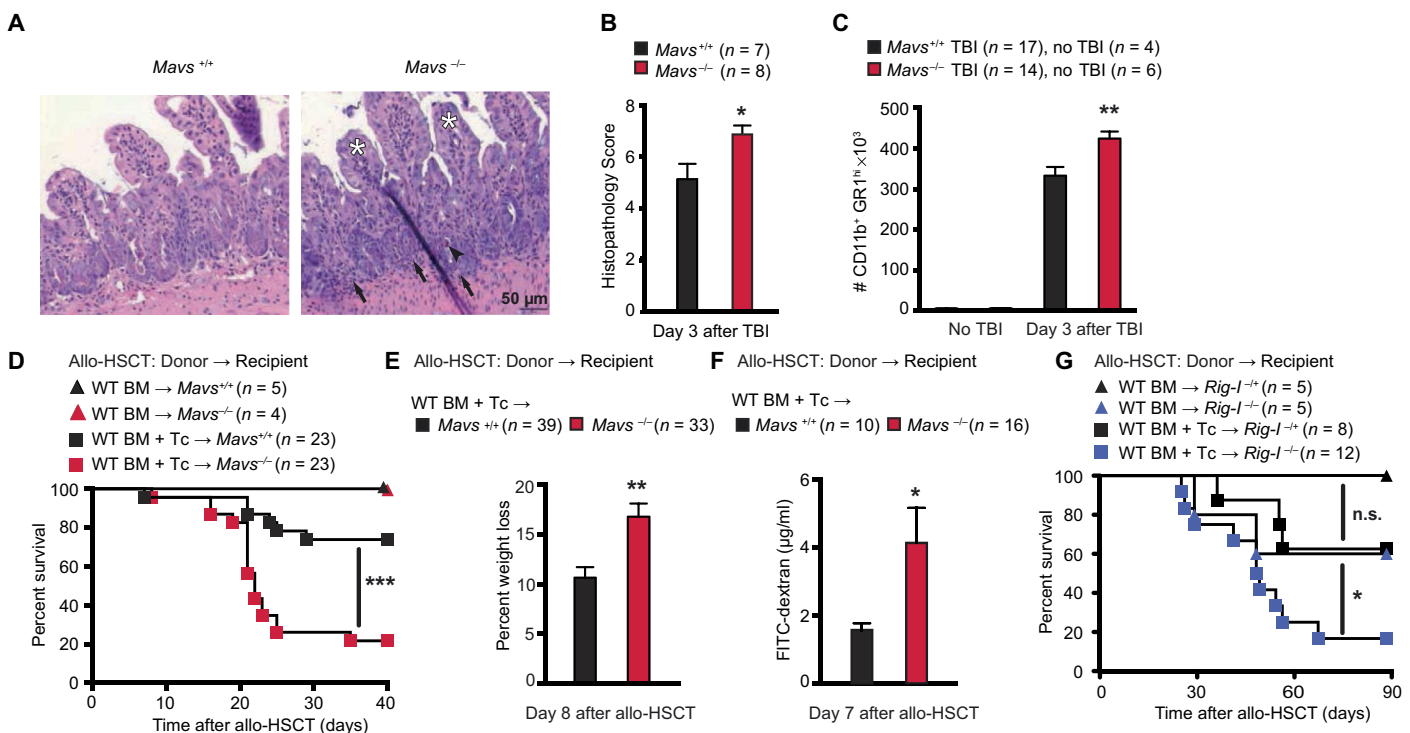

Fig. 1. Endogenous RIG-I/MAVS signaling reduces intestinal tissue damage in mice. (**A**) Representative images of tissue damage in hematoxylin and eosin–stained small intestine biopsies from mice after an 11-Gy TBI conditioning regimen. White asterisks, villus stunting; black arrowhead, crypt apoptosis; black arrows, granulocyte infiltration. (**B**) Histopathological score from (A); pooled data from two independent experiments. (**C**) Number of leukocytes infiltrating the mouse gut lamina propria after TBI (11 Gy) analyzed by flow cytometry. Pooled data from four independent experiments. Survival (**D**) and weight loss (**E**) in mouse allo-HSCT recipients transplanted with 5×10^6 BM $\pm$ 2×10^6 T cells (donor BALB/c WT and C57BL/6 *MAVS*$^{+/+}$ or *MAVS*$^{-/-}$ recipients). Pooled data from four independent experiments. (**F**) FITC-dextran concentrations in plasma after allo-HSCT [described in (D) and (E)]. Pooled data from two independent experiments. (**G**) Survival of *Rig-I*$^{-/+}$ and *Rig-I*$^{-/-}$ mouse recipients after transplant with 5×10^6 BM and 1×10^6 T cells (donor C57BL/6 WT, recipient 129/sv *Rig-I*$^{-/+}$ or *Rig-I*$^{-/-}$). Animal numbers per group (*n*) are depicted in the figure panels. Survival was analyzed using the log-rank test. All other experiments were analyzed using two-tailed unpaired *t* test. *$P < 0.05$, **$P < 0.01$, and ***$P < 0.001$. Data are means $\pm$ SEM. n.s., not significant.

loss (Fig. 1E and fig. S1, B and C) and reduced intestinal barrier integrity as measured by translocation of intraluminal fluorescein isothiocyanate (FITC)–dextran into the systemic circulation on day 7 after allogeneic transplantation (Fig. 1F and fig. S1D). $Rig\text{-}I^{-/-}$ ($Ddx58^{-/-}$) allo-HSCT recipients of donor BM and T cells also displayed increased mortality and weight loss compared to $Rig\text{-}I^{+/-}$ littermates (Fig. 1G and fig. S1E). We observed a nonsignificant trend toward higher mortality and more weight loss of $Rig\text{-}I^{-/-}$ recipients of allogeneic donor BM (Fig. 1G and fig. S1E).

MAVS signaling in nonhematopoietic cells maintains intestinal barrier function and attenuates GVHD in mice

Given that the RIG-I/MAVS pathway senses bacterial RNA (18), one hypothesis to explain our findings is that there may be mouse strain–specific differences in the intestinal bacterial microbiota. We could not detect differences between the intestinal bacterial composition of co-housed $Mavs^{-/-}$ and $Mavs^{+/+}$ littermates as assessed by 16S ribosomal RNA (rRNA) sequencing (Fig. 2A). To define the effects of RIG-I/MAVS deficiency in a compartment-specific manner, we generated BM chimeras with either a MAVS-deficient or MAVS-sufficient hematopoietic system or non-hematopoietic system, respectively. This approach yielded donor chimerism of >99% among intestinal myeloid cells (fig. S2A). BM chimeras with MAVS deleted in the nonhematopoietic system (MAVS$^{+/+}$ BM transplanted into $Mavs^{-/-}$ recipients) showed higher mortality after allo-HSCT (Fig. 2B) and more intestinal pathology in the small intestine (Fig. 2C) compared to WT recipients of WT BM (MAVS$^{+/+}$ BM transplanted into $Mavs^{+/+}$ recipients) or WT recipients with MAVS deleted in the hematopoietic system (MAVS$^{-/-}$ BM transplanted into $Mavs^{+/+}$ recipients). We next analyzed gene expression of integrin β_6 ($Itgb6$) in small intestine RNA isolates as an indicator of epithelial cell integrity after damage (19, 20) and of the antimicrobial peptide $RegIII\gamma$, which is produced by Paneth cells and protects the inner mucus layer from bacterial colonization (21). Both $Itgb6$ and $RegIII\gamma$ gene expressions were reduced in $Mavs^{-/-}$ allo-HSCT recipients compared to $Mavs^{+/+}$ littermates (Fig. 2D). Because reduced gut epithelial barrier function may promote allogeneic T cell reactivity, we next analyzed donor-derived CD4 and CD8 T cell expansion and IFN-γ production of $Mavs^{+/+}$ versus $Mavs^{-/-}$ allo-HSCT recipient mice. We observed increased T cell proliferation in the spleen of $Mavs^{-/-}$ recipients early after allo-HSCT (day 4 after transplant) but similar T cell effector function at later time points in the small intestine (day 8 after transplant) (fig. S2, B and C).

RIG-I/MAVS pathway activation protects mice from intestinal tissue damage after conditioning therapy

We observed that a single dose of intravenous 3pRNA, a RIG-I agonist, 1 day before allo-HSCT reduced mortality (Fig. 3A), weight loss (Fig. 3B and fig. S3A), and damage to the small intestine compared to control WT recipients who did not receive 3pRNA (Fig. 3C and fig. S3B). It was critical that RIG-I agonists were administered before (day −1) or at the same time as allo-HSCT (day 0), given that administration after allo-HSCT (day +1) failed to achieve a benefit (Fig. 3D and fig. S3C). Non-triphosphorylated RNA that does not activate RIG-I (22) did not reduce weight loss or improve survival (fig. S3D). This suggested that activation of the RIG-I/MAVS pathway protects from intestinal damage. Administration of 3pRNA (day −1) led to decreased gut mucosal permeability as measured by FITC-dextran translocation (Fig. 3E) and to enhanced intestinal expression of $RegIII\gamma$ in the small intestine after allo-HSCT (Fig. 3F). Similarly, pretreatment with 3pRNA lowered systemic bacteremia
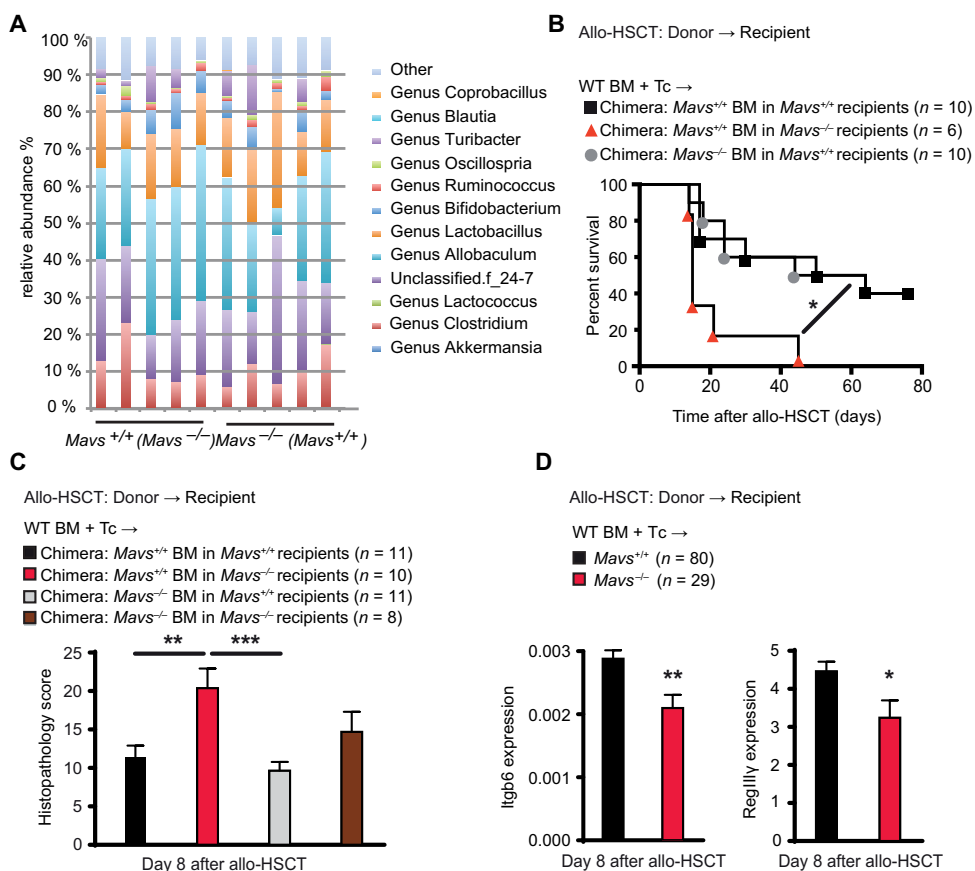

Fig. 2. MAVS signaling in nonhematopoietic cells maintains intestinal barrier function. (**A**) Average relative abundance of bacterial genera in the intestinal microbiota of cohoused $Mavs^{+/+}$ ($n = 5$) and $Mavs^{-/-}$ ($n = 5$) littermates. One representative experiment of two independent experiments. (**B**) Survival of C57BL/6 BM chimeric mice, which were Mavs-deficient either in the hematopoietic or in the nonhematopoietic compartment. These mice were analyzed after a second allo-HSCT with BM and T cells from B10.BR WT donor mice. (**C**) GVHD histopathological score for small intestine biopsies from C57BL/6 BM chimeric mice, which were Mavs-deficient either in the hematopoietic or in the nonhematopoietic compartment. These mice were analyzed after a second allo-HSCT with BM and T cells from BALB/c WT donor mice. Pooled data from two independent experiments. (**D**) Quantitative polymerase chain reaction (qPCR) of $Itgb6$ and $RegIII\gamma$ expression in the small intestine after allo-HSCT with BM and T cells from BALB/c WT mouse donors into C57BL/6 MAVS$^{+/+}$ or MAVS$^{-/-}$ recipients. Pooled data from five independent experiments. Animal numbers per group (n) are depicted above panels. Survival was analyzed using the log-rank test. Other experiments were analyzed using ordinary one-way analysis of variance (ANOVA) for multiple comparisons or two-tailed unpaired t test. *$P < 0.05$, **$P < 0.01$, and ***$P < 0.001$. Data are means ± SEM.
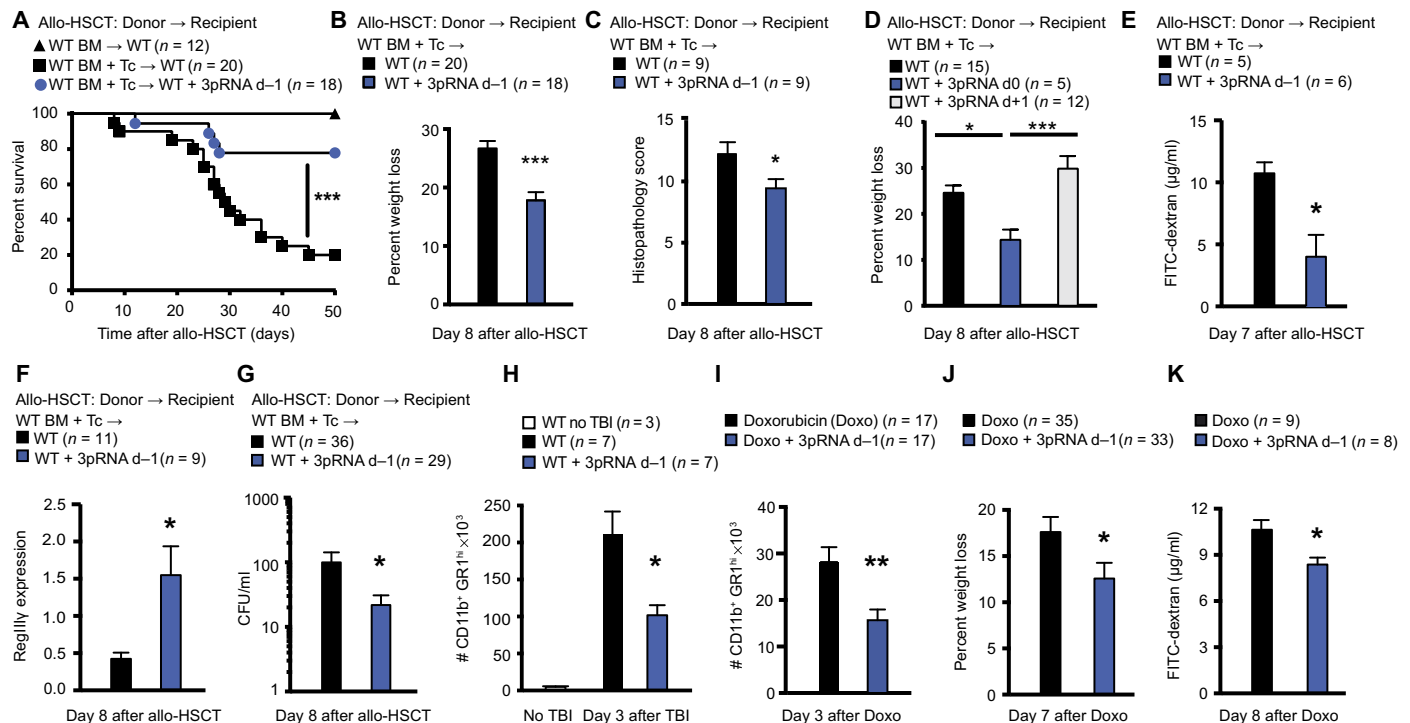
Fig. 3. RIG-I/MAVS pathway activation protects from intestinal tissue damage after TBI. Survival (**A**) and weight loss (**B**) after allo-HSCT involving transplant of 5×10^6 BM $\pm 1 \times 10^6$ T cells from C57BL/6 WT donor mice into BALB/c WT recipients with or without 3pRNA treatment on day −1. Pooled data from four independent experiments. (**C**) Histopathological score of small intestine tissue after allo-HSCT from C57BL/6 WT donor mice to BALB/c WT mouse recipients with or without 3pRNA treatment on day −1. Pooled data from two independent experiments. (**D**) Weight loss in mouse recipients from (C) after allo-HSCT with or without 3pRNA treatment on day 0 (d0) or day +1 (d+1). Pooled data from three independent experiments. (**E**) FITC-dextran concentrations in plasma after allo-HSCT from C57BL/6 WT donor mice to BALB/c WT recipient mice with or without 3pRNA treatment on day −1. (**F**) qPCR of *RegIIIγ* expression in mouse gut epithelial cells after allo-HSCT from C57BL/6 WT donor mice into BALB/c WT recipient mice with or without 3pRNA treatment on day −1. Pooled data from three independent experiments. (**G**) Bacterial colony-forming units (CFU) in sera from mouse recipients after allo-HSCT [described in (F)]. Pooled data from three independent experiments. (**H**) Leukocytes in the small intestine lamina propria of BALB/c mice after TBI (9 Gy) analyzed by flow cytometry. Pooled data from two independent experiments. (**I**) Leukocytes in the small intestine lamina propria of C57BL/6 mice after treatment with chemotherapy (doxorubicin) analyzed by flow cytometry. Pooled data from three independent experiments. (**J**) Weight loss in C57BL/6 mice that received doxorubicin (20 mg/kg). Pooled data from six independent experiments. (**K**) FITC-dextran concentrations in plasma from C57BL/6 mice after doxorubicin treatment (20 mg/kg). One representative experiment of four independent experiments is shown. Animal numbers per group (*n*) are depicted above figure panels. 3pRNA treatment was always performed on day −1 in indicated groups except for (D). All experiments were analyzed using one-tailed (G) or two-tailed unpaired *t* test or ordinary one-way ANOVA for multiple comparisons. Survival was analyzed using the log-rank test. *$P < 0.05$, **$P < 0.01$, and ***$P < 0.001$. Data are means ± SEM.

after allo-HSCT (Fig. 3G) and reduced neutrophil infiltration after TBI (Fig. 3H) but did not result in altered production of the proinflammatory cytokines interleukin-6 (IL-6) and tumor necrosis factor–α compared to TBI alone (fig. S3E). 3pRNA treatment before barrier-disrupting chemotherapy with doxorubicin also reduced neutrophil infiltration and decreased weight loss and translocation of FITC-dextran (Fig. 3, I to K, and fig. S3F). Consistent with the concept that avoiding breaching the epithelial barrier could prevent GVHD, 3pRNA pretreatment reduced allogeneic T cell activation in the spleen and intestine of allo-HSCT recipient WT mice (fig. S3, G and H). Decreased allogeneic T cell activity and GVHD may be accompanied by a reduction in the beneficial graft-versus-leukemia (GVL) response. However, application of 3pRNA on day −1 before allo-HSCT along with A20-Luc–transduced lymphoma cells did not diminish GVL activity against the latter compared to control allo-HSCT recipient WT mice who did not receive 3pRNA (fig. S3, I and J).

RIG-I–induced type I IFN signaling mediates intestinal tissue protection and prevents GVHD in mice
We next analyzed the role of IFN-I in intestinal tissue protection and prevention of GVHD. Systemic application of 3pRNA led to a rapid increase in IFN-α and IFN-β in the serum (fig. S4A), enhanced IFN-β luciferase reporter activity in the intestine of IFN-β luciferase reporter mice (fig. S4B) (*22*), and increased expression of IFN-induced genes, including RIG-I (*Ddx58*) and *Mx1*, in IECs isolated from the small intestine (fig. S4C). We then performed RNA sequencing with tissue samples from the small intestine of WT mice that received TBI before 3pRNA treatment and antibody-mediated blockade of the IFN-α/β receptor (IFNAR) (fig. S4D). 3pRNA treatment before TBI resulted in increased expression of IFN-inducible genes in the small intestine. Blockade of IFNAR signaling abrogated 3pRNA-mediated up-regulation of IFN-induced genes, demonstrating that RIG-I–induced gene regulation depends on IFN-I. Upon temporary blockade of IFNAR signaling directly before 3pRNA treatment, RIG-I agonists failed to improve overall mouse survival and early weight loss after allo-HSCT (Fig. 4A). This indicated that RIG-I agonists required IFN-I signaling to be protective. In line with our findings with 3pRNA (Fig. 3, B and D, and fig. S3C), the induction of IFN-I was only effective before TBI-induced damage. Blocking IFNAR 48 hours before tissue damage abrogated the effects of 3pRNA, whereas blockade of IFNAR 24 hours after damage did not (Fig. 4B and fig. S4E). Consistent with these results, blockade of
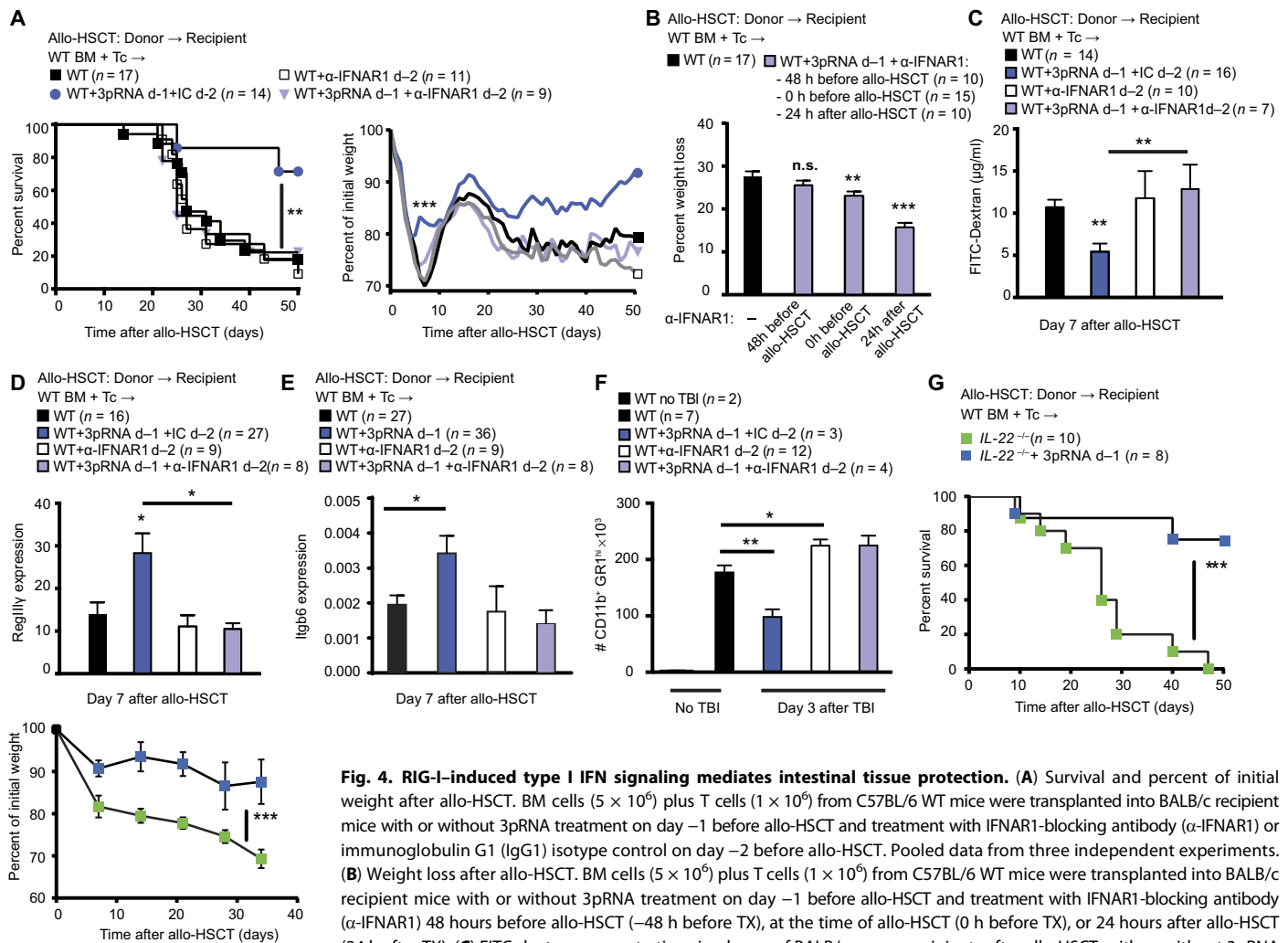
Fig. 4. RIG-I–induced type I IFN signaling mediates intestinal tissue protection. (**A**) Survival and percent of initial weight after allo-HSCT. BM cells (5×10^6) plus T cells (1×10^6) from C57BL/6 WT mice were transplanted into BALB/c recipient mice with or without 3pRNA treatment on day −1 before allo-HSCT and treatment with IFNAR1-blocking antibody (α-IFNAR1) or immunoglobulin G1 (IgG1) isotype control on day −2 before allo-HSCT. Pooled data from three independent experiments. (**B**) Weight loss after allo-HSCT. BM cells (5×10^6) plus T cells (1×10^6) from C57BL/6 WT mice were transplanted into BALB/c recipient mice with or without 3pRNA treatment on day −1 before allo-HSCT and treatment with IFNAR1-blocking antibody (α-IFNAR1) 48 hours before allo-HSCT (−48 h before TX), at the time of allo-HSCT (0 h before TX), or 24 hours after allo-HSCT (24 h after TX). (**C**) FITC-dextran concentrations in plasma of BALB/c mouse recipients after allo-HSCT, with or without 3pRNA treatment on day −1 before allo-HSCT, and treatment with IFNAR1-blocking antibody (α-IFNAR1) or IgG1 isotype control (IC) on day −2 before allo-HSCT. Pooled data from three independent experiments. (**D** and **E**) qPCR of RegIIIγ and Itgb6 expression in small intestine biopsies from BALB/c recipient mice after allo-HSCT, with or without 3pRNA treatment on day −1 before allo-HSCT, and treatment with IFNAR1-blocking antibody (α-IFNAR1) or IgG1 isotype control on day −2 before allo-HSCT. Pooled data from three (D) and six (E) independent experiments. (**F**) Flow cytometry analysis of leukocyte infiltration into the small intestine lamina propria of BALB/c mice after TBI (9 Gy), with or without 3pRNA treatment on day −1 before TBI, and treatment with IFNAR1-blocking antibody (α-IFNAR1) or IgG1 isotype control on day −2 before TBI. Pooled data from two independent experiments. (**G**) Survival and weight loss in BALB/c mouse recipients lacking IL-22 (Il-22−/−) after allo-HSCT with BM and T cells from C57BL/6 WT mice with or without 3pRNA treatment on day −1 before allo-HSCT. Pooled data from two independent experiments. Animal numbers per group (n) are depicted above figure panels. Treatment time points for 3pRNA and α-IFNAR1 antibody are indicated. All experiments were analyzed using two-tailed unpaired t test or ordinary one-way ANOVA for multiple comparisons. Survival was analyzed using the log-rank test. *P < 0.05, **P < 0.01, and ***P < 0.001. Data are means ± SEM.

IFN-I signaling 2 days before TBI-induced damage abrogated the 3pRNA-induced increase in barrier function (Fig. 4C) and the increase in RegIIIγ and Itgb6 expression during GVHD (Fig. 4, D and E), and reversed the inhibition of neutrophil influx into the gut mucosa after TBI-induced intestinal damage in WT mice (Fig. 4F). Notably, recipient-derived IL-22 has been shown to protect against tissue damage caused by conditioning therapy and GVHD (23, 24) by protecting intestinal epithelial integrity. However, 3pRNA was effective in reducing GVHD and weight loss in IL-22−/− allo-HSCT recipient mice (Fig. 4G). This suggested that IFN-I, but not IL-22, may be the mediator of RIG-I–induced protection.

RIG-I–induced type I IFN signaling in nonhematopoietic cells promotes proliferation of the ISC compartment

The observed increase in gut barrier function and increased IFN-β production in the intestine after 3pRNA administration (fig. S4B) suggested a prominent role for the nonhematopoietic system including IECs as IFN-I targets in vivo. We therefore generated BM chimeric mice with either an IFNAR1 (IFN-α/β receptor α-chain)–deficient hematopoietic compartment or an IFNAR1-deficient nonhematopoietic compartment and used them as allo-HSCT recipients with or without previous 3pRNA treatment. Mice with IFNAR1 deficiency in the nonhematopoietic system developed more severe GVHD than did those with

IFNAR1 deficiency in the hematopoietic system (fig. S5A). There was a nonstatistically significant trend toward improved survival after RIG-I agonist treatment in allo-HSCT recipients with an IFNAR1-deficient hematopoietic system but not in allo-HSCT recipients with an IFNAR1-deficient nonhematopoietic system (fig. S5A). Although these data may suggest a prominent role for IFNAR1, in the nonhematopoietic system, the origin and target of IFNs produced in vivo remain unclear. DCs are a main hematopoietic target population of IFN-I activity in vivo (25), which prompted us to analyze the effects of 3pRNA on the course of GVHD in mice in which CD11c⁺ DCs did not express IFNAR1. We found more early weight loss during GVHD in $CD11cCre\ Ifnar1^{fl/fl}$ mice, compared to cohoused $Ifnar1^{fl/fl}$ mice (Fig. 5A), whereas overall

survival was not significantly different (fig. S5B). However, 3pRNA-mediated prevention of early weight loss was unchanged (Fig. 5A), confirming a predominant role of the nonhematopoietic system in mediating the effects of IFN-I. We thus postulated that prophylactic RIG-I–triggered protection from tissue injury could be mediated by IFN signaling in IECs. To assess the direct impact of RIG-I signaling and IFN-I on IECs, we used an ex vivo organoid system composed of mouse primary small intestine crypts (26). Each of these epithelial "mini-guts" contained a functional ISC compartment that consisted of LGR5⁺ ISCs and supportive niche cells (Paneth cells) (26). Crypts cultured ex vivo grew into organoids with crypt buds that recapitulated the in vivo intestinal organization including crypt villus structures and
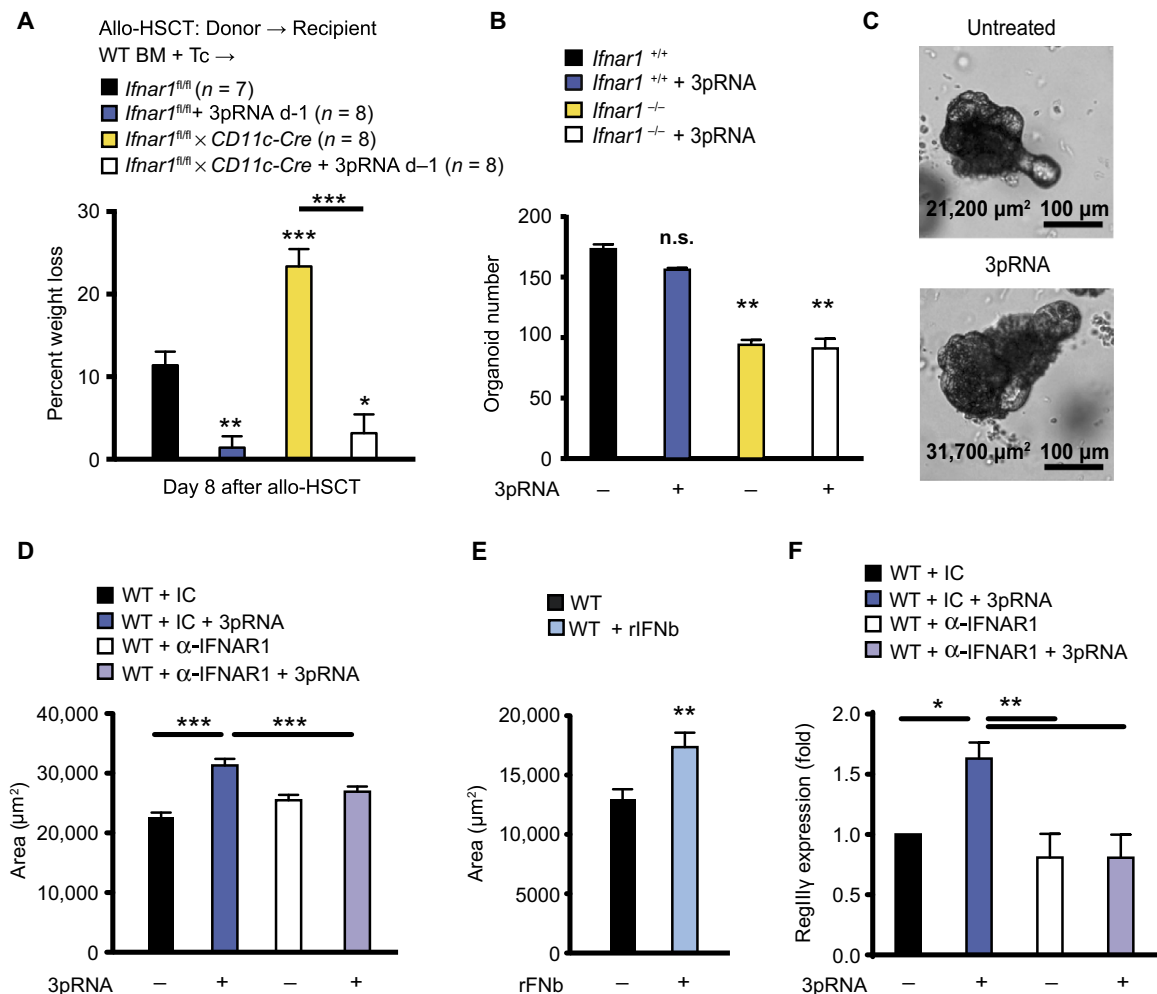
Fig. 5. RIG-I–induced type I IFN signaling in nonhematopoietic cells promotes regeneration of the ISC compartment. (**A**) Weight loss after allo-HSCT. BM cells (5×10^6) plus T cells (5×10^6) from BALB/c donor mice transplanted into C57BL/6 recipient mice (genotypes are indicated in the figure) with or without 3pRNA treatment on day −1. Pooled data from two independent experiments. (**B**) Number of organoids after 5 days in culture with or without the addition of 3pRNA (2 μg/ml) on day 1 of culture; organoids were derived from C57BL/6 IFNAR1⁺/⁺ or IFNAR1⁻/⁻ mice. One representative experiment of three independent experiments. (**C**) Representative images of organoids derived from C57BL/6 WT mice after 5 days in culture with or without the addition of 3pRNA (2 μg/ml) on day 1 of culture. Organoid area is shown. (**D**) Measurement of organoids from C57BL/6 WT mice after 5 days in culture with or without the addition of 3pRNA (2 μg/ml) or α-IFNAR1–blocking antibody (10 μg/ml) on day 1 of culture. One representative experiment of three independent experiments. (**E**) Size of organoids derived from C57BL/6 WT mice after 7 days in culture with or without the addition of recombinant murine IFN-β (20 U/ml) on day 1 of culture. One representative experiment of three independent experiments. (**F**) qPCR of RegIIIγ expression in organoids 24 hours after stimulation with indicated combinations of 3pRNA and α-IFNAR1–blocking antibody or IgG1 isotype control. Pooled data from three independent experiments. All experiments were analyzed using two-tailed unpaired t test or ordinary one-way ANOVA for multiple comparisons. Survival was analyzed using the log-rank test. *P < 0.05, **P < 0.01, and ***P < 0.001. Data are means ± SEM.

central lumen markers (27). Fewer epithelial organoids were derived from $Ifnar1^{-/-}$ compared to $Ifnar1^{+/+}$ mice, suggesting a crucial role for type I IFN signaling in epithelial regeneration (Fig. 5B). Although ex vivo stimulation with 3pRNA did not increase the number of intestinal organoids (Fig. 5B), it did increase organoid size (Fig. 5, C and D, and fig. S5C), suggesting that RIG-I activation stimulated the ISC compartment, resulting in epithelial tissue regeneration.

Similar to our in vivo findings demonstrating that 3pRNA-induced augmentation of gut barrier function was mediated by IFNAR signaling (Fig. 4, C to F), organoid growth after ex vivo 3pRNA stimulation was dependent on IFN-I produced via MAVS (fig. S5D). IFNAR blockade abrogated 3pRNA-mediated increase in organoid size (Fig. 5D and fig. S5C), whereas addition of recombinant IFN-β increased organoid size (Fig. 5E and fig. S5E). Neither recombinant IFN-β nor IFNAR blockade could influence the number of organoids (fig. S5, F and G). Yet, 3pRNA stimulation of organoid-forming crypts ex vivo also induced IFN-I–dependent RegIIIγ expression (Fig. 5F), consistent with our in vivo findings (Fig. 4D). Unlike the case with IFNAR$^{-/-}$ organoids, we could not detect an inherent difference in organoid formation between small intestine crypts isolated from $Mavs^{+/+}$ or $Mavs^{-/-}$ littermates (fig. S6A).

Furthermore, no differences in Paneth cell numbers between $Mavs^{+/+}$ and $Mavs^{-/-}$ littermates could be detected (fig. S6B), suggesting that MAVS signaling in the intestine may not be required for mediating gut homeostasis in the steady state but is required for the induction of epithelial regeneration after tissue damage. We found that the Paneth cell–derived antimicrobial peptide Lysozyme P and the ISC marker Lgr5 were both reduced in $Mavs^{-/-}$ mice compared to $Mavs^{+/+}$ littermates after allo-HSCT (Fig. 6A). We found elevated numbers of Paneth cells in allo-HSCT recipients pretreated with 3pRNA on day −1 (Fig. 6B) and elevated gene expression of Lysozyme P and the ISC marker Lgr5 (Fig. 6C). Congruent with a lack of benefit for GVHD, we found that delaying 3pRNA treatment until day +1 after allo-HSCT did not protect ISCs and Paneth cells. Lysozyme P and Lgr5 expression was reduced in mice that received 3pRNA on day +1 after allo-HSCT (Fig. 6D). We also observed that Lysozyme P and Lgr5 expression was reduced in mice 24 hours after TBI, suggesting that the lack of efficacy of 3pRNA after allo-HSCT could at least in part be due to fewer target cells in the intestinal epithelium (fig. S6C).

To determine the impact of endogenous RIG-I/MAVS signaling on intestinal regeneration during ongoing GVHD, we next analyzed the
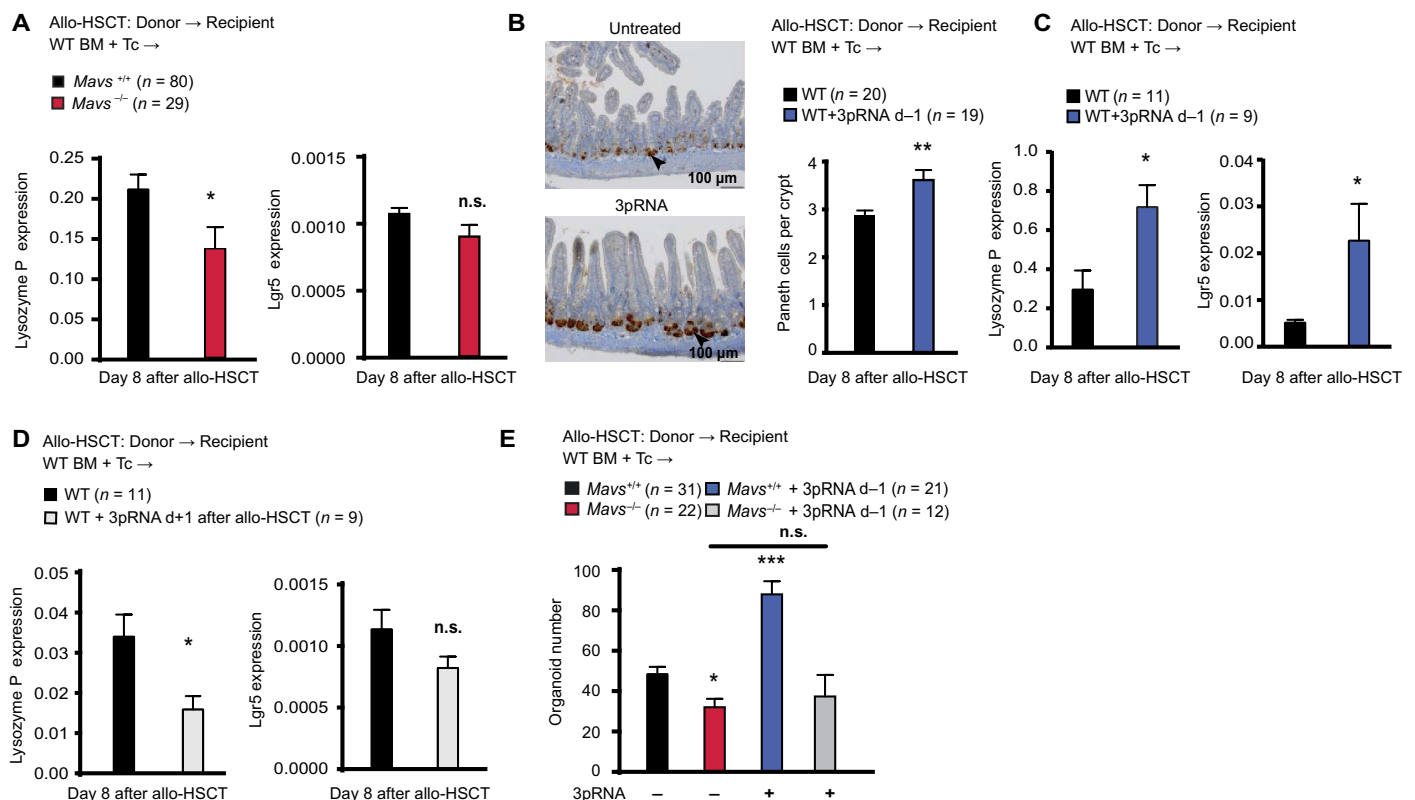

Fig. 6. RIG-I activation protects ISCs after allo-HSCT. (**A**) qPCR expression of Lysozyme P and Lgr5 in small intestine biopsies from $MAVS^{+/+}$ or $MAVS^{-/-}$ C57BL/6 recipient mice after allo-HSCT with 5×10^6 BM cells and 2×10^6 T cells from BALB/c WT donor mice. Pooled data from five independent experiments. (**B**) Analysis of allo-HSCT BALB/c recipients in the presence or absence of 3pRNA treatment on day −1. Immunohistochemistry showing lysozyme staining of the small intestine of BALB/c recipients 8 days after allo-HSCT. Lysozyme-positive gut Paneth cells are indicated by black arrowheads. Histogram shows number of Paneth cells per crypt. Representative images and pooled data from three independent experiments. (**C**) qPCR showing expression of Lysozyme P and Lgr5 in IECs from the small intestine of BALB/c recipient mice 8 days after allo-HSCT with or without 3pRNA treatment on day −1 before allo-HSCT. Pooled data from three independent experiments. (**D**) qPCR of Lysozyme P and Lgr5 expression in the small intestine of BALB/c recipient mice after allo-HSCT with or without 3pRNA treatment on day +1. Data from one experiment. (**E**) Number of organoids derived from C57BL/6 recipient mice on day 8 after allo-HSCT with or without 3pRNA treatment on day −1 before allo-HSCT. Pooled data from four independent experiments. Animal numbers per group (n) are depicted above figure panels. All experiments were analyzed using two-tailed unpaired t test or ordinary one-way ANOVA for multiple comparisons. *P < 0.05, **P < 0.01, and ***P < 0.001. Data are means ± SEM.

capacity to form intestinal organoids ex vivo in $Mavs^{+/+}$ compared to $Mavs^{-/-}$ allo-HSCT recipients. Strikingly, fewer organoids could be retrieved from $Mavs^{-/-}$ allo-HSCT recipients than from $Mavs^{+/+}$ littermates (Fig. 6E). We also found that in vivo 3pRNA treatment before (day −1) allo-HSCT induced more organoid growth compared to untreated WT recipients. This effect was absent in $Mavs^{-/-}$ allo-HSCT recipients (Fig. 6E), demonstrating that 3pRNA engages the RIG-I/MAVS pathway in vivo to exert its protective function.

STING signaling protects allo-HSCT recipients from GVHD and regulates intestinal organoid growth

Considering the protective role of RIG-I/MAVS against genotoxic tissue damage, we wondered whether other IFN-I–inducing cytosolic nucleic acid sensors would have similar effects. We therefore transplanted STING Goldenticket ($Sting^{gt/gt}$) mice with allogeneic BM and T cells. Similar to our observation in $Mavs^{-/-}$ mice, we found that $Sting^{gt/gt}$ allo-HSCT recipients showed increased mortality compared to cohoused WT mice (Fig. 7A). The composition of the gut microbiota was comparable between cohoused WT and $Sting^{gt/gt}$ mice (Fig. 7B). In parallel with our 3pRNA results, we found that allo-HSCT recipients treated with IFN-stimulatory DNA on day −1 showed reduced mortality (Fig. 7C) and weight loss (Fig. 7D). Administration of IFN-stimulatory DNA induced production of IFN-α and IFN-β in serum and, like 3pRNA, did not change TBI-induced production of proinflammatory cytokines (fig. S7, A and B). Administration of IFN-stimulatory DNA also reduced translocation of FITC-dextran across the mouse gut epithelia. This effect could be reproduced after injection of calf thymus DNA, which, in contrast to IFN-stimulatory DNA, contained CpG motifs (28) and induced IFN-I via the STING pathway (Fig. 7E) (29). Finally, STING signaling and stimulation of organoids with IFN-stimulatory DNA contributed to growth of intestinal organoids in vitro and RegIIIγ expression in an IFN-I–dependent manner (Fig. 7, F to H).

Given that pretransplant conditioning with either TBI or chemotherapy leads to accumulation of aberrant self-DNA found in apoptotic bodies, the extracellular space, and cytosol resulting in IFN-I production (30), we hypothesized that the STING pathway might mediate protection through detection of endogenous DNA. We observed increased dsDNA in the plasma of mice undergoing TBI compared to untreated mice (Fig. 7I). We next used the luciferase reporter mouse system to analyze IFN-β production in the intestine 24 hours after TBI. In comparison to untreated mice, TBI induced IFN-I signaling in the small intestine (fig. S7C).

We did not succeed in detecting endogenous RNA in mouse plasma. If endogenous RNA was released into the extracellular space upon damage, then we presumed it was rapidly degraded. Given that commensal microbiota including bacteria in the gut could potentially deliver endogenous ligands required for activation of RIG-I (18), we tested whether RNA isolated from mouse feces could induce RIG-I–dependent IFN-I signaling in IECs. Feces-derived RNA induced a RIG-I–dependent IFN-I response in MODE-K cells, a murine IEC line with morphological and phenotypic characteristics of normal enterocytes (31), arguing that 3pRNA and RNA derived from commensals including viruses, phage, or bacteria could potentially induce protective IFN-I signaling through activation of RIG-I (fig. S7, D to G).

Together, our data suggest that activation of the RIG/MAVS and STING pathways, either through endogenous or applied ligands (IFN-stimulatory DNA, 3pRNA), may be essential for protection of gut epithelial integrity after TBI or chemotherapy and for the prevention of GVHD after allo-HSCT.

DISCUSSION

Previous studies have proposed a protective function of IFN-I in the setting of allo-HSCT (32) and of stromal MAVS signaling in a dextran sodium sulfate (DSS)–induced mouse model of colitis (18), but the mechanisms by which IFN-I contributes to this protection remain ill defined. Li and co-workers (18) used a model of low-dose DSS to induce chronic tissue damage and demonstrated that MAVS signaling in stromal cells controlled tissue homeostasis by monitoring commensal bacteria. However, erosive epithelial damage by DSS is an artificial experimental approach that does not mirror common clinical scenarios, in which patients suffer from tissue damage after cytotoxic chemotherapy or radiation therapy or through immune activation. Here, we have used a series of genetically modified ($Ddx58^{-/-}$, $Mavs^{-/-}$, and $Sting^{gt/gt}$) and chimeric mice to analyze clinically relevant models of injury (TBI and chemotherapy) to the ISC compartment and immune-mediated acute tissue damage (allo-HSCT/GVHD). We have demonstrated the role of the RIG-I/MAVS/IFN-I and STING/IFN-I pathways for the maintenance of intestinal barrier function and prevention of GVHD. Specifically, we have shown that defective MAVS or STING signaling leads to breakdown of intestinal barrier function and increased GVHD pathology. Given that cohoused WT and $Mavs^{-/-}$ or $Sting^{gt/gt}$ mice harbored similar intestinal bacterial populations, it is unlikely that differences in bacterial composition contributed to the protective role of MAVS or STING during GVHD development, unlike what has been proposed for IFN-I–mediated control of Paneth cell function (33). $Rig-I^{-/-}$ mouse recipients of allogeneic BM and T cells similarly suffered from worse GVHD, and there was a nonsignificant trend toward higher mortality and more weight loss in $Rig-I^{-/-}$ mouse recipients receiving allogeneic BM only. This is reminiscent of the colitis-like phenotype of $Rig-I^{-/-}$ mice and their increased susceptibility to DSS-induced colitis (34). However, because $Rig-I^{-/-}$ mice seemed to be viable only on the 129/sv background, their higher susceptibility to external insults may be attributable to strain-specific differences.

We showed that exogenous stimulation of the RIG-I and STING pathways with 3pRNA or IFN-stimulatory DNA in a preventive setting (1 day before allo-HSCT) promoted intestinal barrier function (as measured by FITC-dextran translocation), Paneth cell function (measured by expression of Lysozyme P), Lgr5 marker expression, and the production of mucosal homeostatic factors (expression of Itgb6 and RegIIIγ), ultimately protecting the recipient from the lethal consequences of systemic GVHD. In contrast, application of RIG-I agonists 1 day after allo-HSCT did not result in protection and even decreased expression of Lysozyme P and Lgr5. As we also noticed reduced expression of Lysozyme P and Lgr5 in the gut after TBI and allo-HSCT, we speculated that this lack of therapeutic efficacy of 3pRNA could at least in part be explained by the loss of targetable IECs after pretransplant conditioning. We elucidated the temporal requirements for effective IFN-I–dependent signaling: IFNAR needed to be activated at the time of tissue damage, because early blockade of IFNAR before allo-HSCT but not late blockade after allo-HSCT totally abolished the protective effect of 3pRNA. An earlier study has reported reduction of GVHD if recombinant IFN-α was applied 1 day before allo-HSCT (32). Emphasizing the nonredundant role of the RIG-I/MAVS/IFN-I pathway in epithelial protection, RIG-I ligand–mediated protection was independent of IL-22, a cytokine that enhanced intestinal barrier integrity during allo-HSCT via protection of the ISC compartment (23, 35).

Mechanistically, IFN-I (both RIG-I–/STING-induced and recombinant IFN-β) triggered growth of primary intestinal crypt cultures, an effect that was abrogated by blocking IFNAR. Growth of these epithelial
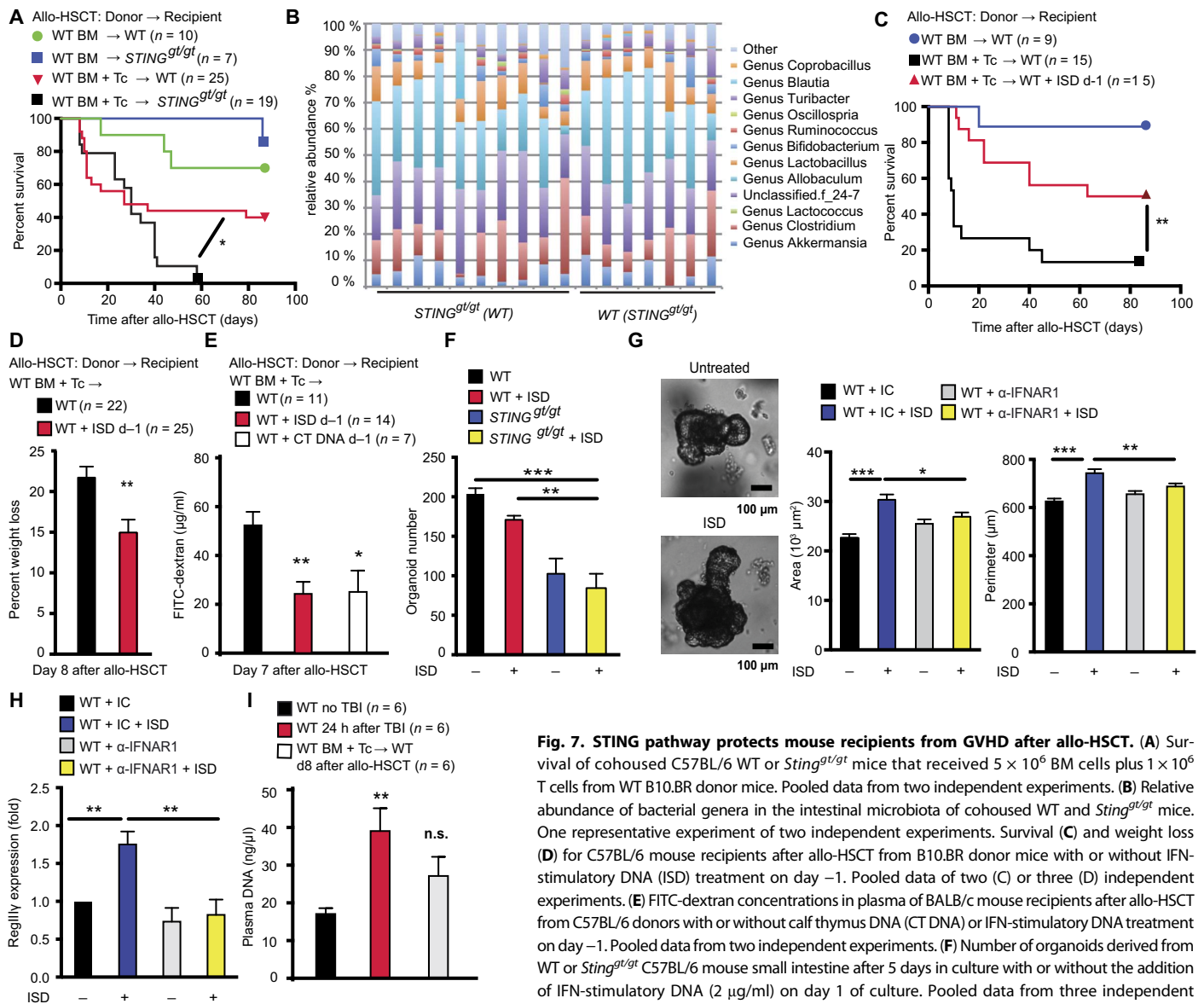
Fig. 7. STING pathway protects mouse recipients from GVHD after allo-HSCT. (A) Survival of cohoused C57BL/6 WT or $Sting^{gt/gt}$ mice that received 5×10^6 BM cells plus 1×10^6 T cells from WT B10.BR donor mice. Pooled data from two independent experiments. **(B)** Relative abundance of bacterial genera in the intestinal microbiota of cohoused WT and $Sting^{gt/gt}$ mice. One representative experiment of two independent experiments. Survival **(C)** and weight loss **(D)** for C57BL/6 mouse recipients after allo-HSCT from B10.BR donor mice with or without IFN-stimulatory DNA (ISD) treatment on day −1. Pooled data of two (C) or three (D) independent experiments. **(E)** FITC-dextran concentrations in plasma of BALB/c mouse recipients after allo-HSCT from C57BL/6 donors with or without calf thymus DNA (CT DNA) or IFN-stimulatory DNA treatment on day −1. Pooled data from two independent experiments. **(F)** Number of organoids derived from WT or $Sting^{gt/gt}$ C57BL/6 mouse small intestine after 5 days in culture with or without the addition of IFN-stimulatory DNA (2 μg/ml) on day 1 of culture. Pooled data from three independent experiments. **(G)** Organoids derived from C57BL/6 mouse small intestine. Measurement of organoid size after 5 days in culture with or without the addition of IFN-stimulatory DNA (2 μg/ml), α-IFNAR1–blocking antibody (10 μg/ml), or IgG1 isotype control on day 1 of culture. The experiment was performed three times, and images of one representative experiment are shown. **(H)** qPCR of $RegIII\gamma$ expression in organoids derived from C57BL/6 WT mice 24 hours after stimulation with indicated combinations of IFN-stimulatory DNA, α-IFNAR1–blocking antibody, or IgG1 isotype control. Pooled data from three independent experiments. **(I)** DNA in plasma of BALB/c mice 24 hours after TBI (9 Gy) or allo-HSCT. Pooled data from three independent experiments. Animal numbers per group (n) are depicted above figure panels. All experiments were analyzed using two-tailed unpaired t test or ordinary one-way ANOVA for multiple comparisons. Survival was analyzed using the log-rank test. *$P < 0.05$, **$P < 0.01$, and ***$P < 0.001$. Data are means ± SEM.

mini-guts relies on sufficient expansion of Lgr5$^+$ ISCs that eventually give rise to transient amplifying cells and, ultimately, to mature IECs. Here, we found that organoid formation capacity and production of Paneth cell–derived signals (Lysozyme P) were both reduced in $Mavs^{-/-}$ allo-HSCT recipients compared to $Mavs^{+/+}$ allo-HSCT recipients. In contrast, we could not detect any differences in organoid formation or Paneth cell numbers between $Mavs^{+/+}$ and $Mavs^{-/-}$ mice in the steady state, suggesting that MAVS and IFN-I might exert their protective functions during acute damage by activation of the ISC compartment. Along these lines, $Sting^{gt/gt}$ and $Ifnar1^{-/-}$ mice also showed defects in organoid formation.

Given that Paneth cells constitute the ISC niche and produce factors that are critical for homeostasis of Lgr5$^+$ ISCs and self-renewal in the small intestine (27, 36) including WNT, EGF (epidermal growth factor), and Notch ligands, accurately timed RIG-I– or STING-induced IFN-I signaling could modulate the production of these Paneth cell–derived signals during acute tissue damage. We observed that RIG-I ligands protected Paneth cells in allo-HSCT mouse recipients and enhanced expression of Lysozyme P and Lgr5. Moreover, RIG-I– and STING-induced IFN-I enhanced the production of $RegIII\gamma$ that could contribute to limiting intestinal tissue damage by sustaining a protective shield against bacterial colonization and translocation (21, 37). Finally, we

Fischer et al., Sci. Transl. Med. **9**, eaag2513 (2017)   19 April 2017

9 of 13

found that administration of 3pRNA before allo-HSCT allowed retrieval of more organoids from the small intestine of treated recipients compared to untreated control recipients and required the RIG-I adaptor MAVS to induce epithelial regeneration. Engagement of RIG-I in vivo thus augmented ISC function and epithelial regeneration during allo-HSCT. Given that expression of RIG-I, MAVS, and STING has previously been identified in Lgr5+ ISCs in a proteomic screen (38), future studies will clarify whether endogenous RIG-I and STING ligands and IFN-I enhance organoid growth by directly acting on Lgr5+ ISCs. Alternatively, Bmi+ ISCs, considered to be injury-inducible cells with full potential for epithelial regeneration shortly after irradiation damage (39), could be targets for RIG-I/MAVS–, STING–, or IFN-I–dependent signals.

Under conditions of chronic viral challenge and chronic IFN-I signaling, myeloid cells are the main target of IFN-I signals, controlling epithelial barrier integrity through secretion of apolipoproteins L9a/b (10). In addition, natural killer cells (both donor or recipient) reduce inflammation after irradiation-induced gut epithelial barrier loss and GVHD in several mouse models (40) and are activated by IFN-I after 3pRNA injection (22). Non-IEC IFN-I targets could contribute to the 3pRNA-induced protection against gut barrier loss and GVHD. 3pRNA increased expression of apolipoproteins L9a/b in the small intestine of irradiated WT mice, an effect that was entirely dependent on IFN-I signaling. In contrast, weight loss during GVHD in $Ifnar1^{fl/fl}$ CD11cCre mice was higher, but reduction of GVHD-associated weight loss by RIG-I activation was not affected. This suggested that although IFN-I signaling through DCs appears to be important for limiting tissue damage under certain conditions, protection from tissue injury in GVHD via RIG-I activation is not mediated by IFN-I signaling in DCs.

Our data suggested that endogenous RIG-I/MAVS and STING signaling resulted in protective IFN-I signaling to maintain epithelial barrier integrity, specifically in the context of tissue damage induced by TBI, chemotherapy, and GVHD. In this respect, identifying endogenous ligands that engage these pathways and mediate protection is of particular interest.

There are a number of limitations to our study. First, the links among the effects of IFN-I signaling on IECs, protection of gut epithelial barrier function, and reduction of GVHD are still correlative, and causal relationships remain to be formally proven. More detailed, large-scale experiments with BM chimeras and inducible, epithelia- or mesenchyme-specific IFNAR$^{-/-}$ mouse recipients are needed. Second, testing the role of RIG-I/MAVS, STING, and IFN-I in additional minor mismatch models of allo-HSCT may allow more general conclusions to be drawn about the relevance of these pathways in allo-HSCT. Similarly, exploring the role of RIG-I/MAVS, STING, and IFN-I activation in additional models of chemotherapy-induced tissue injury might extend our findings that are currently limited to doxorubicin treatment and the analysis of the RIG-I/MAVS pathway. Third, although RIG-I has been shown to be down-regulated in the intestinal epithelium of patients with Crohn's disease (41), the role of cytosolic nucleic acid sensors in human allo-HSCT and GVHD remains unclear. Intestinal gene expression analysis in patients with varying grades of GVHD may provide insights into the role of cytosolic nucleic acid sensors and open the way for prospective studies using RIG-I agonists, which are currently being developed for clinical application. Finally, given that the cytosolic DNA receptor cGAS has been shown to bind to a variety of DNA molecules including IFN-stimulatory DNA (4), we can only speculate that cGAS could be the main sensor upstream of STING to induce the protective function of dsDNA, but this requires further evaluation.

In summary, we have shown that correctly timed therapeutic activation of RIG-I or STING may offer a strategy to reduce gut epithelial barrier dysfunction and promote epithelial integrity during acute tissue damage caused by chemotherapy or TBI and thus help to prevent the development of GVHD.

MATERIALS AND METHODS
Study design
The goal of this study was to evaluate the impact of RIG-I/MAVS and STING signaling on gut integrity during acute tissue injury and GVHD in mice. To assess this, acute tissue damage was induced by TBI, cytotoxic chemotherapy, and mouse models of allo-HSCT. GVHD intensity was quantified using survival, weight loss, histopathology, and immunohistochemistry. Intestinal barrier function was analyzed using FITC-dextran translocation, expression of antimicrobial peptides, and neutrophil influx into the lamina propria. Bacteremia was measured in the serum by counting CFU. Organoid cultures of mouse small intestinal crypts were used as an indicator for epithelial regeneration. Damage-associated DNA release was quantified using total DNA isolated from mouse plasma. qPCR was performed for gene expression analysis of IFN signaling, antimicrobial peptide production, and small intestine stem or Paneth cell marker expression. 16S rRNA sequencing was performed to detect potential differences in the intestinal bacterial composition of WT, $Mavs^{-/-}$, or $Sting^{gt/gt}$ mice. For animal studies, sample sizes were chosen according to the power of the statistical test of each experiment. For all studies, animal numbers are depicted in the figures, and the number of independent experiments is listed in the figure legends. WT and genetically modified mice were randomized into experimental groups and randomly assigned to different cages. Experienced GVHD pathologists performed histopathological scoring of intestinal damage after allo-HSCT in a blinded fashion. All mouse antibodies used in this study were validated with flow cytometry by the supplier, either eBioscience, BD Biosciences, or BioLegend. Mouse antibodies and their clones are listed in table S1 (clone number, 1DegreeBio, reference ID). Cell lines were tested for mycoplasma at frequent intervals. We did not exclude outliers in any experiment. For all results, statistical tests are described in the figure legends.

Mice
$Mavs^{-/-}$ (C57BL/6) were provided by the late J. Tschopp. $Rig-I^{-/-}$ mice (129/sv) were provided by Z.-G. Wang (34). $Ifnar1^{fl/fl} \times CD11c$-Cre mice were provided by U. Kalinke (Hannover, Germany). $Sting^{gt/gt}$ mice were from the Jackson Laboratory. We used cohoused mice ($Sting^{gt/gt}$) or littermates derived from heterozygous breeding pairs as indicated in the results or figure legends.

BM transplantation
Allogeneic BM transplantation was performed as previously described (42). Recipients were given 5×10^6 T cell–depleted BM cells directly after lethal TBI. T cell depletion of BM cells was performed as previously described (43). T cell doses (MACS enrichment, Miltenyi) varied depending on the transplant model.

In vivo permeability assay
FITC-dextran assay was performed as previously described (35). FITC-dextran (#FD4-1G, Sigma) was administered by oral gavage at a concentration of 50 mg/ml in water (750 mg/kg). Four and a half hours later, plasma was collected and analyzed on a plate reader.

Fischer et al., Sci. Transl. Med. 9, eaag2513 (2017)   19 April 2017

10 of 13

In vivo analysis of neutrophil infiltration
Mice were lethally irradiated or treated with doxorubicin. On day 3, lamina propria leukocytes were isolated and neutrophils were analyzed by flow cytometry as previously described (44).

Analysis of T cell proliferation in vivo
In vivo T cell analysis was performed as previously described (45). Carboxyfluorescein diacetate succinimidyl ester (15×10^6) (eBioscience)–stained T cells were transplanted into lethally irradiated allogeneic recipients as described above.

Crypt isolation
Isolation of intestinal epithelial crypts was performed as previously described (26). Briefly, small intestines were opened longitudinally, washed, and incubated in 10 mM EDTA for 25 min (4°C). Supernatant containing crypts was collected.

Organoid culture
Two hundred fifty crypts per well were suspended in growth factor–reduced Matrigel (Corning) (33% ENR medium; 66% Matrigel) at 4°C and plated in 30-μl drops, each containing about 250 crypts. Five hundred microliters of ENR-medium [Advanced DMEM/F-12 (Life Technologies), 2 mM L-glutamine (Sigma), 10 mM Hepes (Life Technologies), penicillin (100 U/ml)/streptomycin (100 μg/ml) (Life Technologies), 1.25 mM N-acetyl cysteine (Sigma), 1 × B27 supplement (Life Technologies), 1 × N2 supplement (Life Technologies), mEGF (50 ng/ml) (PeproTech), recombinant murine Noggin (100 ng/ml) (PeproTech), 5% human R-spondin-1–conditioned medium of hR-spondin-1–transfected human embryonic kidney (HEK) 293T cells] was added to crypt cultures. Medium was replaced every 2 to 3 days. 3pRNA and IFN-stimulatory DNA were complexed with Lipofectamine 2000 (Invitrogen). Recombinant murine IFN-β [PBL (12400-1)] and/or IFNAR1 antibody/IgG1 isotype control were added with medium change.

Quantitative PCR
Total RNA was isolated and transcribed using standard methods and kits according to the manufacturer's protocols (RNeasy Mini Kit, Qiagen; SuperScript III Reverse Transcriptase, Invitrogen). The qPCR Core Kit for SYBR Green I (Eurogentec) and the LightCycler 480 II (Roche) Real-Time PCR System were used as indicated by the manufacturer. The relative transcript level of each gene was calculated according to the 2^{-Ct}, for unnormalized genes, and the $2^{-\Delta\Delta Ct}$ method, for genes normalized to β-actin.

Assessment of epithelial regeneration in intestinal organoid cultures
To determine organoid size and morphology, bright-field microscopy images were taken using a Zeiss Axiovision Observer microscope with a 5× objective lens. Two-dimensional area and perimeter were analyzed using border perimeter tracing of organoids of each well using ImageJ software.

Reagents
Double-stranded in vitro–transcribed 3pRNA (sense, 5′-UCAAACAGUC-CUCGCAUGCCUAUAGUGAGUCG-3′) was generated as described (22).

Treatments before allo-HSCT
Mice were treated at indicated time points with 3pRNA or IFN-stimulatory DNA (25 μg if not indicated otherwise). 3pRNA or IFN-stimulatory DNA was complexed in 3.5 μl of in vivo-jetPEI (Polyplus) and injected intravenously. In some experiments, mice were treated intraperitoneally with 500 μg of IFNAR1-blocking antibody/IgG1 control.

Statistics
Animal numbers per group (n) are depicted in the figure legends. We never used technical replicates. GraphPad Prism version 6 was used for statistical analysis. Survival was analyzed using the log-rank test. Differences between means of experimental groups were analyzed using two-tailed unpaired t test or ordinary one-way ANOVA. We used ordinary one-way ANOVA for multiple comparisons and always performed Dunnett's test for multiple test corrections. Applied statistical tests are indicated in the figure legends. Significance was set at $*P < 0.05$, $**P < 0.01$, and $***P < 0.001$. Data are means ± SEM.

REFERENCES AND NOTES
1. Z. Abdullah, M. Schlee, S. Roth, M. A. Mraheil, W. Barchet, J. Böttcher, T. Hain, S. Geiger, Y. Hayakawa, J. H. Fritz, F. Civril, K.-P. Hopfner, C. Kurts, J. Ruland, G. Hartmann, T. Chakraborty, P. A. Knolle, RIG-I detects infection with live Listeria by sensing secreted bacterial nucleic acids. EMBO J. 31, 4153–4164 (2012).
2. V. Hornung, J. Ellegast, S. Kim, K. Brzozka, A. Jung, H. Kato, H. Poeck, S. Akira, K.-K. Conzelmann, M. Schlee, S. Endres, G. Hartmann, 5′-Triphosphate RNA is the ligand for RIG-I. Science 314, 994–997 (2006).
3. A. Pichlmair, O. Schulz, C. P. Tan, T. I. Näslund, P. Liljeström, F. Weber, C. Reis e Sousa, RIG-I-mediated antiviral responses to single-stranded RNA bearing 5′-phosphates. Science 314, 997–1001 (2006).
4. G. N. Barber, STING-dependent cytosolic DNA sensing pathways. Trends Immunol. 35, 88–93 (2014).
5. H. Poeck, M. Bscheider, O. Gross, K. Finger, S. Roth, M. Rebsamen, N. Hannesschläger, M. Schlee, S. Rothenfusser, W. Barchet, H. Kato, S. Akira, S. Inoue, S. Endres, C. Peschel, G. Hartmann, V. Hornung, J. Ruland, Recognition of RNA virus by RIG-I results in activation of CARD9 and inflammasome signaling for interleukin 1β production. Nat. Immunol. 11, 63–69 (2010).
6. M. Yoneyama, K. Onomoto, M. Jogi, T. Akaboshi, T. Fujita, Viral RNA detection by RIG-I-like receptors. Curr. Opin. Immunol. 32, 48–53 (2015).
7. J. Pothlichet, I. Meunier, B. K. Davis, J. P.-Y. Ting, E. Skamene, V. von Messling, S. M. Vidal, Type I IFN triggers RIG-I/TLR3/NLRP3-dependent inflammasome activation in influenza A virus infected cells. PLOS Pathog. 9, e1003256 (2013).
8. L. Franchi, T. Eigenbrod, R. Muñoz-Planillo, U. Ozkurede, Y.-G. Kim, A. Chakrabarti, M. Gale Jr., R. H. Silverman, M. Colonna, S. Akira, G. Nuñez, Cytosolic double-stranded RNA activates the NLRP3 inflammasome via MAVS-induced membrane permeabilization and K⁺ efflux. J. Immunol. 193, 4214–4222 (2014).
9. J. Gregorio, S. Meller, C. Conrad, A. Di Nardo, B. Homey, A. Lauerma, N. Arai, R. L. Gallo, J. Digiovanni, M. Gilliet, Plasmacytoid dendritic cells sense skin injury and promote wound healing through type I interferons. J. Exp. Med. 207, 2921–2930 (2010).
10. L. Sun, H. Miyoshi, S. Origanti, T. J. Nice, A. C. Barger, N. A. Manieri, L. A. Fogel, A. R. French, D. Piwnica-Worms, H. Piwnica-Worms, H. W. Virgin, D. J. Lenschow, T. S. Stappenbeck, Type I interferons link viral infection to enhanced epithelial turnover and repair. Cell Host Microbe 17, 85–97 (2015).

11. J.-Y. Yang, M.-S. Kim, E. Kim, J. H. Cheon, Y.-S. Lee, Y. Kim, S.-H. Lee, S.-U. Seo, S.-H. Shin, S. S. Choi, B. Kim, S.-Y. Chang, H.-J. Ko, J.-W. Bae, M.-N. Kweon, Enteric viruses ameliorate gut inflammation via toll-like receptor 3 and toll-like receptor 7-mediated interferon-β production. *Immunity* **44**, 889–900 (2016).

12. L. W. Peterson, D. Artis, Intestinal epithelial cells: Regulators of barrier function and immune homeostasis. *Nat. Rev. Immunol.* **14**, 141–153 (2014).

13. S. Heidegger, M. R. M. van den Brink, T. Haas, H. Poeck, The role of pattern-recognition receptors in graft-versus-host disease and graft-versus-leukemia after allogeneic stem cell transplantation. *Front. Immunol.* **5**, 337 (2014).

14. B. R. Blazar, W. J. Murphy, M. Abedi, Advances in graft-versus-host disease biology and therapy. *Nat. Rev. Immunol.* **12**, 443–458 (2012).

15. R. R. Jenq, M. R. M. van den Brink, Allogeneic haematopoietic stem cell transplantation: Individualized stem cell and immune therapy of cancer. *Nat. Rev. Cancer* **10**, 213–221 (2010).

16. L. Schwab, L. Goroncy, S. Palaniyandi, S. Gautam, A. Triantafyllopoulou, A. Mocsai, W. Reichardt, F. J. Karlsson, S. V. Radhakrishnan, K. Hanke, A. Schmitt-Graeff, M. Freudenberg, F. D. von Loewenich, P. Wolf, F. Leonhardt, N. Baxan, D. Pfeifer, O. Schmah, A. Schönle, S. F. Martin, R. Mertelsmann, J. Duyster, J. Finke, M. Prinz, P. Henneke, H. Häcker, G. C. Hildebrandt, G. Häcker, R. Zeiser, Neutrophil granulocytes recruited upon translocation of intestinal bacteria enhance graft-versus-host disease via tissue damage. *Nat. Med.* **20**, 648–654 (2014).

17. S. Viaud, F. Saccheri, G. Mignot, T. Yamazaki, R. Daillère, D. Hannani, D. P. Enot, C. Pfirschke, C. Engblom, M. J. Pittet, A. Schlitzer, F. Ginhoux, L. Apetoh, E. Chachaty, P.-L. Woerther, G. Eberl, M. Berard, C. Ecobichon, D. Clermont, C. Bizet, V. Gaboriau-Routhiau, N. Cerf-Bensussan, P. Opolon, N. Yessaad, E. Vivier, B. Ryffel, C. O. Elson, J. Dorè, G. Kroemer, P. Lepage, I. G. Boneca, F. Ghiringhelli, L. Zitvogel, The intestinal microbiota modulates the anticancer immune effects of cyclophosphamide. *Science* **342**, 971–976 (2013).

18. X.-D. Li, Y.-H. Chiu, A. S. Ismail, C. L. Behrendt, M. Wight-Carter, L. V. Hooper, Z. J. Chen, Mitochondrial antiviral signaling protein (MAVS) monitors commensal bacteria and induces an immune response that prevents experimental colitis. *Proc. Natl. Acad. Sci. U.S.A.* **108**, 17390–17395 (2011).

19. J. M. Breuss, J. Gallo, H. M. DeLisser, I. V. Klimanskaya, H. G. Folkesson, J. F. Pittet, S. L. Nishimura, K. Aldape, D. V. Landers, W. Carpenter, Expression of the β6 integrin subunit in development, neoplasia and tissue repair suggests a role in epithelial remodeling. *J. Cell Sci.* **108** (Pt. 6), 2241–2251 (1995).

20. J. M. Breuss, N. Gillett, L. Lu, D. Sheppard, R. Pytela, Restricted distribution of integrin beta 6 mRNA in primate epithelial tissues. *J. Histochem. Cytochem.* **41**, 1521–1527 (1993).

21. S. Vaishnava, M. Yamamoto, K. M. Severson, K. A. Ruhn, X. Yu, O. Koren, R. Ley, E. K. Wakeland, L. V. Hooper, The antibacterial lectin RegIIIγ promotes the spatial segregation of microbiota and host in the intestine. *Science* **334**, 255–258 (2011).

22. H. Poeck, R. Besch, C. Maihoefer, M. Renn, D. Tormo, S. S. Morskaya, S. Kirschnek, E. Gaffal, J. Landsberg, J. Hellmuth, A. Schmidt, D. Anz, M. Bscheider, T. Schwerd, C. Berking, C. Bourquin, U. Kalinke, E. Kremmer, H. Kato, S. Akira, R. Meyers, G. Hacker, M. Neuenhahn, D. Busch, J. Ruland, S. Rothenfusser, M. Prinz, V. Hornung, S. Endres, T. Tüting, G. Hartmann, 5′-Triphosphate-siRNA: Turning gene silencing and Rig-I activation against melanoma. *Nat. Med.* **14**, 1256–1263 (2008).

23. J. A. Dudakov, A. M. Hanash, M. R. M. van den Brink, Interleukin-22: Immunobiology and pathology. *Annu. Rev. Immunol.* **33**, 747–785 (2015).

24. J. A. Dudakov, A. M. Hanash, R. R. Jenq, L. F. Young, A. Ghosh, N. V. Singer, M. L. West, O. M. Smith, A. M. Holland, J. J. Tsai, R. L. Boyd, M. R. M. van den Brink, Interleukin-22 drives endogenous thymic regeneration in mice. *Science* **336**, 91–95 (2012).

25. A. Dann, H. Poeck, A. L. Croxford, S. Gaupp, K. Kierdorf, M. Knust, D. Pfeifer, C. Maihoefer, S. Endres, U. Kalinke, S. G. Meuth, H. Wiendl, K. P. Knobeloch, S. Akira, A. Waisman, G. Hartmann, M. Prinz, Cytosolic RIG-I–like helicases act as negative regulators of sterile inflammation in the CNS. *Nat. Neurosci.* **15**, 98–106 (2012).

26. T. Sato, R. G. Vries, H. J. Snippert, M. van de Wetering, N. Barker, D. E. Stange, J. H. van Es, A. Abo, P. Kujala, P. J. Peters, H. Clevers, Single Lgr5 stem cells build crypt-villus structures in vitro without a mesenchymal niche. *Nature* **459**, 262–265 (2009).

27. B.-K. Koo, H. Clevers, Stem cells marked by the R-spondin receptor LGR5. *Gastroenterology* **147**, 289–302 (2014).

28. K. Yasuda, P. Yu, C. J. Kirschning, B. Schlatter, F. Schmitz, A. Heit, S. Bauer, H. Hochrein, H. Wagner, Endosomal translocation of vertebrate DNA activates dendritic cells via TLR9-dependent and -independent pathways. *J. Immunol.* **174**, 6129–6136 (2005).

29. H. Ishikawa, Z. Ma, G. N. Barber, STING regulates intracellular DNA-mediated, type I interferon-dependent innate immunity. *Nature* **461**, 788–792 (2009).

30. J. Ahn, D. Gutman, S. Saijo, G. N. Barber, STING manifests self DNA-dependent inflammatory disease. *Proc. Natl. Acad. Sci. U.S.A.* **109**, 19386–19391 (2012).

31. K. Vidal, I. Grosjean, J. P. Evillard, C. Gespach, D. Kaiserlian, Immortalization of mouse intestinal epithelial cells by the SV40-large T gene. Phenotypic and immune characterization of the MODE-K cell line. *J. Immunol. Methods* **166**, 63–73 (1993).

32. R. J. Robb, E. Kreijveld, R. D. Kuns, Y. A. Wilson, S. D. Olver, A. L. J. Don, N. C. Raffelt, N. A. De Weerd, K. E. Lineburg, A. Varelias, K. A. Markey, M. Koyama, A. D. Clouston, P. J. Hertzog, K. P. A. Macdonald, G. R. Hill, Type I-IFNs control GVHD and GVL responses after transplantation. *Blood* **118**, 3399–3409 (2011).

33. M. Tschurtschenthaler, J. Wang, C. Fricke, T. M. J. Fritz, L. Niederreiter, T. E. Adolph, E. Sarcevic, S. Kunzel, F. A. Offner, U. Kalinke, J. F. Baines, H. Tilg, A. Kaser, Type I interferon signalling in the intestinal epithelium affects Paneth cells, microbial ecology and epithelial regeneration. *Gut* **63**, 1921–1931 (2014).

34. Y. Wang, H.-X. Zhang, Y.-P. Sun, Z.-X. Liu, X.-S. Liu, L. Wang, S.-Y. Lu, H. Kong, Q.-L. Liu, X.-H. Li, Z.-Y. Lu, S.-J. Chen, Z. Chen, S.-S. Bao, W. Dai, Z.-G. Wang, *Rig-I⁻/⁻* mice develop colitis associated with downregulation of Gαi2. *Cell Res.* **17**, 858–868 (2007).

35. A. M. Hanash, J. A. Dudakov, G. Hua, M. H. O'Connor, L. F. Young, N. V. Singer, M. L. West, R. R. Jenq, A. M. Holland, L. W. Kappel, A. Ghosh, J. J. Tsai, U. K. Rao, N. L. Yim, O. M. Smith, E. Velardi, E. B. Hawryluk, C. Liu, L. A. Fouser, R. Kolesnick, B. R. Blazar, M. R. M. van den Brink, Interleukin-22 protects intestinal stem cells from immune-mediated tissue damage and regulates sensitivity to graft versus host disease. *Immunity* **37**, 339–350 (2012).

36. L. Pellegrinet, V. Rodilla, Z. Liu, S. Chen, U. Koch, L. Espinosa, K. H. Kaestner, R. Kopan, J. Lewis, F. Radtke, Dll1- and dll4-mediated notch signaling are required for homeostasis of intestinal stem cells. *Gastroenterology* **140**, 1230–1240.e7 (2011).

37. R. L. Gallo, L. V. Hooper, Epithelial antimicrobial defence of the skin and intestine. *Nat. Rev. Immunol.* **12**, 503–516 (2012).

38. J. Muñoz, D. E. Stange, A. G. Schepers, M. van de Wetering, B.-K. Koo, S. Itzkovitz, R. Volckmann, K. S. Kung, J. Koster, S. Radulescu, K. Myant, R. Versteeg, O. J. Sansom, J. H. van Es, N. Barker, A. van Oudenaarden, S. Mohammed, A. J. Heck, H. Clevers, The Lgr5 intestinal stem cell signature: Robust expression of proposed quiescent '+4' cell markers. *EMBO J.* **31**, 3079–3091 (2012).

39. K. S. Yan, L. A. Chia, X. Li, A. Ootani, J. Su, J. Y. Lee, N. Su, Y. Luo, S. C. Heilshorn, M. R. Amieva, E. Sangiorgi, M. R. Capecchi, C. J. Kuo, The intestinal stem cell markers Bmi1 and Lgr5 identify two functionally distinct populations. *Proc. Natl. Acad. Sci. U.S.A.* **109**, 466–471 (2012).

40. S. C. Nalle, J. R. Turner, Intestinal barrier loss as a critical pathogenic link between inflammatory bowel disease and graft-versus-host disease. *Mucosal Immunol.* **8**, 720–730 (2015).

41. B. Funke, F. Lasitschka, W. Roth, R. Penzel, S. Meuer, M. Saile, N. Gretz, B. Sido, P. Schirmacher, F. Autschbach, Selective downregulation of retinoic acid-inducible gene I within the intestinal epithelial compartment in Crohn's disease. *Inflamm. Bowel Dis.* **17**, 1943–1954 (2011).

42. D. Jankovic, J. Ganesan, M. Bscheider, N. Stickel, F. C. Weber, G. Guarda, M. Follo, D. Pfeifer, A. Tardivel, K. Ludigs, A. Bouazzaoui, K. Kerl, J. C. Fischer, T. Haas, A. Schmitt-Graff, A. Manoharan, L. Muller, J. Finke, S. F. Martin, O. Gorka, C. Peschel, J. Ruland, M. Idzko, J. Duyster, E. Holler, L. E. French, H. Poeck, E. Contassot, R. Zeiser, The Nlrp3 inflammasome regulates acute graft-versus-host disease. *J. Exp. Med.* **210**, 1899–1910 (2013).

43. Ö. Alpdogan, S. J. Muriglan, J. M. Eng, L. M. Willis, A. S. Greenberg, B. J. Kappel, M. R. M. van den Brink, IL-7 enhances peripheral T cell reconstitution after allogeneic hematopoietic stem cell transplantation. *J. Clin. Invest.* **112**, 1095–1107 (2003).

44. K. Neumann, M. Castiñeiras-Vilariño, U. Höckendorf, N. Hannesschlager, S. Lemeer, D. Kupka, S. Meyermann, M. Lech, H.-J. Anders, B. Kuster, D. H. Busch, A. Gewies, R. Naumann, O. Groß, J. Ruland, Clec12a is an inhibitory receptor for uric acid crystals that regulates inflammation in response to cell death. *Immunity* **40**, 389–399 (2014).

45. T. D. Kim, T. H. Terwey, J. L. Zakrzewski, D. Suh, A. A. Kochman, M. E. Chen, C. G. King, C. Borsotti, J. Grubin, O. M. Smith, G. Heller, C. Liu, G. F. Murphy, O. Alpdogan, M. R. M. van den Brink, Organ-derived dendritic cells have differential effects on alloreactive T cells. *Blood* **111**, 2929v2940 (2008).

Fischer et al., *Sci. Transl. Med.* **9**, eaag2513 (2017)   19 April 2017

12 of 13

Citation: J. C. Fischer, M. Bscheider, G. Eisenkolb, C.-C. Lin, A. Wintges, V. Otten, C. A. Lindemans, S. Heidegger, M. Rudelius, S. Monette, K. A. Porosnicu Rodriguez, M. Calafiore, S. Liebermann, C. Liu, S. Lienenklaus, S. Weiss, U. Kalinke, J. Ruland, C. Peschel, Y. Shono, M. Docampo, E. Velardi, R. R. Jenq, A. M. Hanash, J. A. Dudakov, T. Haas, M. R. M. van den Brink, H. Poeck, RIG-I/MAVS and STING signaling promote gut integrity during irradiation- and immune-mediated tissue injury. *Sci. Transl. Med.* **9**, eaag2513 (2017).

Fischer *et al.*, *Sci. Transl. Med.* **9**, eaag2513 (2017)   19 April 2017

13 of 13

Editor's Summary

A STING in the tail for GVHD

RIG-I/MAVS and cGAS/STING are innate recognition pathways that sense specific RNA or DNA patterns and induce IFN-I expression. Fischer *et al.* now show that endogenous and targeted activation of these pathways reduces intestinal injury after irradiation or chemotherapy and during graft-versus-host disease after allogeneic hematopoietic stem cell transplantation. Activation of RIG-I/MAVS and STING results in an IFN-I response that protects intestinal mucosal barrier function in vivo and promotes growth of intestinal organoids in vitro. IFN-I–mediated promotion of gut integrity correlates with attenuated graft-versus-host disease. Targeting these pathways may allow amelioration of intestinal tissue injury and regeneration of the intestinal stem cell niche.

The following resources related to this article are available online at http://stm.sciencemag.org.
This information is current as of April 19, 2017.

Article Tools	Visit the online version of this article to access the personalization and article tools: http://stm.sciencemag.org/content/9/386/eaag2513
Supplemental Materials	*"Supplementary Materials"* http://stm.sciencemag.org/content/suppl/2017/04/17/9.386.eaag2513.DC1
Permissions	Obtain information about reproducing this article: http://www.sciencemag.org/about/permissions.dtl

Science Translational Medicine

AAAS

Supplementary Materials for

RIG-I/MAVS and STING signaling promote gut integrity during irradiation- and immune-mediated tissue injury

Julius C. Fischer, Michael Bscheider, Gabriel Eisenkolb, Chia-Ching Lin,
Alexander Wintges, Vera Otten, Caroline A. Lindemans, Simon Heidegger,
Martina Rudelius, Sébastien Monette, Kori A. Porosnicu Rodriguez, Marco Calafiore,
Sophie Liebermann, Chen Liu, Stefan Lienenklaus, Siegfried Weiss, Ulrich Kalinke,
Jürgen Ruland, Christian Peschel, Yusuke Shono, Melissa Docampo, Enrico Velardi,
Robert R. Jenq, Alan M. Hanash, Jarrod A. Dudakov, Tobias Haas,
Marcel R. M. van den Brink,* Hendrik Poeck*

*Corresponding author. Email: hendrik.poeck@tum.de (H.P.); m-van-den-brink@ski.mskcc.org
(M.R.M.v.d.B.)

This PDF file includes:

Materials and Methods

Mice

C57BL/6 (H-2k^b, Thy-1.2), BALB/c (H-2k^d, Thy-1.2) were purchased from Janvier Labs (France). *Mavs$^{-/-}$* (C57BL/6) were provided by the late J. Tschopp. *Ifnar1$^{-/-}$* (C57BL/6) mice were provided by Joseph C. Sun (MSKCC), *Il-22$^{-/-}$* (Balb/c) mice were provided by Genentech. *Rig-I$^{-/-}$* mice (129/sv) were provided by Zhu-gang Wang (State Key Laboratory of Medical Genomics, Shanghai Jiao Tong University School of Medicine, Shanghai 200025, P.R.China) (*34*). *Ifn-β$^{Δβ-luc}$* mice used for in vivo imaging were backcrossed to C57BL/6 albino background (*42*). Floxed Ifnar1 mice (C57BL/6) crossed with CD11c-Cre mice (C57BL/6) were provided by U. Kalinke (Twincore, Hannover, Germany). *Sting$^{gt/gt}$* mice were from Jackson (Stock number 017537). Mice were used between 6 and 12 weeks of age at the onset of experiments and were maintained in specific pathogen free conditions. We used littermates derived from heterozygous breeding pairs (*Mavs$^{-/-}$*, *Mavs$^{+/+}$*; Ifnar1$^{fl/fl}$ CD11c-Cre$^+$, Ifnar1$^{fl/fl}$ CD11c-Cre$^-$; *Rig-I$^{-/-}$* , *Rig-I$^{+/-}$*) or cohoused mice as indicated in the results or figure legends. Animal studies were approved by the local regulatory agencies (Regierung von Oberbayern, Munich, and Landesamt für Verbraucherschutz und Lebensmittelsicherheit (LAVES), Oldenburg, Germany) and by the Memorial Sloan-Kettering Cancer Center (MSKCC) Institutional Animal Care and Use Committee (IACUC).

Bone marrow transplantation model

Allogeneic bone marrow transplants were performed as previously described (*43*). Briefly, recipients were given 5x10^6 BM cells directly after lethal total body irradiation (TBI) with 2x4.5Gy (BALB/c), 2x5.5Gy (C57BL/6) or 2x5Gy (129/sv). T cell doses (CD4/CD8 or CD5 MACS enrichment, Miltenyi) varied depending on the transplant model: Donor C57BL/6 into recipient BALB/c (0.5x10^6 or 1x10^6 when indicated), donor BALB/c into recipient C57BL/6 (2x10^6), donor C57BL/6 into recipient 129/sv (1x10^6), donor B10.BR into C57BL/6 (1x10^6). We used T cell depleted BM in all allo-HSCT experiments with BM only controls. T cell depletion of BM cells was performed as previously described (*44*)

Generation of chimeric recipients with *Mavs* or *Ifnar1* deficiency of hematopoietic or non-hematopoietic tissues

WT, *Mavs$^{-/-}$* and *Ifnar1$^{-/-}$* recipients (C57BL/6J) were injected as syngeneic bone marrow transplantation (BMT) with 5 x 10^6 WT or *Mavs$^{-/-}$* or *Ifnar1$^{-/-}$* BM cells (C57Bl/6) intravenously directly after TBI with 2x5.5Gy. Between 45 and 90 days after first syngeneic BMT, allogeneic HSCT (donor BALB/c into recipient C57Bl/6: T cell dose 2x10^6, TBI 2x5.5Gy; donor B10.BR into recipient C57BL/6: T cell dose 1x10^6, TBI 2x4.5 Gy) was performed.

In vivo permeability assay (FITC-dextran)

FITC-dextran Assay was performed as previously described (*35*). Mice were kept without food and water for 8 hours and then FITC-dextran (#FD4-1G, Sigma) was administered by oral gavage at a concentration of 50 mg/ml in water (750mg/kg). 4.5 hours later, plasma was collected from peripheral blood (8800rcf, 10min), then mixed 1:1 with PBS and

analyzed on a plate reader at an excitation wavelength of 485 nm and an emission wavelength of 535 nm.

Determination of bacteremia
To determine bacteremia, peripheral blood was collected and centrifuged at 400g for 5 min, supernatant (blood plasma) was collected, plated and incubated at 37°C under anaerobic conditions using Columbia Agar plates. After 48h CFUs were counted and bacteremia was quantified in CFUs per ml blood plasma.

Isolation of Lamina Propria Leukocytes and intestinal epithelial cells (IEC) from the small intestine
Isolation was performed as previously described (*43*). Briefly, Peyer's patches were excised from ileum (defined as distal 1/3 of small intestine) and ileums were flushed with cold PBS and cut into 2 cm pieces. Longitudinally opened intestines were washed and incubated with HBSS solution containing 2mM EDTA, 10 mM HEPES, 10% FCS (Hyclone), 1% Penicillin-Streptomycin, 1 % L-Glutamine and 1 mM DTT (all Sigma-Aldrich). After incubation on a shaker (225 rpm) at 37°C for 2 x 15 min, tissues were washed and filtered through a 100 µm strainer (BD 352360). The flow-through were centrifuged for 5 min at 1,500 r.p.m and the remaining pellet was lysed in TRIzol (Ambion) for subsequent RNA extraction. Next, intestines were incubated for 45min in PBS$^{+Ca/+Mg}$ supplemented with FCS (10%), Collagenase II (200 U/ml; Worthington), and DNase I (0.05 mg/ml; Roche) on a shaker at 37°C. Lamina Propria Leukocytes (LPL) in suspension were then purified on a 40/80% Percoll gradient (Biochrom).

In vivo analysis of neutrophil infiltration
Phenotypical analysis of neutrophils was performed as previously described (*45*). For assessment of neutrophil infiltration after TBI or doxorubicin treatment, 6-12 weeks old mice were irradiated with 9Gy (Balb/c) or 11Gy (C57BL/6) or treated with doxorubicin injected intraperitoneally (i.p.) (7.5mg/KG body weight, unless indicated otherwise). On day 3 after intervention mice were sacrificed, Lamina Propria Leukocytes were isolated, counted and neutrophils within the LPLs were analyzed by flow cytometry and normalized to the absolute number of averagely isolated cells ($1x10^6$)

Flow cytometry
Cell suspensions were stained in PBS with 3% FCS. Fluorochrome-coupled antibodies were purchased from eBioscience or BioLegend and are listed Table 1. For intracellular cytokine staining (ICS), T cells were activated with 80 nM Phorbol-12-myristat-13- acetat (PMA; Sigma), 1µM ionomycin (Merck Millipor) and Brefeldin A for 4 hours. For ICS, the Foxp3 Transcription Factor Fixation/Permeabilization Kit (eBioscience) was used according to manufacturer's instructions. Data were acquired on a FACS Canto II (BD Biosciences) and analyzed using FlowJo software (TreeStar).

Analysis of T cell proliferation *in vivo*
In vivo T cell analysis was performed as previously described (*46*). T cell and BM preparation was performed as described above. T cells were stained with 3.5 µM carboxyfluorescein diacetate succinimidyl ester (CFSE, eBioscience) for 12 minutes at

37°C, washed and counted. 15 x 10^6 stained cells were transplanted into lethally irradiated allogeneic recipients as described above. Spleens were harvested on day 3 and analyzed with FACS.

Crypt isolation
Isolation of intestinal epithelial crypts was performed as previously described (26). Briefly, after harvesting small intestines, the organs were opened longitudinally and washed. Small intestine was incubated in 10 mM ethylenediamine-tetraacetic acid (EDTA) for 25 min (4°C) to dissociate the crypts. The supernatant containing crypts was collected.

Organoid culture
250 crypts per well were suspended in liquefied growth factor reduced Matrigel (Corning) (33% ENR-medium; 66% growth factor reduced Matrigel) at 4°C. Then, they were plated in delta-surface Nunc 24-well plates in 30 µL drops, each containing approximately 250 crypts. After the Matrigel drops polymerized, 500ul complete crypt culture medium was added to small intestine crypt cultures (ENR-medium: advanced DMEM/F12 (Life technologies), 2 mM L-glutamine (Sigma), 10 mM HEPES (Life technologies), 100 U/ml penicillin/100 µg/ml streptomycin (Life technologies), 1.25 mM N-acetyl cysteine (Sigma), 1x B27 supplement (Life technologies), 1x N2 supplement (Life technologies), 50 ng/ml mEGF (Peprotech), 100ng/ml rec. mNoggin (Peprotech), 5% human R-spondin-1 conditioned medium of hR-spondin-1-transfected HEK 293T cells). Together with the crypt culture medium, 2µg/ml of 3pRNA or 2µg/ml of ISD complexed with Lipofectamine 2000 (Invitrogen) or recombinant murine (rm) IFN-β (20U/ml; PBL (12400-1)) was added. All plates were incubated at 37 °C/5% CO2 and medium was replaced every 2-3 days. IFN-β was added again with every medium change. For IFNαR1 blockade, 10ug/ml of antibody were added to the matrigel before polymerization and with every medium change (MAR1-5A3 anti-mIFNalphaR1 antibody or MOPC-21 Mouse IgG1 as isotype control (BioXCell)).

Histopathologic analysis
Intestines were harvested 8 days after allo-HSCT or 72 hours after TBI for histopathologic assessment of intestinal tissue injury. Samples were formalin-preserved, paraffin-embedded, sectioned, and stained with hematoxylin and eosin (H&E). For evaluation of intestinal GVHD after allo-HSCT, blinded scoring was performed by experienced pathologists (C.L. or M.R.) as previously described (47). For evidence of intestinal tissue damage after TBI, tissues were examined by four established criteria in a blinded fashion by a pathologist (S.M.): crypt apoptosis (% of crypt containing at least 1 apoptotic cell), crypt abscesses (Absent (0), Present (1)), granulocytic infiltrates (Absent (0), minimal (1), mild (2), moderate (3), marked (4)) and villus atrophy (absent (0), minimal (1), mild (2), moderate (3), marked (4)). Each mouse was given an individual cumulative score (histopathology score) based on the above criteria.

Immunohistochemistry
Intestines of mice 8 days after allo-HSCT were harvested, formalin-fixed, paraffin embedded. The immunohistochemical detection of Lysozyme was performed using Discovery XT processor (Ventana Medical Systems). The tissue sections were

deparaffinized with EZPrep buffer (Ventana Medical Systems), antigen retrieval was performed with CC1 buffer (Ventana Medical Systems) and sections were blocked for 30 minutes with Background Buster solution (Innovex). Slides were incubated with anti-Lysozyme antibodies (DAKO; cat# A099; 2ug/ml) for 5h, followed by 60 minutes incubation with biotinylated goat anti-rabbit IgG (Vector labs, cat#PK6101) at 1:200 dilution. The detection was performed with DAB detection kit (Ventana Medical Systems) according to manufacturer´s instruction. Slides were counterstained with hematoxylin (Ventana Medical Systems) and coverslipped with Permount (Fisher Scientific). To quantify Lysozyme$^+$ Paneth cells, the number of positive cells per crypt was evaluated over a 5000 µm length of intestinal mucosa. Lysozyme$^+$ Paneth cells are depicted as mean Paneth cell number / crypt. Quantification was performed in a blinded fashion by S.M.

Detection of bioluminescence and in vivo imaging

Ifn-β$^{\Delta\beta\text{-luc}}$ mice were injected i.v. with 100 µl luciferin (30 mg/ml in PBS)/20 g mouse weight and anesthesized using isoflurane. Within 10 min after luciferin injection, mice or isolated organs were analyzed with an in vivo imaging instrument (IVIS 200; PerkinElmer). The acquired images were analyzed using Living Image 4.4. software.

Quantitative PCR

RNA was isolated from cells lysed in TRIzol (ambion) or from whole tissue homogenates. Tissue homogenates were prepared as follows: 1 cm large or small intestine was flushed and longitudinally opened pieces were frozen in 500ul TRIzol reagent using liquid nitrogen. After thawing, samples were supplemented with stainless stell beads 5mm (Qiagen) and homogenized using a Tissuelyser II (Qiagen) 1 min with 30Hz (1800 oscillations/minute). Total RNA was isolated and transcribed using standard methods and kits according to manufacturer´s protocols (RNeasy Mini Kit, Qiagen; SuperScript III Reverse Transcriptase, invitrogen). The specific primer pairs were as follows: mRegIII*γ* fwd TTCCTGTCCTCCATGATCAAAA, rev CATCCACCTCTGTTGGGTTCA; mActin fwd CACACCCGCCACCAGTTCG, rev CACCATCACACCCTGGTGC; mLgr5 fwd ACCCGCCAGTCTCCTACATC rev GCATCTAGGCGCAGGGATTG; mLysozymeP fwd CAG GCCAAGGTCTACAATCG, rev TTGATCCCACAGGCATTCTT.; mItgb6 fwd ATTGTCATTCCCAATGATGG, rev CATAGTTCTCATACAGATGGAC. The qPCR Core kit for SYBR Green I (Eurogentec) and a LightCycler 480 II (Roche) Real-Time PCR System were used as indicated by the manufacturer. The relative transcript level of each gene was calculated according to the 2−Ct, for unnormalized genes, and the 2−ΔΔCt method, for the genes normalized to *β-Actin*. Alternatively, the following Taqman Expression Assay IDs were used: BETA-ACTIN Mm01205647_g1; IFNB1 Mm00439552_s1; REG3G Mm00441127_m1;

Measurement of cytokines

TNF and IL-6 were analyzed using the Cytometric Bead Array Enhanced Sensitivity Flex Set System (BD) according to manufacturer's instructions. IFNα and IFNβ were analyzed by ELISA (PBL Assay Science) according to manufacturer's instructions.

Assessment of epithelial regeneration in intestinal organoid cultures
To determine the effect of 3pRNA / interferon stimulatory DNA / rmIFN-β on organoid size and morphology, bright-field microscopy images were taken using a Zeiss Axiovision Observer microscope with a 5x objective lens after 5 or 7 days in culture. 2D area and perimeter were analyzed using border perimeter tracing of organoids found in four representative fields of each well using Image J software. For assessment of gene expression by quantitative (q) PCR, organoids were subjected to RNA extraction 24 hours after culture using Trizol reagent (Invitrogen) according to manufacturer's protocol. Isolated RNA was reverse-transcribed using the Quantitect Reverse Transcription Kit (Qiagen). Gene expression was assessed by quantitative real-time PCR using Taqman Expression Assay pre-designed probes (Applied Biosystems). Signals were normalized to *β-Actin*. mRNA expression. Normalized values were used to calculate relative expression by ΔΔCt analysis or absolute expression by ΔCt. Taqman IDs are depicted below (qPCR).

Reagents
OptiMEM reduced-serum medium was from Invitrogen. Double-stranded in vitro-transcribed 3pRNA (sense, 5′- UCA AAC AGU CCU CGC AUG CCU AUA GUG AGU CG -3′) was generated as described (*22*). Synthetic dsRNA with the same sequence but lacking the 5′-triphosphate (synRNA) was purchased from Eurofins (Ebersberg, Germany). Interferon stimulatory DNA was purchased from Invivogen.

Drug treatment
Mice were treated on indicated time points with 3pRNA or interferon stimulatory DNA (25 µg if not indicated otherwise). 3pRNA / interferon stimulatory DNA was complexed in 3.5 µl in vivo-jetPEI (Polyplus) and injected intravenously. In some experiments mice were treated i.p. with 500ug IFNaR1 blocking antibody (Clone: MAR1-5A3, BioXCell, West Lebanon, NH) or IgG1 Isotype control (Clone: MOPC-21, BioXCell, West Lebanon, NH) as indicated.

16S RNA gene Sequencing
Stool specimens were stored at -80°C. DNA was purified using a phenol-chloroform extraction technique with mechanical disruption (bead-beating) based on a previously described protocol (*48*) and analyzed using the Illumina MiSeq platform to sequence the V4-V5 region of the 16S rRNA gene. Sequence data were compiled and processed using mothur version 1.34(*49*), screened and filtered for quality (*50*), then classified to the species level (*51*) using a modified form of the Greengenes reference database (*52*), screened and filtered for quality (*50*), then classified to the species level (*51*) using a modified form of the Greengenes reference database (*52*).

Quantification of Plasma DNA levels
Mouse plasma was collected from peripheral blood (8800rcf, 10min). Plasma samples of 3-4 mice were combined to a final volume of 400-500µl and DNA extracted using the QIAamp Circulating Nucleic Acids Kit (Qiagen). dsDNA was quantified using a Qubit 2.0 Fluorometer with the Qubit dsDNA HS Assay Kit (Thermo Fisher Scientific).

GVT model and bioluminescence imaging

A20-TGL (H-2^d), a BALB/c B-cell lymphoma, were generated as described previously (*53*). A20-TGL tumor cells were inoculated via separate intravenous injection on the day of allo-BMT (*54*). To visualize and quantify tumor burden, A20-TGL inoculated mice were administered D-luciferin (Goldbio), anesthetized, and imaged using in vivo bioluminescence imaging systems (Caliper Life Sciences)

Cell lines, culture and RNA transfection, feces RNA isolation

Mode-K cells were purchased from Dominique Kaiserlian (French Institute of Health and Medical Research, Unit of Immunity Infection Vaccination, France) and cultured as previously described (*31*). Cell lines were tested as mycoplasma negative. Where indicated, MODE-K cells were transfected with mouse RIG-I siRNA (100μM, Eurofins Genomics,) or control siRNA (Qiagen) using Lipofectamine 2000 (Life Technologies) according to manufacturer's instructions. After 48 h, cells were transfected with 3pRNA (0.8μg/mL) or mouse feces-derived RNA complexed to Lipofectamine 2000. Supernatants were collected and RNA was extracted 18h after transfection followed by IFN-β measurement with ELISA (PBL Assay Science) or by assessment of IFN-β mRNA by qPCR. Mouse feces from healthy WT mice was diluted (RNAprotect Reagent, Quiagen) and homogenized with Glass beads (Sigma) and a Tissuelyser II (Qiagen). After centrifugation, supernatant was subtracted and total feces RNA was isolated using standard methods and kits according to manufacterers' protocols.

Gene Expression Profiling Analysis

For gene expression profiling analysis, (i) Balb/c mice were solely irradiated (9Gy) (n=3), (ii) pretreated with 3pRNA prior (d-1) to irradiation (n=3) or (iii) pre-treated with 3pRNA (d-1) + α-IFNaR1 blocking antibody (d-2) prior to irradiation (n=3). RNA from small intestines was isolated 12 h after irradiation and used for RNA sequencing. Poly(A) RNA sequencing was performed with three biological replicates for each group and analyzed with an Illumina HiSeq2500 platform. The heatmap depicted in Fig. S4D shows all genes listed in the interferome database (*55*) that show significantly changed gene expression of 3pRNA pretreated and irradiated mice compared to both the other groups simultaneously.

Data Analyis

The output data (FASTQ files) were mapped to the target genome using the rnaStar aligner that maps reads genomically and resolves reads across splice junctions. We used the 2 pass mapping method in which the reads are mapped twice. The first mapping pass used a list of known annotated junctions from Ensemble. Novel junctions found in the first pass were then added to the known junctions and a second mapping pass was done. After mapping we computed the expression count matrix from the mapped reads using HTSeq (www-huber.embl.de/users/anders/HTSeq) and one of several possible gene model databases. The raw count matrix generated by HTSeq was then processed using the R/Bioconductor package DESeq (www-huber.embl.de/users/anders/DESeq) which was used to both normalize the full dataset and analyze differential expression between sample groups.

A heatmap was generated using the heatmap.2 function from the gplots R package. The data plot was the mean centered normalized log2 expression of the top 100 significant

genes. For simple hierarchical clustering the correlation metric was used (Dij = 1 - cor(Xi,Xj)) with the Pearson correlation on the normalized log2 expression values.

Statistics

Animal numbers per group (n) are depicted in the figure legends. We never used technical replicates. GraphPad Prism version 6 was used for statistical analysis. Survival was analyzed using the Log-rank test. Differences between means of experimental groups were analyzed using two-tailed unpaired t test or ordinary one-way Anova correspondingly to the distribution shape of our observations. We used ordinary one-way Anova for multiple comparisons and always performed Dunnett's test for Multiple-test corrections. Applied statistical tests are indicated in the figure legends. Significance was set at p values < 0.05, p < 0.01 and p < 0.001 and was then indicated with asterisks (*, ** and ***). Data are presented as mean ± S.E.M.

Table S1. Antibodies.

Target structure	Clone#	1DegreeBio ID
CD11b	M1/70	1DB-001-0001021785
CD11c	N418	1DB-001-0000839554
CD3	17A2	1DB-001-0001110661
CD4	GK1.5	1DB-001-0000263404
CD45.1	A20	1DB-001-0000839250
CD45.2	104	1DB-001-0000839196
CD8a	53-6.7	1DB-001-0000263247
IFNaR1	MAR1-5A3	1DB-001-0000840263
IFN γ	XMG1.2	1DB-001-0001110823
Ly-6G/Ly-6C (Gr-1)	RB6-8C5	1DB-001-0000839101
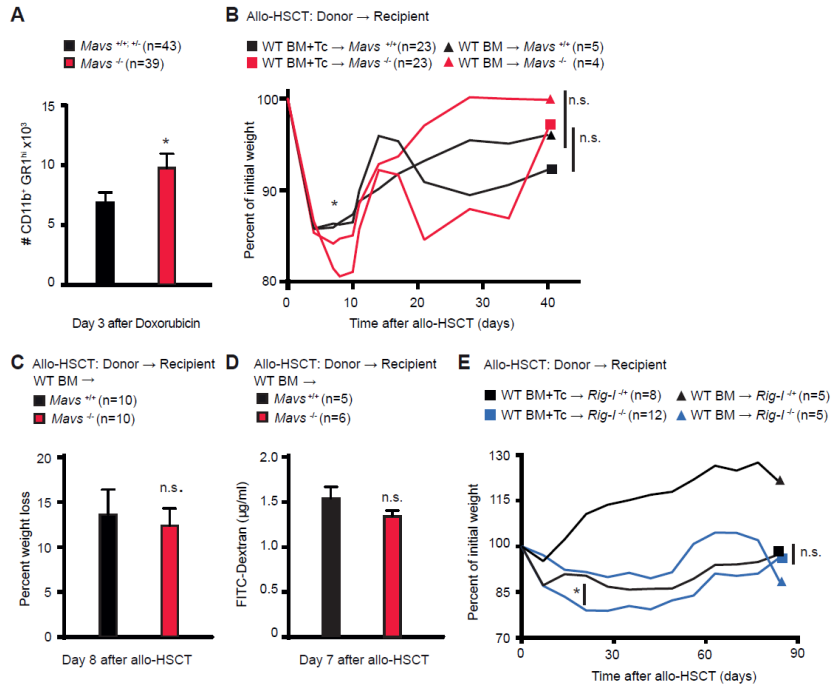
Figure S1. Endogenous RIG-I / MAVS signaling reduces intestinal tissue damage by conditioning therapy and attenuates GVHD. (A) LPL isolated from small intestines of *Mavs*^{+/+}/ *Mavs*^{+/-} and *Mavs*^{-/-} mice were analyzed by flow cytometry on day 3 after treatment with doxorubicin (20mg/kg). Pooled data of 3 independent experiments. Animal numbers per group (n) are depicted. **(B)** Weight loss of *Mavs*^{+/+} and *Mavs*^{-/-} animals after TBI + 5×10^6 BM alone or BM with 2×10^6 T cells (donor BALB/c into recipient C57BL/6). Pooled data of 4 independent experiments. Animal numbers per group (n) are depicted. **(C)** Weight loss on day 8 after allo-HSCT of *Mavs*^{+/+} and *Mavs*^{-/-} animals after TBI + 5×10^6 BM alone (donor BALB/c into recipient C57BL/6). Pooled data of (B) and one additional independent experiment. Animal numbers per group (n) are depicted. **(D)** FITC-dextran concentrations in the serum of *Mavs*^{+/+} and *Mavs*^{-/-} recipients on d7 after TBI + 5×10^6 BM alone (donor BALB/c into recipient C57BL/6). Animal numbers per group (n) are depicted. **(E)** Weight loss of *Rig-I*^{-/+} and *Rig-I*^{-/-} animals after TBI + 5×10^6 BM alone or BM with 1×10^6 T cells (donor C57BL/6 into recipient 129/sv). Animal numbers per group (n) are depicted. Experiments were analyzed using two-tailed unpaired t test. Significance was set at p values < 0.05, p < 0.01 and p < 0.001 and was then indicated with asterisks (*, ** and ***). Data are presented as mean ± S.E.M

Figure S2. Donor-derived T cells show enhanced alloreactivity in *Mavs*$^{-/-}$ allo-HSCT recipients. (A) CD45.2^{+} C57BL/6 recipients (n=3) received TBI (11Gy) and 5×10^{6} syngeneic CD45.1^{+} BM and were analyzed 43 days after BMT and compared to CD45.2^{+} animals that did not receive TBI and BMT (n=3). Shown is the analysis of small intestine live lamina propria leukocytes (LPL) of one representative animal per group. **(B)** *Mavs*$^{+/+}$ and *Mavs*$^{-/-}$ littermates received TBI + 5×10^{6} BM cells and 15×10^{6} CFSE labeled T cells (donor BALB/c into recipient C57BL/6). On day 4 after allo-HSCT splenic cells were analyzed by flow cytometry to identify proliferating CFSE labeled donor T-cells. Pooled data of 2 independent experiments. Animal numbers per group (n) are depicted. **(C)** LPL isolated from small intestines of *Mavs*$^{+/+}$ and *Mavs*$^{-/-}$ mice that received TBI + 5×10^{6} BM cells and 2×10^{6} T cells (donor BALB/c into recipient C57BL/6) were analyzed on day 8 after allo-HSCT by flow cytometry. Pooled data of 2 independent experiments. Animal numbers per group (n) are depicted. All experiments were analyzed using two-tailed unpaired t test. Significance was set at p values < 0.05, p < 0.01 and p < 0.001 and was then indicated with asterisks (*, ** and ***). Data are presented as mean ± S.E.M.
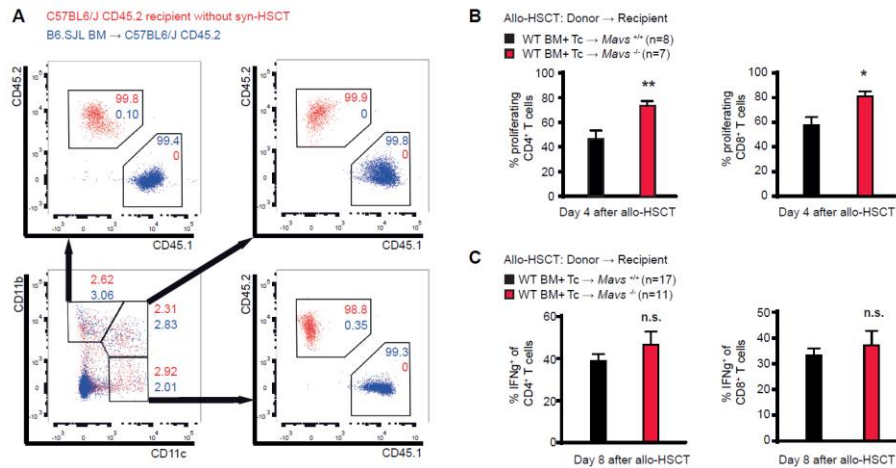
A Allo-HSCT: Donor → Recipient
▲ WT BM → WT (n=12)
■ WT BM + Tc → WT (n=20)
● WT BM + Tc + 3pRNA d-1 → WT (n=18)

B Allo-HSCT: Donor → Recipient
WT BM + Tc →
■ WT (n=16)
■ WT + 3pRNA d-1 (n=15)

C Allo-HSCT: Donor → Recipient
WT BM + Tc →
■ WT (n=15)
● WT + 3pRNA d0 (n=5)
▲ WT + 3pRNA d+1 (n=12)

D Allo-HSCT: Donor → Recipient
■ WT BM+Tc → WT (n=14)
● WT BM+Tc → WT + 3pRNA d-1 (n=14)
▲ WT BM+Tc → WT + synRNA d-1 (n=14)

E
■ WT (n=7)
■ WT + 3pRNA d-1 (n=8)

F
■ WT+ Doxorubicin (n=35)
● WT+ Doxorubicin + 3pRNA d-1 (n=33)

G Allo-HSCT: Donor → Recipient
■ WT BM + Tc → WT (n=3)
■ WT BM + Tc → WT + 3pRNA d-1 (n=3)

H Allo-HSCT: Donor → Recipient
■ WT BM + Tc → WT (n=11)
■ WT BM + Tc → WT + 3pRNA d-1 (n=8)

I Allo-HSCT: Donor → Recipient
WT BM + A20-TGL → ▲ WT (n=8)
WT BM + A20-TGL+Tc → ■ WT (n=11)
WT BM + A20-TGL+Tc → ● WT + 3pRNA d-1 (n=8)

J Day 21 after allo-HSCT
BM + A20-TGL
BM + A20-TGL + Tcells (0.5M)
BM + A20 -TGL + T cells (0.25M)
BM + A20-TGL + T cells (0.5M) + 3pRNA d-1
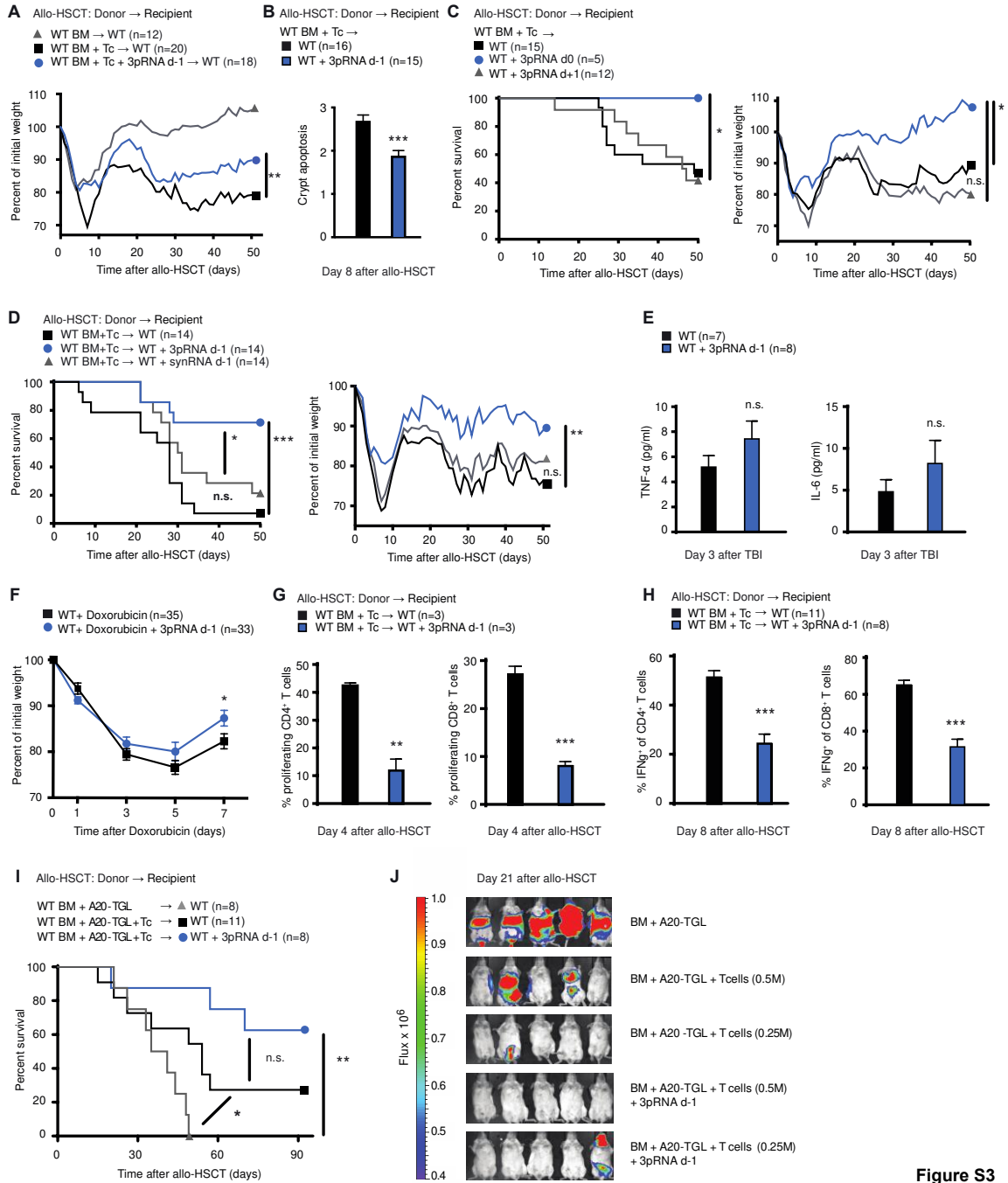BM + A20-TGL + T cells (0.25M) + 3pRNA d-1

Figure S3

Figure S3. RIG-I ligands have to be applied before or during allo-HSCT to exert their protective effects and do not affect GVL. (**A**) Weight loss of animals after 9Gy TBI + $5x10^6$ BM alone with $1x10^6$T cells (donor C57BL/6 into recipient BALB/c). Indicated mice were either left untreated or treated with 3pRNA on day -1. Pooled data of 4 independent experiments. Animal numbers per group (n) are depicted. (**B**) Histopathological analysis of crypt apoptosis of small intestines from allo-HSCT recipients (donor C57BL/6 into recipient BALB/c). Indicated mice were either left untreated or treated with 3pRNA on day -1. Pooled data of 3 independent experiments. Animal numbers per group (n) are depicted. (**C**) Survival and weight loss of allo-HSCT recipients (donor C57BL/6 into recipient BALB/c). Indicated mice were either left untreated or treated with 3pRNA on day 0 or d+1. Pooled data of 3 independent experiments. Animal numbers per group (n) are depicted. (**D**) Survival and weight loss of allo-HSCT recipients (donor C57BL/6 into recipient BALB/c, 9Gy TBI + $5x10^6$ BM + $1x10^6$T cells). Indicated mice were left untreated or treated with 3pRNA or non-triphosphorylated control RNA (synRNA) on day -1. Pooled data of 2 independent experiments. Animal numbers per group (n) are depicted. (**E**) Measurement of serum cytokines of BALB/c mice on day 3 after TBI (9 Gy) using cytometric bead array (CBA). Indicated mice were left untreated or treated with 3pRNA on d-1. Pooled data of 3 independent experiments. Animal numbers per group (n) are depicted. (**F**) Weight loss of WT mice (C57BL/6) receiving doxorubicin (20mg/kg). Indicated animals were treated with 3pRNA on d-1 or were left untreated. Pooled data of 6 independent experiments. Animal numbers per group (n) are depicted. (**G**) BALB/c mice received TBI + $5x10^6$ BM cells and $15x10^6$ CFSE labeled T cells (donor C57BL/6 into recipient BALB/c). On day 4 after allo-HSCT splenic cells were analyzed by flow cytometry to identify proliferated CFSE labeled donor T cells. Shown is one representative of 2 independent experiments. Animal numbers per group (n) are depicted. (**H**) Lamina propria leukocytes (LPL) isolated from small intestines of BALB/c mice on day 8 after allo-HSCT (donor C57BL/6 into recipient BALB/c) were analyzed by flow cytometry. Indicated mice were left untreated or treated with 3pRNA on d-1. Pooled data of 3 independent experiments. Animal numbers per group (n) are depicted. (**I**) Survival of BALB/c mice that received 8.5Gy TBI + $5x10^6$ BM alone or $5x10^6$ BM and $0.5x10^6$ T cells (donor C57BL/6 into recipient BALB/c) and that were inoculated with $0.25x10^6$ A20 tumor cells. Pooled data of 2 independent experiments. Animal numbers per group (n) are depicted. (**J**) Allo-HSCT recipients were inoculated with A20-TGL and *in vivo* bioluminescence imaging was conducted to determine tumor burden. Bioluminescence of one representative experiment on d21 after allo-HSCT is shown. All experiments were analyzed using two-tailed unpaired t test or ordinary one-way Anova for multiple. Survival was analyzed using the Log-rank test. Significance was set at p values < 0.05, p < 0.01 and p < 0.001 and was then indicated with asterisks (*, ** and ***). If not otherwise indicated, significance was calculated compared to untreated groups. Data are presented as mean ± S.E.M.

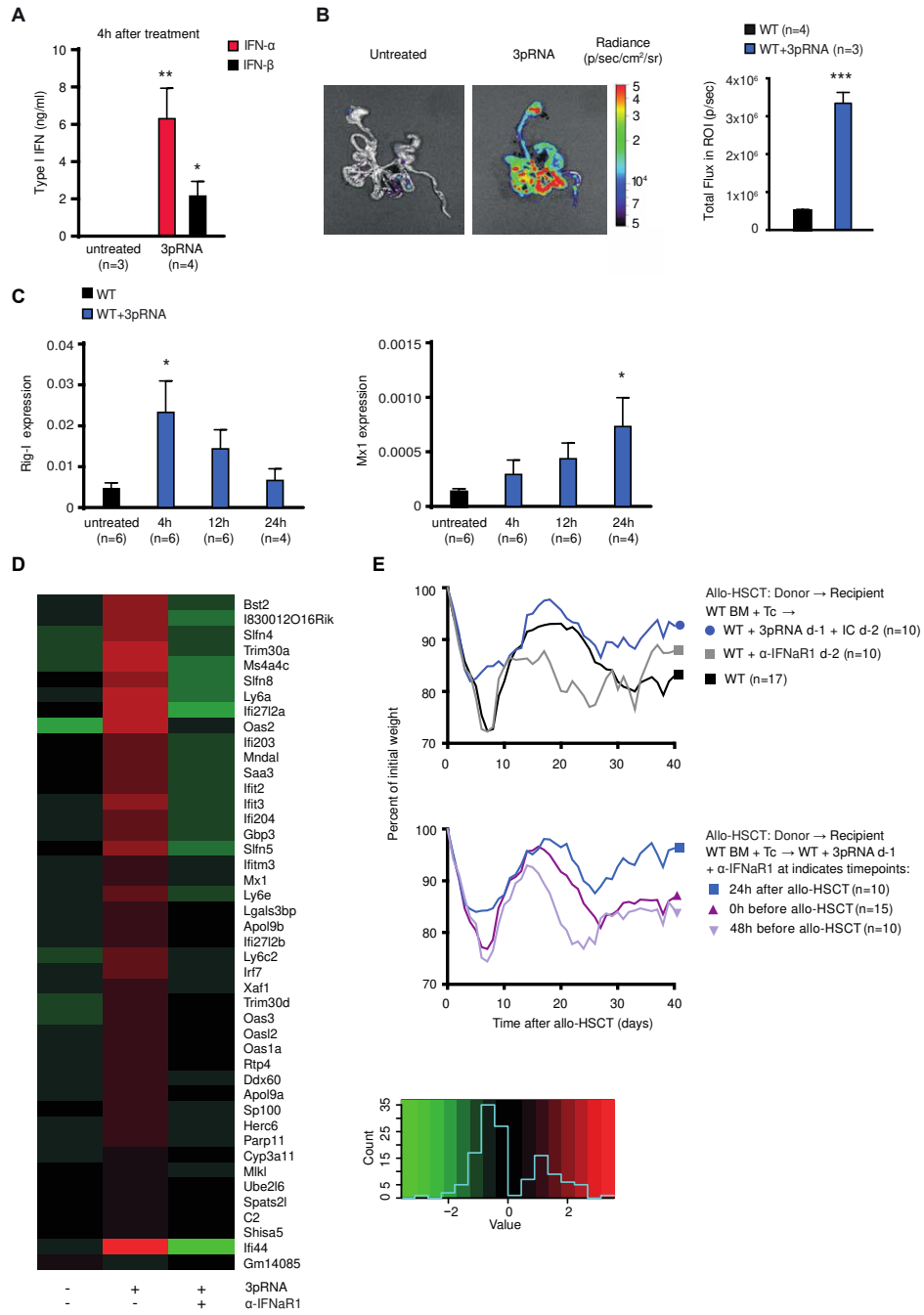Figure S4

Figure S4. RIG-I–induced treatment effects are mediated by IFN-Is. (**A**) Serum Type I IFN levels of untreated or 3pRNA treated BALB/c WT mice were determined 4 h after i.v. injection of 25ug 3pRNA or vehicle control (jetPEI). Animal numbers per group (n) are depicted. (**B**) Left panel: Albino C57BL/6 mice carrying an IFN-$\beta^{\Delta\beta\text{-luc}}$ allele were injected i.v. with 25 µg 3pRNA. 24 hours later, luciferin was injected i.v., and luciferase activity of isolated intestines was determined by bioluminescence imaging (one representative image is shown). Right Panel: The luciferase activity was quantified in a region of interest covering the small intestine (n=4 mice in untreated group; n=3 mice in the 3pRNA treated group). One representative experiment is shown. (**C**) *Rig-I* mRNA transcript expression (left panel) and *Mx1* mRNA transcript expression (right panel) was determined in small intestinal epithelial cells of untreated or 3pRNA-treated BALB/c mice at the indicated time points. Relative transcript levels were normalized to the housekeeping gene *β-Actin*. Shown are pooled data of 2 independent experiments. Animal numbers per group (n) are depicted. (**D**) Heatmap depicting interferon regulated genes of Balb/c mice that were solely irradiated (9Gy) (n=3, **left lane**), (ii) pretreated with 3pRNA prior (d-1) to irradiation (n=3, **middle lane**) or (iii) pre-treated with 3pRNA (d-1) + α-IFNaR1 blocking antibody (d-2) prior to irradiation (n=3; **right lane**). RNA from small intestines was isolated 12 h after irradiation and used for RNA sequencing. The heatmap shows all genes listed in the interferome database that show significantly changed gene expression of 3pRNA pretreated and irradiated mice compared to both the other groups simultaneously. (**E**) Weight loss of allo-HSCT recipients. Indicated mice received 3pRNA on d-1 and/or α-IFNaR1 blocking. Both upper and lower panel show pooled data of the same 3 independent experiments. The lower panel shows mice that received combination treatment of 3pRNA and α-IFNaR1 blocking Ab at indicated time points. Animal numbers per group (n) are depicted. All experiments were analyzed using two-tailed unpaired t test or ordinary one-way Anova for multiple comparisons. Survival was analyzed using the Log-rank test. Significance was set at p values < 0.05, p < 0.01 and p < 0.001 and was then indicated with asterisks (*, ** and ***). If not otherwise indicated, significance was calculated compared to untreated groups. Data are presented as mean ± S.E.M.
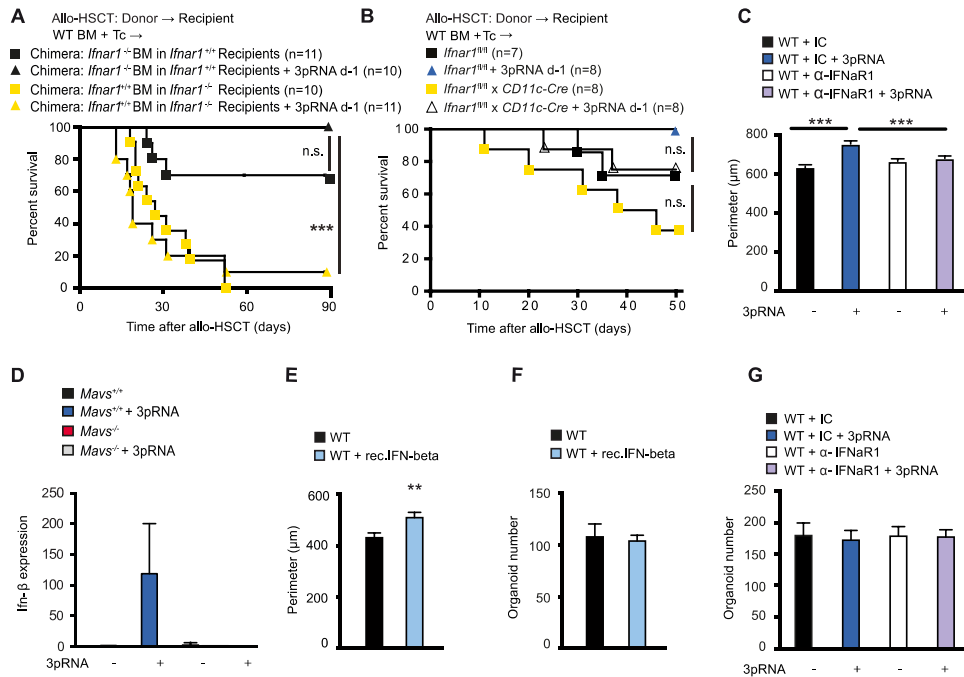
Figure S5. RIG-I–induced IFN-Is enhance epithelial regeneration through stimulation of the ISC compartment. (**A**) 90 days after syngeneic bonemarrow transplantation between *Ifnar1*^{-/-} and *Ifnar1*^{+/+} mice (C57BL/6), bonemarrow chimera were lethally irradiated and transplanted with 5×10^6 BM cells with 1×10^6 T cells from donor B10.BR mice and monitored for survival. Indicated mice were either left untreated or treated with 3pRNA on d-1. Pooled data of 2 independent experiments. Animal numbers per group (n) are depicted. (**B**) Survival of either *Ifnar1*^{fl/fl} or *Ifnar1*^{fl/fl} *CD11cCre* allo-HSCT recipients (donor BALB/c into recipient C57BL/6) in the presence or absence of 3pRNA (d-1). Pooled data of 2 independent experiments. Animal numbers per group (n) are depicted (**C**) Measurement of organoid size (perimeter) of C57BL/6 small intestinal organoids after 5 days in culture. Indicated crypts were treated with 3pRNA (2µg/ml), α-IFNaR1 blocking Ab (10ug/ml) or IgG1 Isotype control (IC). The experiment was performed 3 times and one representative experiment is shown. (**D**) *IFN-β* mRNA transcript expression 24 hours after 3pRNA stimulation of *Mavs*^{+/+} or *Mavs*^{-/-} small intestinal organoids. The experiment was performed 3 times and resulting data were pooled. (**E**) Measurement of organoid size (perimeter) of C57BL/6 small intestinal organoids after 5 days in culture. Indicated crypts were treated with rec. IFN-β (20U/ml). The experiment was performed 3 times and one representative experiment is shown. (**F**) Number of organoids of C57BL/6 small intestinal organoids after 7 days in culture. Indicated Crypts were treated with rec. IFN-β (20U/ml). (**G**) Number of C57BL/6 small intestinal organoids treated as in (**C**) after 7 days in culture. Survival was analyzed using the Log-rank test. All other experiments were analyzed using two-tailed unpaired t test or ordinary one-way Anova for multiple comparisons. Significance was set at p values < 0.05, p < 0.01 and p < 0.001 and was then indicated with asterisks (*, ** and ***). Data are presented as mean ± S.E.M.
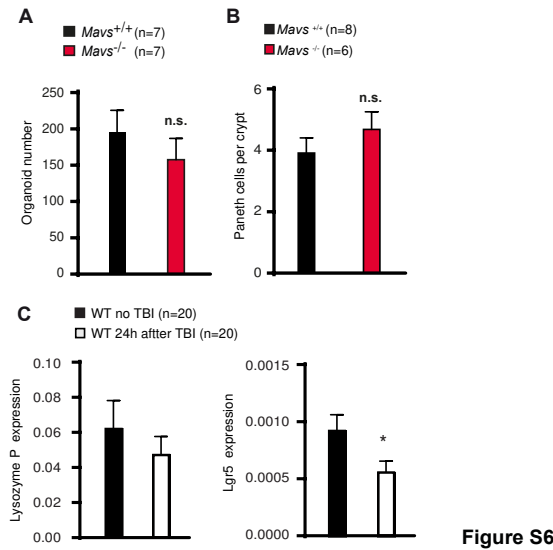
Figure S6. MAVS-deficient mice do not display an inherent defect in organoid formation or in the number of Paneth cells. (A) Number of organoids grown *ex vivo* from small intestinal crypts of *Mavs*$^{+/+}$ and *Mavs*$^{-/-}$ mice after 5 days in culture. Pooled data of 7 independent experiments. Animal numbers per group (n) are depicted. **(B)** Determination of Lysozyme^{+} paneth cells per crypt in the ileum of untreated *Mavs*$^{+/+}$ and *Mavs*$^{-/-}$ mice using immunohistochemistry (IHC). Pooled data of 2 independent experiments. Animal numbers per group (n) are depicted. **(C)** RNA of small intestines from Balb/c WT mice isolated 24 hours after irradiation (9Gy). Gene expression was determined by qPCR. Relative transcript levels of *Lysozyme* P and *Lgr5* were normalized to the housekeeping gene *β-Actin*. Pooled data of 2 independent experiments. Animal numbers per group (n) are depicted. All experiments were analyzed using two-tailed unpaired t test or ordinary one-way Anova for multiple comparisons or. Significance was set at p values < 0.05, p < 0.01 and p < 0.001 and was then indicated with asterisks (*, ** and ***). Data are presented as mean ± S.E.M.
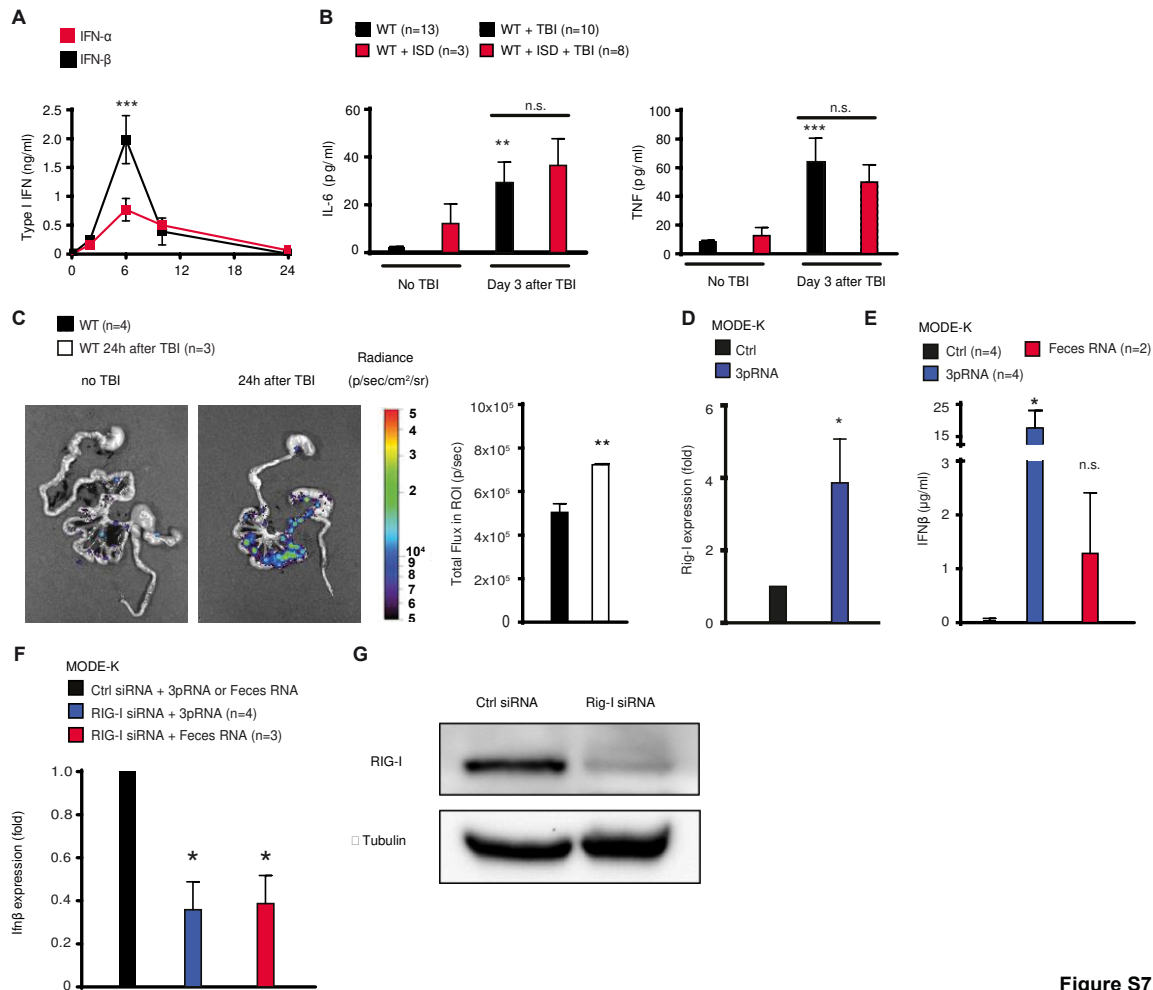
Figure S7. TBI and IFN-stimulatory DNA induce a systemic IFN-I response and feces-derived RNA triggers a RIG-I-dependent IFN-I response in IECs. (A) Serum levels of IFN-α and IFN-β were determined at the indicated time points (hours) after *i.v.* injection of 50µg interferon-stimulatory DNA (ISD) into C57BL/6. Pooled data of n=2 independent experiments (n=2-5 per time point). **(B)** Serum levels of IL-6 (left panel) and TNF-α (right panel) of untreated or irradiated (9Gy), ISD or TBI + ISD stimulated BALB/c mice. Serum levels of the indicated proteins were determined by cytometric bead array (CBA). Pooled data of 2 independent experiments. Animal numbers per group (n) are depicted. **(C)** Left panel: Albino C57BL/6 mice carrying an IFN-β$^{Δβ\text{-luc}}$ allele received TBI (11Gy). 24 hours later, luciferin was injected *i.v.* and luciferase activity of isolated intestine was determined. Right Panel: The luciferase activity was quantified in a region of interest covering the small intestine (n=4 mice in untreated group; n=3 mice in the TBI group). **(D)** *Rig-I* mRNA transcript expression and **(E)** IFN-β protein expression in murine MODE-K cells 18 hours after treatment with feces-derived RNA or 3pRNA.

Number of pooled experiments depicted. **(F)** Ifn-β mRNA transcript expression 18 hours after stimulation of control- or *Rig-I*-siRNA transfected murine MODE-K cells with mouse feces-derived RNA or 3pRNA. Number of pooled experiments depicted. **(G)** RIG-I protein expression in control- or *Rig-I*-siRNA transfected murine MODE-K cells was analyzed using western blot. Number of pooled experiments depicted. The experiments were analyzed using two-tailed unpaired t test or ordinary one-way Anova for multiple comparisons. Significance was set at p values < 0.05, p < 0.01 and p < 0.001 and was then indicated with asterisks (*, ** and ***). Data are presented as mean ± S.E.M.

IV. Danksagung

Mein wichtigster Dank gilt meiner Familie und Freunden, deren vielschichtige Unterstützung den Ausgang der vorliegenden Arbeit grundgelegt und gesichert hat.

Für die herausragende und sehr enge Betreuung, die mit intensiven Auseinandersetzungen mit einer Vielzahl an wissenschaftlichen Fragestellungen, Problemen und persönlichen Entscheidungen verbunden war, danke ich Hendrik Poeck und Tobias Haas in einem besonders großen Maße.

Michael Bscheider gilt mein spezieller und besonderer Dank für seine Einführung in die Durchführung wissenschaftlicher Arbeiten und vor allem für seinen wissenschaftlichen Enthusiasmus, der mich nachhaltig angesteckt hat.

Für die freundschaftliche Zusammenarbeit danke ich besonders Gabriel Eisenkolb, Vera Otten und Martina Schmickl, sowie allen meinen Mitdoktoranden und Arbeitskollegen, die mich von 2012-2017 begleitet und unterstützt haben.

Eidesstattliche Erklärung

Ich erkläre an Eides statt, dass ich die bei der promotionsführenden Einrichtung bzw. Fakultät
Klinik und Poliklinik für Innere Medizin III, Hämatologie und Onkologie, Klinikum rechts der Isar der
medizinischen Fakultät der TU München
der TUM zur Promotionsprüfung vorgelegte Arbeit mit dem Titel:

Die Rolle zytosolischer Nukleinsäurerezeptoren bei Strahlentherapie- oder Chemotherapie-induziertem
intestinalen Gewebeschaden und der Graft-versus-host disease

in
Klinik und Poliklinik für Innere Medizin III, Hämatologie und Onkologie, Klinikum rechts der Isar der
medizinischen Fakultät der TU München

(Lehrstuhl bzw. Fachgebiet oder Klinik)

unter der Anleitung und Betreuung durch

PD. Dr. Hendrik Poeck

ohne sonstige Hilfe erstellt und bei der Abfassung nur die gemäß § 6 Abs. 6 und 7 Satz 2
angegebenen Hilfsmittel benutzt habe.

(x) Ich habe keine Organisation eingeschaltet, die gegen Entgelt Betreuerinnen und
Betreuer für die Anfertigung von Dissertationen sucht, oder die mir obliegenden
Pflichten hinsichtlich der Prüfungsleistungen für mich ganz oder teilweise erledigt.

(x) Ich habe die Dissertation in dieser oder ähnlicher Form in keinem anderen
Prüfungsverfahren als Prüfungsleistung vorgelegt.

(   ) Die vollständige Dissertation wurde in ....

veröffentlicht. Die promotionsführende Einrichtung...
hat der Vorveröffentlichung zugestimmt.

(x) Ich habe den angestrebten Doktorgrad **noch nicht** erworben und bin **nicht** in einem
früheren Promotionsverfahren für den angestrebten Doktorgrad endgültig gescheitert.

(   ) Ich habe bereits am ....

bei der Fakultät für ....

der Hochschule ....

unter Vorlage einer Dissertation mit dem Thema ....

....

die Zulassung zur Promotion beantragt mit dem Ergebnis:

....

Die öffentlich zugängliche Promotionsordnung der TUM ist mir bekannt, insbesondere habe ich die
Bedeutung von § 28 (Nichtigkeit der Promotion) und § 29 (Entzug des Doktorgrades) zur Kenntnis
genommen. Ich bin mir der Konsequenzen einer falschen Eidesstattlichen Erklärung bewusst.

Mit der Aufnahme meiner personenbezogenen Daten in die Alumni-Datei bei der TUM bin ich

(x) einverstanden
(   ) nicht einverstanden

München, den 7.6.18 ....
                                                              Unterschrift